IONIC POLISHING OF FUSED SILICA

by

Raymond Gale Wilson

A Dissertation Submitted to the Faculty of the

COMMITTEE ON OPTICAL SCIENCES

In Partial Fulfillment of the Requirements
For the Degree of

DOCTOR OF PHILOSOPHY

In the Graduate College

THE UNIVERSITY OF ARIZONA

1971

THE UNIVERSITY OF ARIZONA

GRADUATE COLLEGE

I hereby recommend that this dissertation prepared under my direction by Raymond Gale Wilson

entitled Ionic Polishing of Fused Silica

be accepted as fulfilling the dissertation requirement of the degree of Doctor of Philosophy

R. H. Noble — Dissertation Director

16 April 71 — Date

After inspection of the final copy of the dissertation, the following members of the Final Examination Committee concur in its approval and recommend its acceptance:*

Stanley Ballard — 4/16/71

John O. Stoner, Jr. — 16 April 1971

Quentin M. Stevenson — 19 April 1971

Roland V. Shack — 19 APRIL 1971

*This approval and acceptance is contingent on the candidate's adequate performance and defense of this dissertation at the final oral examination. The inclusion of this sheet bound into the library copy of the dissertation is evidence of satisfactory performance at the final examination.

STATEMENT BY AUTHOR

This dissertation has been submitted in partial fullfillment of requirements for an advanced degree at The University of Arizona and is deposited in the University Library to be made available to borrowers under the rules of the Library.

Brief quotations from this dissertation are allowable without special permission, provided that accurate acknowledgment of source is made. Requests for permission for extended quotation from or reproduction of this manuscript in whole or in part may be granted by the head of the major department or the Dean of the Graduate College when in his judgment the proposed use of the material is in the interests of scholarship. In all other instances, however, permission must be obtained from the author.

SIGNED: Raymond L. Wilson

ACKNOWLEDGMENTS

I am indebted to the administration of Illinois Wesleyan University for allowing me a two year study leave of absence during which time a major portion of this research and study was completed. It was supported during the two years partly by Illinois Wesleyan and mainly by the National Science Foundation through a Science Faculty Fellowship for which I am most grateful.

My wife and children were understanding about being uprooted for two years and an additional summer, but I'm sure the Tucson stay was valuable to all of them also.

I would like to thank the Office of Naval Research whose funding provided the main support for this project.

I am grateful to Dr. Robert H. Noble, my advisor, for encouraging my participation in this research. It has provided me with a most valuable experience.

TABLE OF CONTENTS

Page

LIST OF ILLUSTRATIONS vi

LIST OF TABLES. x

ABSTRACT. xi

1. INTRODUCTION. 1
   - Brief Explanation of the Ionic Polishing Process. 2
   - Review of Past Research 4
     - Erosion Ratios 4
     - Structure and Nature of the Eroded Surface 15
     - Contaminant Film 21
     - Surface Layer Alterations. 22
     - Secondary Electron Emission. 27
     - Gas Trapping and Release 27
     - Other Effects. 30
   - Summary and Conclusions Based upon Past Research. 30

2. THE IONIC POLISHING SYSTEM. 32
   - The Vacuum System 32
   - The Cooling Systems 36
   - The Ion Source and Lens 39
   - Electronics for the Ion Source and Lens 43
   - The Target Chamber and Monitoring System. 50

3. EXPERIMENTAL PROCEDURES 56
   - Target Alignment and Preparation. 56
   - Ion Beam Production and Monitoring. 61
   - A Vacuum Problem. 65
   - Target Temperature. 65

4. POST-BOMBARDMENT MEASUREMENTS AND CALCULATIONS. 68
   - Determination of Eroded Mass and Eroded Mass Error. . . . 68
   - Determination of Ion Dose and Ion Dose Error. 70
   - Display and Tabulation of Erosion Ratios. 73

5. EXAMINATION OF POLISHED SURFACES. 83
   - Gross Observations of Gross Surfaces. 83
   - Examination by Electron Microscopy. 86
   - An Indirect Roughness Estimate. 98

6. SUMMARY AND CONCLUSIONS 100

TABLE OF CONTENTS--Continued

Page

APPENDIX I: CALCULATION OF ION DOSES. 106

APPENDIX II: TABULATION OF ERODED MASSES 112

LIST OF REFERENCES. 117

LIST OF ILLUSTRATIONS

Figure		Page
1.	Erosion Ratio, Kr on Fused Silica and Glass.	5
2.	Erosion Ratio, Xe on Vitreous Silica	6
3.	Erosion Ratio, Ar on Silica.	9
4.	Equivalent DC Erosion Ratios	10
5.	Comparison of Erosion Ratios	11
6.	Eroded Depth as a Function of Temperature.	12
7.	Eroded Depth Experimental Arrangement.	13
8.	Eroded Depth as a Function of Angle.	14
9.	Glass Polished at 80°.	17
10.	Glass Polished at 60°.	17
11.	Glass Polished at 45°.	18
12.	Glass Polished at 30°.	18
13.	Glass Polished at 0°	19
14.	Glass Polished at 60° while Rotating	19
15.	Reflection Coefficient of Glass.	23
16.	Reflection Coefficient Ratio of Quartz	24
17.	Refractive Index Increase of Vitreous Silica	25
18.	Refractive Index Decrease of Quartz.	25
19.	Effective Depth of Bombarded Layer	26
20.	Reflection Coefficient Ratio vs. Integrated Flux . . .	26
21.	H_2^+ and D_2^+ Range in Quartz.	28
22.	He^+ Range in Quartz.	28
23.	Secondary Electron Emission, 0 - 2.5 keV	29

LIST OF ILLUSTRATIONS--Continued

Figure		Page
24.	Secondary Electron Emission, 0 - 30 keV	29
25.	Schematic Diagram of the Ionic Polishing Vacuum System	34
26.	Ion Beam System	37
27.	Schematic Diagram of the Ionic Polishing Cooling Systems	38
28.	Duoplasmatron Schematic Diagram	40
29.	Einzel Lens Schematic Diagram	41
30.	Power Supply for Duoplasmatron Filament	44
31.	Power Supplies for Duoplasmatron Magnet (Top) and Arc (Bottom)	47
32.	Electrical Diagram, the Duoplasmatron and Einzel Lens	48
33.	Ion Beam System	49
34.	Electrical Diagram, Vacuum System and Duoplasmatron Relays and Interlocks	50
35.	Target Assembly Flange.	51
36.	Power Supply for the Neutralization Filament.	52
37.	Temperature and Electron Emission Characteristics of the Neutralization Filament.	53
38.	Typical Faraday Cup Bias Curves	54
39.	Faraday Cup Bias Circuit.	55
40.	Shutter and Faraday Cup Control Circuit	55
41.	Target Assembly Flange on Analog Fixture.	58
42.	Target Assembly Flange, Air Side.	60
43.	Typical Duoplasmatron Operation Curve	62
44.	Target Under Ion Bombardment.	63
45.	Typical Erosion Runs.	64

LIST OF ILLUSTRATIONS--Continued

Figure		Page
46.	Target After Bombardment.	72
47.	Intermediate Electrode Erosion.	72
48.	Erosion Ratio Versus Acceleration Voltage, Neon on Fused Silica.	74
49.	Erosion Ratio Versus Acceleration Voltage, Argon on Fused Silica	75
50.	Erosion Ratio Versus Acceleration Voltage, Krypton on Fused Silica	76
51.	Erosion Ratio Versus Acceleration Voltage, Xenon on Fused Silica	77
52.	Erosion Ratio Versus Acceleration Voltage, Angle of Incidence, 0°	78
53.	Erosion Ratio Versus Acceleration Voltage, Angle of Incidence, 15°	79
54.	Erosion Ratio Versus Acceleration Voltage, Angle of Incidence, 30°	80
55.	Erosion Ratio Versus Acceleration Voltage, Angle of Incidence, 45°	81
56.	Gross Pitting of Fused Silica by 15 KeV Xenon Ions at 45°, Magnification 35X.	84
57.	Gross Pitting of Fused Silica by 15 KeV Xenon Ions at 30°, Magnification 35X.	84
58.	Gross Pitting of Fused Silica by 10 KeV Xenon Ions at 30°, Magnification 35X.	85
59.	Pitting of Fused Silica by 5 KeV Xenon Ions at 0°, Magnification 35X	85
60.	Pitting of Fused Silica by 5 KeV Xenon Ions at 45°, Magnification 100X	87
61.	Comparison Photograph Showing Very Little Pitting on a Target Bombarded by 4.6 KeV Argon Ions at 45°, Magnification 100X	87
62.	SEM Micrograph, Fused Silica, 15 KeV Neon at 45°, Magnification 3,000X.	89

LIST OF ILLUSTRATIONS--Continued

Figure		Page
63.	SEM Micrograph, Fused Silica, 15 KeV Argon at 45°, Magnification 3,000X.	90
64.	SEM Micrograph, Fused Silica, 5 KeV Xenon at 45°, Magnification 3,000X.	92
65.	SEM Micrograph, Unbombarded Surface, Magnification 10,000X	93
66.	TEM Micrograph, Fused Silica, 5 KeV Xenon at 45°, Magnification 4,000X.	94
67.	TEM Micrograph, Fused Silica, 15 KeV Argon at 45°, Magnification 4,500X.	94
68.	TEM Micrograph, Fused Silica, 5 KeV Neon at 45°, Magnification 9,600X.	95
69.	TEM Micrograph, Fused Silica, 5 KeV Xenon at 0°, Magnification 9,600X	96
70.	TEM Micrograph, Fused Silica, 5 KeV Argon at 45°, Magnification 9,600X.	97
71.	FECO Fringes from Bombarded Surface	99

LIST OF TABLES

Table		Page
I.	Erosion Ratios (μgm/μA·hr) as a Function of Ion Energy and Angle of Incidence.	82
II.	Summary of Bombardment Doses, and Estimated Bombardment Dose Error	110
III.	Tabulation of Mass Data.	115

ABSTRACT

Ground and polished surfaces of GE Type 101 clear fused silica were bombarded with positive ions of neon, argon, krypton, and xenon at angles of incidence from normal to 45° and with incident energies generally in the range 5 to 15 keV using a raw focused beam from a duoplasmatron. Bombardment doses averaged near 300 microampere-hours. Attempts were made to neutralize positive surface charge buildup by employing a nearby electron-emitting tungsten filament. Target temperature increase due to bombardment was estimated. Eroded mass was determined by weighing to micrograms. Erosion ratios were calculated in terms of micrograms/microampere-hour; the average value over all runs was near 2 micrograms/microampere-hour. Examination of the polished surfaces revealed, in some instances, gross pitting and etching in unexplainable patterns. Other surfaces which appeared optically smooth at magnifications of 100, revealed at 3,000X and 10,000X by electron microscopy, microfurrowing perpendicular to the ion beam direction. The furrow spacings ranged from 45 to 130 nm and their peak-to-peak roughnesses were estimated to range from 7 to 35 nm. It is suggested that the furrowing is related to micro-cratering in the early stages of bombardment and that the early cratering and other gross pitting is related to the past history of the silica surface. The surface morphology is discussed in relation to possible erosion processes of momentum transfer, thermal spikes, and

blistering and exfoliation due to trapped gas. Experimental improvements are suggested as well as other applications of ion bombardment.

1

INTRODUCTION

Ionic polishing is a new application of a well-known phenomenon, sputtering, which was investigated as early as 1852.[1] The literature concerning metal sputtering is extensive, much of the information having been acquired within the past two decades. There have been some comprehensive reviews of the sputtering process.[2-5] Evidently the lack of applicability and some inherent difficulties, which will be discussed, have held back comparable research in the sputtering in insulators. In recent years, however, research in the sputtering of insulating materials has been stimulated by work in thin films, the use of plasmas and ion beams near insulators, and questions concerning particle irradiation of space probes.[6] In 1965, Meinel, Bashkin, and Loomis[7] discovered that an accelerated ion beam could be used to polish and figure an optical surface; they suggested the term "ionic polishing." It is their discovery that stimulated this research.

Since 1965 several organizations have taken an interest in the ionic polishing of optical materials. In the United States the Perkin-Elmer Corporation[8-10] and the Kollsman Corporation[11,12] have instituted research programs in this field apparently oriented toward the commercial production of optical surfaces. In Great Britain the British Scientific Instrument Research Association (SIRA) is also working along the same lines with a particular

interest in the possible creation of supersmooth surfaces.[13-14] This writer assumes that industrial security has precluded the publication of any detailed accounts of ionic polishing processes. A group at Sussex University in England is also working in this area,[15] and, of course, the work originated at The University of Arizona has continued.

Brief Explanation of the Ionic Polishing Process

It would be well to clarify certain points at the outset of this paper, for this writer noted some surprise when he brought up the question of sputtering glass. The sputtering of metals is a phenomenon that has been well researched, and the experimental procedures are widely known. This is apparently not so for dielectric materials. For a metal to be sputtered, it is subjected to bombardment by positive ions. This is perhaps most easily done by immersing the metal in a gaseous discharge, the metal acting as the discharge cathode. Or the metal can be placed in the path of an ion beam. An interchange of energy takes place between the impinging ions and the metal atoms, some of which leave the surface of the metal and become deposited on the walls of the containing chamber and on objects placed therein. It is a common technique for coating mirrors with aluminum, and the procedure is described by Strong[16] and others.

If such a process is to be used in the polishing and figuring of optical surfaces, it would be desirable to have accurate knowledge of the erosion ratio, i.e., the ratio of the mass of

material eroded to the number of incident ions or some equivalent ratio, such as molecule/ion. One would also need to know something of the nature of the resultant polish obtained by this process.

This research specifically reports erosion ratios for GE Type 101 clear fused silica, a commonly used optical material. Past research in sputtering has shown that the erosion ratio will depend upon a number of parameters, among which are: incident ion mass, incident ion energy, and angle of incidence. The research of this paper reports on the variation of erosion ratio of fused silica for incident ions of neon, argon, krypton, and xenon, with incident energies generally in the range 5 keV to 15 keV and with angles of incidence varying from 0° (normal) to 45°. Selected ionically polished surfaces were examined and we report on the nature of the polished surfaces.

There are a number of problems inherent in the ionic bombardment of insulators, and in order to provide the reader with a better comprehension of this writer's approach to this investigation it would probably be well to review the technique and results of past research in this field.

We have briefly described on page 2 procedures for sputtering a metal, by placing it in a gaseous discharge or in the path of an ion beam. When sputtering a dielectric, however, the experimental procedures of necessity must be altered.

The dielectric can still be placed in a gas discharge, but charge buildup on the surface will create a problem in attempting

to maintain the discharge at the surface. One researcher placed a suitably biased metal grid over the surface[17] and thus maintained the discharge there, but contamination by sputtered grid molecules could occur, and the sputtering conditions for the dielectric were thus poorly defined. It is thought that the dielectric can be maintained electrically neutral by placing an electron-emitting filament near the surface[18] or by means of an electron gun; these electrons would neutralize the charge buildup due to the positive ions. If the dielectric is in a gas discharge, the surface can be kept neutral by the application of an ac potential to the metal substrate supporting the dielectric.[17] If the bombarding ion beam overlaps the edge of the target the beam plasma can provide a conducting path to the target supports. Inadequate surface charge neutralization could conceivably alter the bombarding ion energy and angle of incidence.

Review of Past Research

Let us now look at the results of other workers and their approaches to the above problem. We will be mainly concerned with values of the erosion ratio, but mention will be made of other phenomena accompanying ionic bombardment.

Erosion Ratios

Akishin, Vasil'ev, and Isaev[19] measured erosion ratios for mica, fused silica, and glass using krypton ion beams in the energy range 4 to 30 keV. Apparently the beam they employed was energy analyzed. The beam current density for silica and glass was from

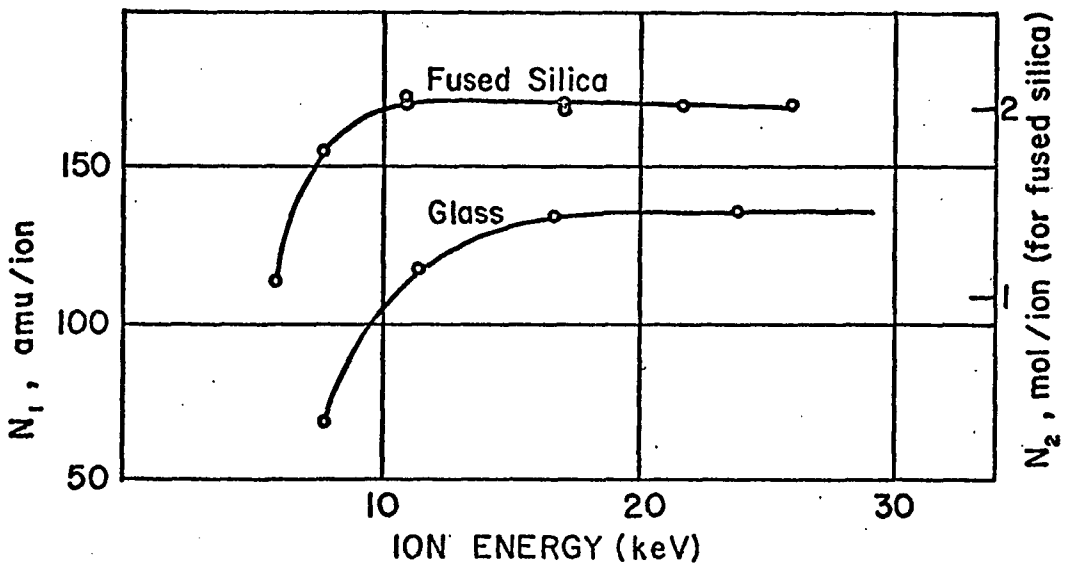

Fig. 1. Erosion Ratio, Kr on Fused Silica and Glass. Variation of cathode erosion ratio N for fused silica and for glass as a function of the Kr ion energy. The N_2 axis, mol/ion, refers to fused silica only. (Akishin et al.[19])

100 to 200μA/cm^2, while the pressure in the vacuum chamber was 3×10^{-4} Torr. The glass and silica were oriented at 60° to the ion beam, but it is not clear whether this is the angle from the normal or from the surface. Positive charge accumulated on the target surface was neutralized by electrons from a nearby cathode of thoriated tungsten. The ion beam current was measured with a Faraday cup, and this agreed, to within 10%, with a measurement obtained from the electron neutralization current. Secondary electron emission was suppressed by a magnetic field and a positive biased ring near the target. Erosion ratios were obtained by

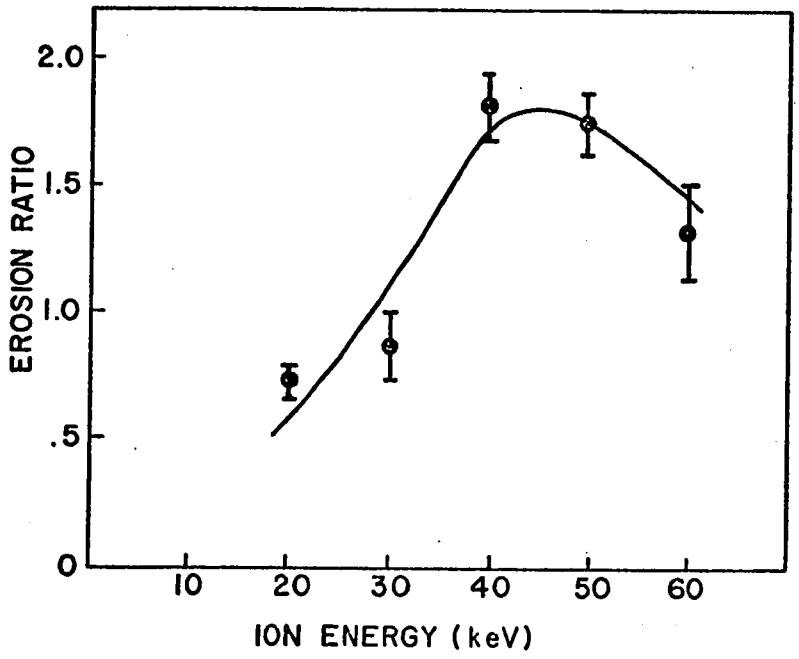

Fig. 2. Erosion Ratio, Xe on Vitreous Silica.
Erosion ratio for vitreous silica bombarded by Xe^+ ions as a function of Xe ion energy. Errors shown are estimated errors made in measuring the volume of the eroded cavity. (Hines and Wallor[20])

weighing before and after bombardment with a weighing accuracy of 5×10^{-5}g. With a bombardment dose of 300μA-hours, the average change in weight was 1 to 2 mg. The target size and mass were not reported, nor was the bombardment time. The erosion ratios are plotted in Fig. 1 as a function of energy. It is not clear how the authors determined that 1 molecule corresponds to 110 amu; the molecular weight of SiO_2 is 60.

Hines and Wallor[20] bombarded vitreous silica with 20 to 60 keV Xe^+ ions at normal incidence in a vacuum of 10^{-5} Torr. A magnetically analyzed beam was used, and charge buildup on the

silica surface was neutralized by electrons from a nearby hot tungsten filament. Beam currents ranged from 0.5 to 3 μA. The amount of material eroded was determined by observing interference fringe contours of the eroded cavity and estimating the volume removed. The results are shown in Fig. 2.

In an earlier paper, Hines and Arndt[18] inferred an erosion ratio of 1.2 with 32 keV Ar^+ ions. They mentioned the appearance of a bluish-silvery film surrounding the bombarded area and conjectured that it was due to oil contamination. Estimates were made of the error to be caused by this contaminant film, but because of questionable validity the error was not included in the results. A formula for estimating the temperature rise of the silica was presented,[21] $\Delta T = Q/\pi Ka$ (where Q = power input to the target, K = thermal conductivity of a semi-infinite target support, and a = radius of bombarded spot), and from this, ΔT for Xe^+ ions at 20 keV and at 59 keV was calculated as 13 C° and 118 C°. (For comparison we note here that Dugdale and Ford[22] measured temperature rises for a 12 keV, 0.1 mA beam of Ar^+ ions incident on alumina at initial temperatures of 20°C, 500°C, and 900°C. Rises were, respectively, 80 C°, 30 C°, and 10 C°.)

Jorgenson and Wehner[23] measured erosion threshold energies and low-energy erosion ratios for films of sputtered silica and Pyrex 7740. The method consisted of depositing onto a Langmuir probe a thin film of silica or Pyrex and then removing the film by dc erosion. The voltage-current characteristics of the probe are very sensitive to deposits of insulating material. The film

deposited is of known thickness, and a known fraction of it is eroded off by enforcing a dc bias voltage on the probe. Different voltages require different times to remove the same amount of material, and this fact was used to determine erosion ratios. (See Fig. 3.) The experiment was carried out in a 10^{-2} Torr argon discharge. It was also determined that the composition of the film sputtered onto the probe was $SiO_{1.6}$. No mention is made of compensation for secondary electron emission. It should be noted that, when insulators are eroded in a gas discharge, one has little control over charge and the angle of incidence of the bombarding ions.

Davidse and Maissel[24] used an interesting rf technique to obtain "equivalent" dc erosion ratios. Among the materials they studied were fused silica, Pyrex 7059 glass, and soda-lime glass. Their experiments were performed in an argon atmosphere at 3×10^{-3} Torr. The dielectric materials were subjected to an rf discharge in the argon with electrode potentials between 1.3 and 3.9 kV, peak-to-peak, at 13.56 MHz. The dielectric material to be eroded was in the form of a plate upon which were placed two smaller samples of materials, germanium and silicon, with known dc erosion ratios. The amount of material removed from all three was determined by weighing. It was assumed that all three were subject to the same erosion conditions. Since the dc erosion ratios were known for germanium and silicon, the relationship between these two ratios could be used to ascertain an "equivalent" dc bombardment voltage, V_{dc}. It resulted that V_{dc} was about 3/4 the rf peak-to-peak voltage although not directly proportional to it. The results

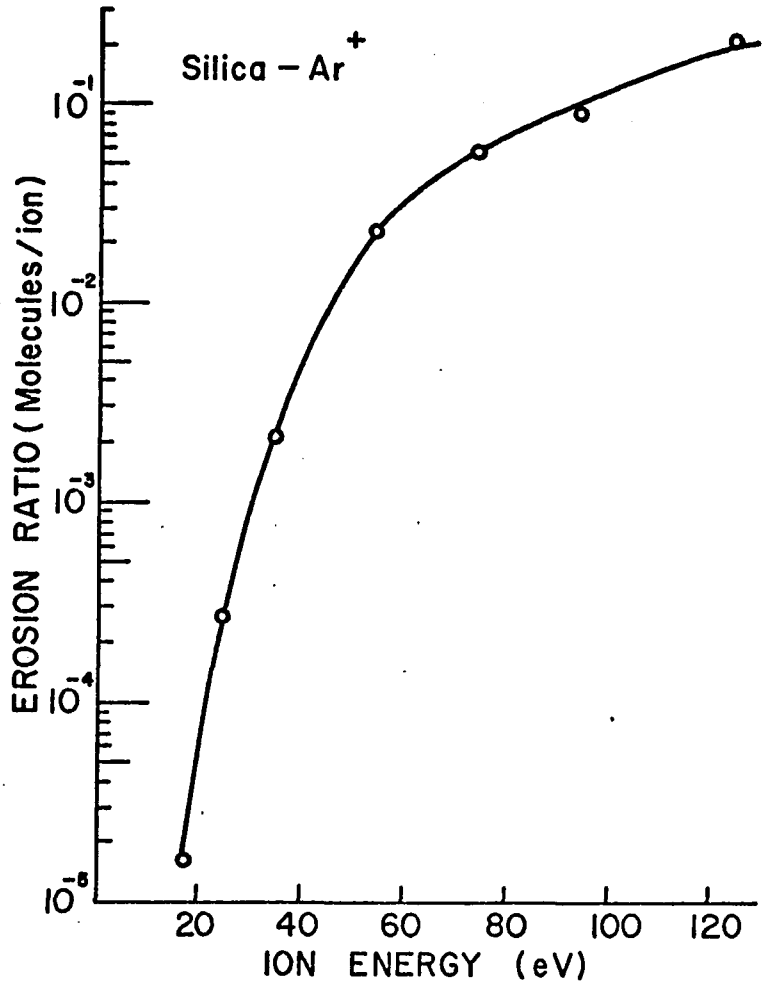

Fig. 3. Erosion Ratio, Ar on Silica.
Erosion ratio vs. bombarding energy.
(Jorgenson and Wehner[23])

of this work are presented in Fig. 4. In the term molecule/ion, "mean molecule" was used based upon mean molecular weight and glass composition. Davidse and Maissel compared their work to that of Hines and Wallor[20] and that of Jorgenson and Wehner,[23] and this is

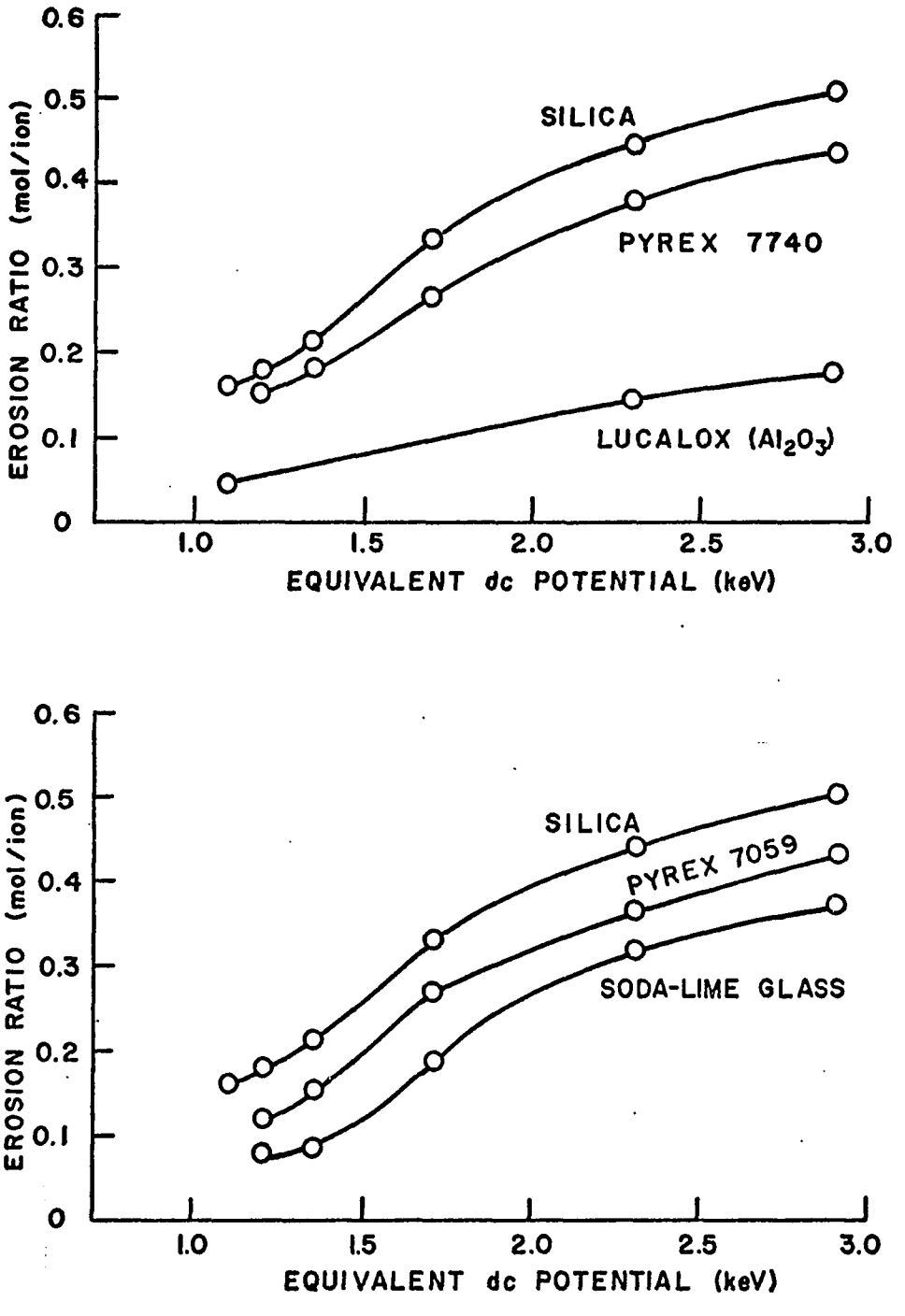

Fig. 4. Equivalent DC Erosion Ratios.
(Top) Equivalent dc erosion ratios for fused silica, Pyrex 7740, and Lucalox. (Bottom) Equivalent dc erosion ratios for Pyrex 7059 and soda-lime glass. (The fused silica curve is shown again for reference.) (Davidse and Maissel[24])

shown in Fig. 5. This comparison serves at least one purpose: to point out that bombardment methods and conditions play a decisive role as concerns erosion ratio.

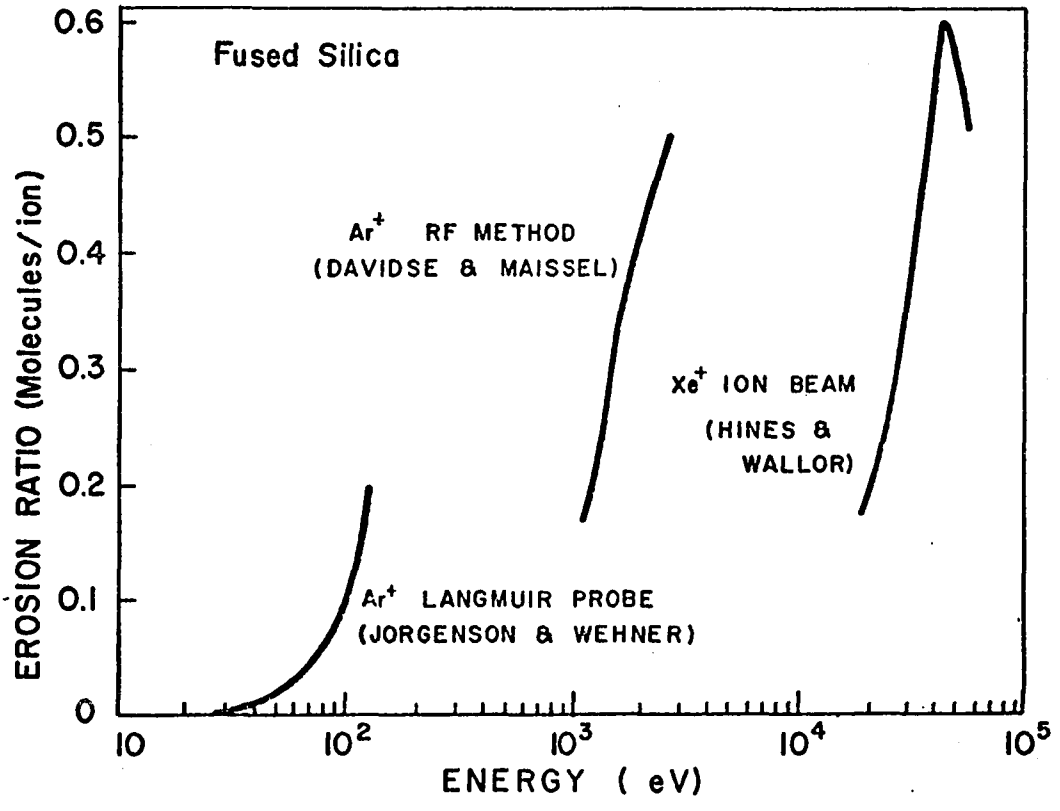

Fig. 5. Comparison of Erosion Ratios.
Comparison of erosion ratios obtained by various methods, for fused silica. (Davidse and Maissel[24])

The need to etch sections of glass and ceramics stimulated Dugdale and Ford[22] to investigate sputtering as the etching process. Their research involved the parameters of voltage, temperature, and angle of incidence in the sputtering of Lucalox alumina, fused silica, and sapphire. An Ar^+ ion beam was used, and the associated plasma in electrical contact with grounded parts of the apparatus supplied the neutralization electrons. Their results working with

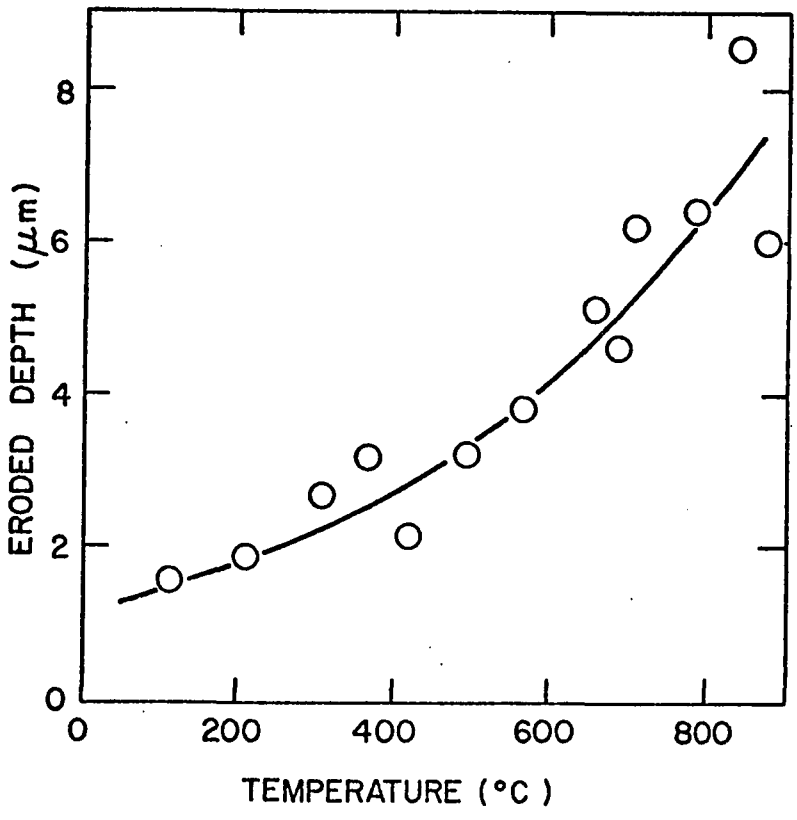

Fig. 6. Eroded Depth as Function of Temperature.
Eroded depth due to bombardment of fused silica by argon at 12 keV, as a function of temperature. (Dugdale and Ford[22])

a 100μA beam of 12 keV Ar^+ ions at normal incidence on a flat surface are shown in Fig. 6, in which erosion depth is plotted as a function of temperature. From these data and Fizeau fringes of the resultant surface, they estimated the erosion ratios at 100°C and 800°C to be, respectively, one and four atoms per ion.

In a second experiment, a 1-mm-diameter cylindrical rod of fused silica was encased in a silica tube, and the assembly was ground flat on one side and placed on a horizontal heated stage

in the path of the ion beam, which was normal to the rod and tube axis at the tube end (Fig. 7). A step was eroded into the rod and then measured with a microscope. This provided erosion depth data as a function of angle of incidence. These results are shown in Fig. 8 for 12 keV Ar^+ ions and temperatures of 300°, 600°, and 900°C. The temperatures are to be regarded as approximate, and, owing to inhomogeneities of the ion beam, calculated erosion rates at glancing angles would be in error. The results, however, clearly indicate the effect on erosion ratio of temperature and angle of incidence. As a mechanism for sputtering, or erosion,

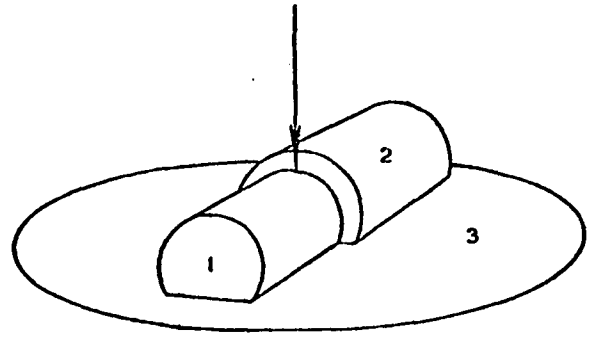

Fig. 7. Eroded Depth Experimental Arrangement. Experimental arrangement to measure erosion of fused silica as a function of angle of incidence: (1) silica rod, (2) close-fitting silica tube, (3) heated stage. (Dugdale and Ford[22])

they conclude that their data are semi-quantitatively consistent with evaporation from thermal spikes, with momentum transfer also playing a role, especially at glancing angles.

The discovery of ionic polishing has been mentioned.[7] Schroeder, Bashkin, and Nester[8] have studied the process in more

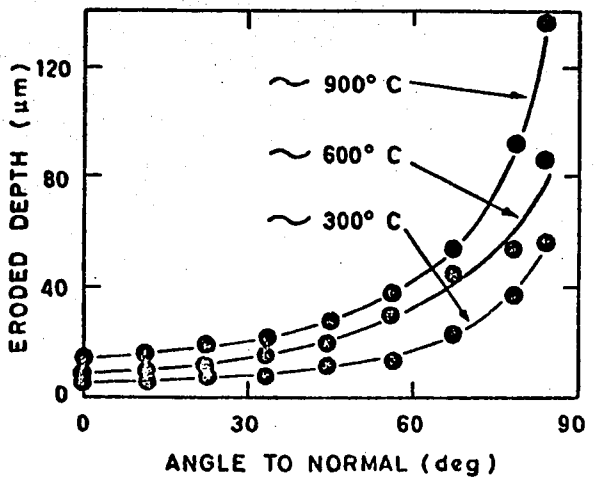

Fig. 8. Eroded Depth as Function of Angle.
Eroded depth due to bombardment of fused silica with argon at 12 keV, as a function of angle of incidence. (Dugdale and Ford[22])

detail using H^+ and Xe^+ ions from a Van de Graaff accelerator. Beam currents ranged from 0.4 to 30 μA and ion energies from 0.5 to 1.8 MeV. The pressure in the chamber was 6 to 8 x 10^{-6} Torr. Most of the work was done at a 60° angle of incidence, and surface charge was neutralized. Starting with surfaces that were flat to λ/10, they removed from 112.5 to 300 nm of material over about 1 cm^2 of surface and estimated an erosion ratio of unity for the materials, which were fused silica, BK-7 optical glass, and Cer-Vit. They also observed a carbon film at the eroded area but were able to eliminate most of it by improvements in vacuum techniques. By placing the sample in one leg of a Twyman-Green interferometer and using laser illumination, they were able to observe interference fringes from the fused silica during bombardment with H^+ ions, but thermal distortion did not allow this with BK-7. Their results

indicate that ionic polishing could be a useful technique in the figuring of optical surfaces. The work just reported was done in 1965. In 1967, Narodny and Tarasevich[11] reported the ionic figuring of an f/6, 10-cm paraboloid of Pyrex. They used a 100 μA Ar^+ ion beam at evidently less than 50 keV focused on the surface. The dwell time of the beam was adjusted along the mirror radius and programmed to remove calculated depths of material as the mirror was rotated.

Structure and Nature of the Eroded Surface

A number of researchers have investigated the surfaces of ionically eroded materials. Dugdale and Ford[22] observed pits on the surface of fused silica after it had been bombarded at normal incidence and 900°C. The pits were shallow compared with the depth of material eroded (about 14 μm), and some had a spiral structure. It was suggested that the pits were part of the equilibrium state of the etched surface. Pitting was also produced at glancing angles and lower target temperatures. (We note that Meckel and Swalin[25] obtained similar figures in bombarding germanium with Ar^+ ions of low energy, about 300 eV. They described it as selective delineation of screw dislocations.)

In a number of studies[26-29] ion bombardment has been used to analyze the structure of ceramic materials and glasses and to determine structural changes brought about by the bombardment. In the specific paper dealing with glass, Krokhina and Spivak[29] found they could obtain different phases of the structural

transformation in the surface layer of a specimen of borosilicate glass. The glass had undergone some heat treatment, which separated out two vitreous phases of different composition: silicate (SiO_2) and boric anhydride (B_2O_3). Using Ne^+ ions at 8 to 10 keV in an atmosphere of at least 5×10^{-2} Torr, and with the glass at 500 to 700°C, they found intense erosion of the boron and sodium with partial elimination of oxygen, leaving the surface layer relatively enriched in silica. Comparison of the microcrystalline surface structure with X-ray powder diffraction patterns indicated that the surface structure corresponded to the hexagonal system of α-quartz. Krokhina and Spivak also noted the formation of furrows on surfaces bombarded at angles of incidence other than normal. They claim that the width of the furrows was determined by the focusing of the ion flux and depended on the straightness and sharpness of the edges of the apertures in the screen or mask that they used over the glass surface. This metal screen provided the neutralization of the dielectric surface. They point out that the furrows are not structural characteristics but are brought about by experimental conditions. This does not seem to be in agreement with the following work which employed no screen or mask.

These furrows are clearly shown in the work of Navez, Sella, and Chaperot,[30] who used an electron microscope to study glass surfaces after ionic bombardment. The glass used was 72% SiO_2 with additional content of Al_2O_3, Na_2O, CaO, and MgO. The surface was bombarded by air ions at 4 keV in an atmosphere of about 10^{-1} Torr. The target support was made of copper and grounded, and they

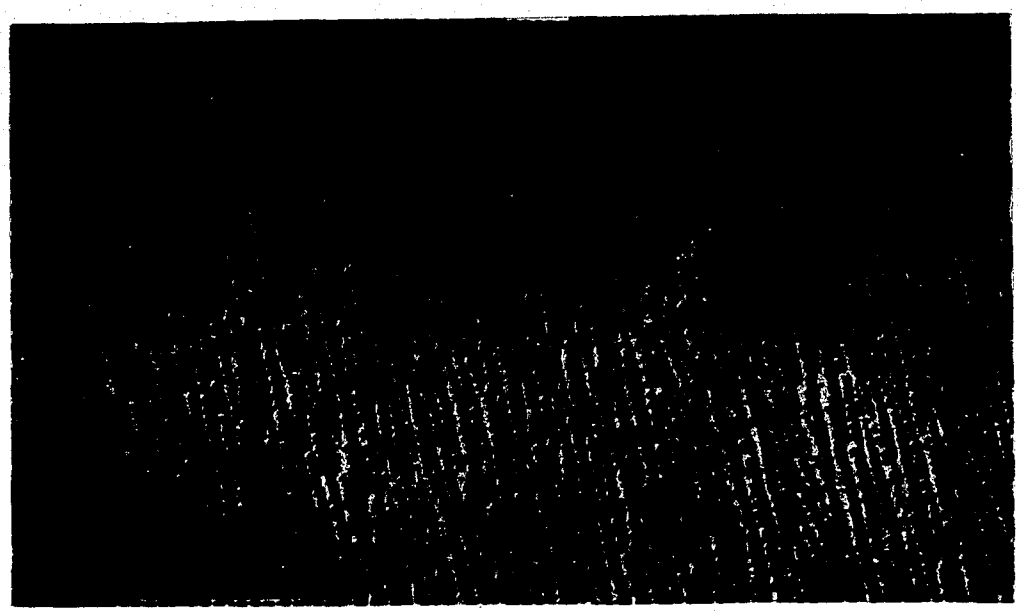

Fig. 9. Glass Polished at 80°.
Polished glass surface bombarded for 6 hours under grazing incidence (80°) by 4 keV ions. Arrow indicates direction of the beam. Striations are parallel to it. (Navez et al.[30])

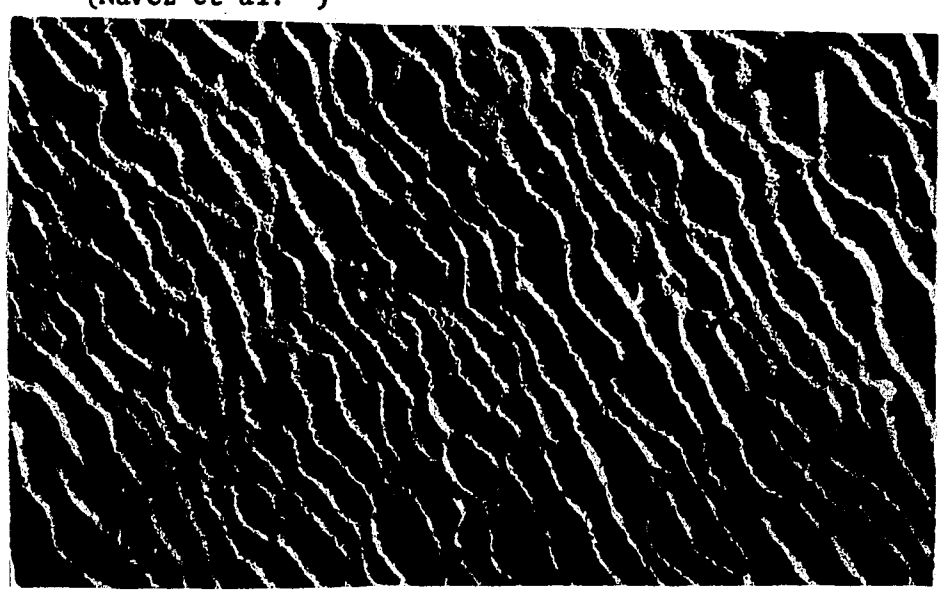

Fig. 10. Glass Polished at 60°.
Polished glass surface bombarded for 2 hours at 60° by a 4 keV ion beam, direction of which is indicated by the arrow. Average distance between ridges is 120 nm. (Navez et al.[30])

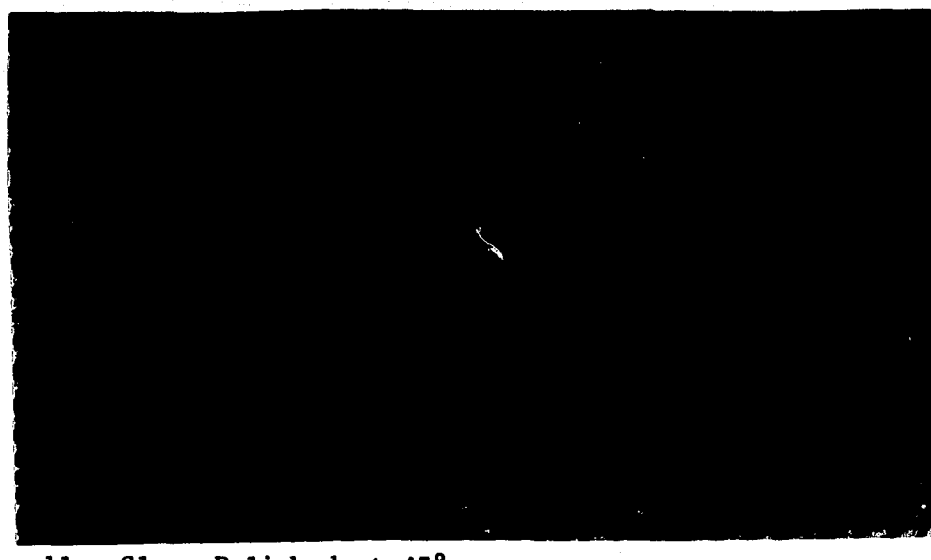

Fig. 11. Glass Polished at 45°.
Polished glass surface bombarded for 2 hours with 4 keV ions at 45°. The ridges are perpendicular to the beam and spaced 100 nm apart. (Navez et al.[30])

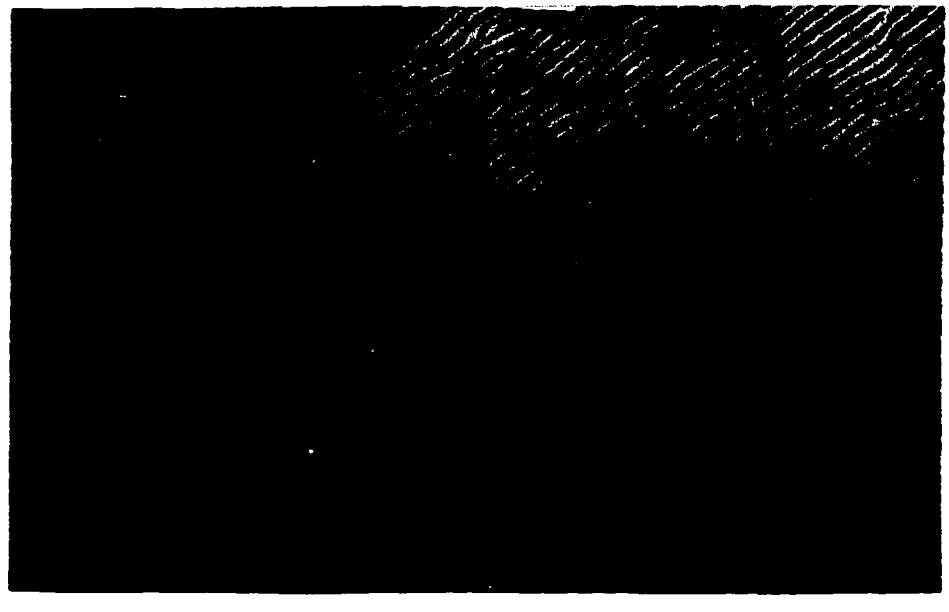

Fig. 12. Glass Polished at 30°.
Polished glass surface bombarded at 30°. The very regular furrows are perpendicular to the beam and spaced 80 nm apart. (Navez et al.[30])

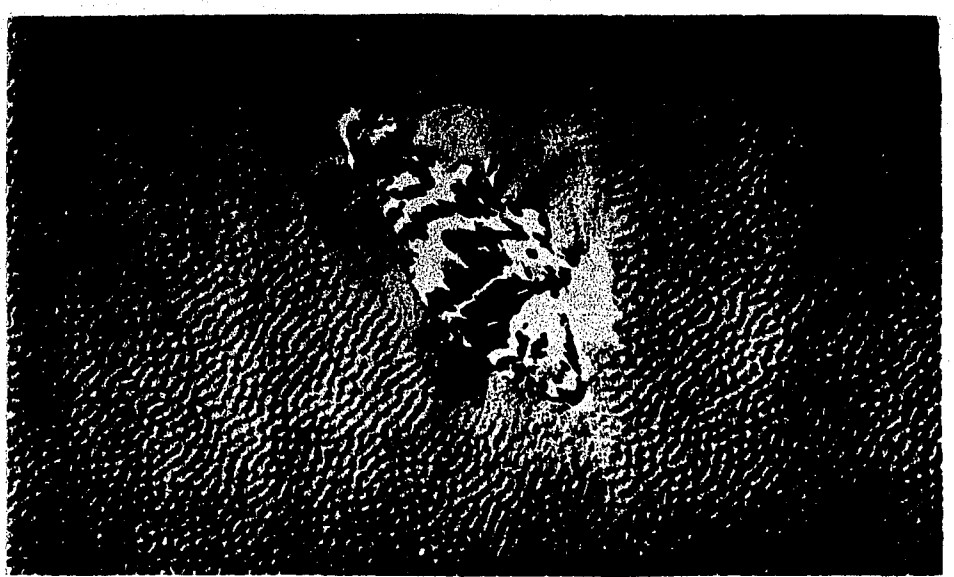

Fig. 13. Glass Polished at 0°.
Polished glass surface bombarded for 1/2 hour at normal incidence. In the center is a prick due to imperfect polishing. The attack figures are quite regular and have a mean diameter of 40 nm. (Navez et al.[30])

Fig. 14. Glass Polished at 60° while Rotating.
Polished glass surface bombarded at 60°, with the sample rotating in its plane. The cellular structure resembles chemical attack figures by hydrofluoric acid solutions. (Navez et al.[30])

comment that gaseous sweeping at this pressure and the high ion density, about 2 $\mu A/mm^2$, eliminate all target contamination, including electric charge. For short attacks they noted only simple cleaning of the surface without observable changes in morphology. However, after bombardment of an hour or more, the surface took on a completely new morphology, which depended on the angle of incidence and which was maintained indefinitely as bombardment continued. A series of electron micrographs made by a double replication technique (Figs. 9 through 14) shows the nature of the furrows. At grazing incidence (more than 80° from the normal) the furrows are parallel to the ion beam direction. At angles from 60° to 20°, the furrows are pendicular to the beam direction. Average spacing between furrows is about 100 nm, which, the authors noted, is the order of magnitude of the depth of atoms perturbed by each incident ion. In the case of normal incidence, one observes a regular structure formed by the juxtaposition of globular elements with an average diameter of 40 nm. This morphological change, due to bombardment, gives credence to the formation of thermal spikes.

Carter and Grant[31] commenting on the above work explained the furrows as follows:

> ...the ions, of range about 10 nm, cause thermal or displacement spikes which are of ellipsoidal structure with the long axis parallel to the ion velocity. As the angle of incidence increases toward the normal, the lateral dimensions of the spikes increase relative to the tangential dimension, and it appears that the ridges can pile up perpendicular to the ion velocity until at normal incidence the spike intersects the surface in circular arrays and voids form.

This writer can find no mention of the depth of the furrows.

The work just cited was carried out with 4 keV ions from air. Meinel, Bashkin, and Loomis[7] reported that the surfaces bombarded with ions near 1 MeV were polished as well as or better than the original, which was the good side of a master optical flat.

Primak[32] has also investigated the surfaces of optical materials bombarded by ions. He describes experiments with quartz and vitreous silica subjected for short periods of time to helium and proton beams in energy ranges 30 to 140 keV and 0 to 2 MeV. Crazing of the vitreous silica surface was observed in the high-energy ranges. He found depressions at the bombarded areas of vitreous silica which were attributable to stress relaxation, not erosion. Also observed on the irradiated surface was contaminant film similar to that observed by Hines and Wallor.[20]

Contaminant Film

The contaminant film accompanying ionic bombardment has been observed by Primak[32]; Schroeder, Bashkin, and Nester[8]; and Hines and Wallor.[20] It is believed that oil in the vapor phase in the vacuum system is adsorbed on objects in the vacuum chamber. Bombardment by electrons or energetic particles causes polymerization of the oil into a low vapor pressure solid. These conclusions were reached after experimentation by Ennos.[33] Hines and Wallor[20] calculated the error that would be contributed to their erosion ratios due to contaminant film formation. The correction was found to be smaller than the probable error arising from the measurement of the eroded volume. They also determined that, with

intense ion beams, the hydrocarbon molecules are sputtered off as fast as they arrive at the surface.

Surface Layer Alterations

Koch[34] reported a change in the reflectivity of glasses after bombardment by H^+ and inert gas ions and attributed the change to an alteration in the surface layer of the glass. Hines[21] obtained quantitative results in experiments with a silica-soda-lime glass irradiated with Ar^+ and N_2^+ ions. The depth and index of the altered layer are determined by fitting a theoretical reflection coefficient curve to the experimental data. The theoretical curves are obtained from the standard thin film equation relating reflection coefficient, thickness, and refractive indices. The depths agree with the theoretical range of Ar^+ ions in glass. Ions of up to 47 keV were used with an analyzed ion beam current of 5 μA and beam diameter of 2 mm. The refractive index of the altered layer is less than that of the original surface and is determined by the integrated flux of positive ions and type of ion (Fig. 15). There is a saturation effect beyond which there is no change in index; the limiting value of the reflection coefficient is thus designated R_∞. R_∞ does not change with the current density of the incident ion beam. It is not thought that sputtering affects these results, and it is believed that sputtering removes the contaminant film.

The effect of retained bombarding atoms is considered to be small. After being bombarded with N_2^+ the glass acquired a bluish tinge, thought to be due to retained N atoms. Annealing in an argon

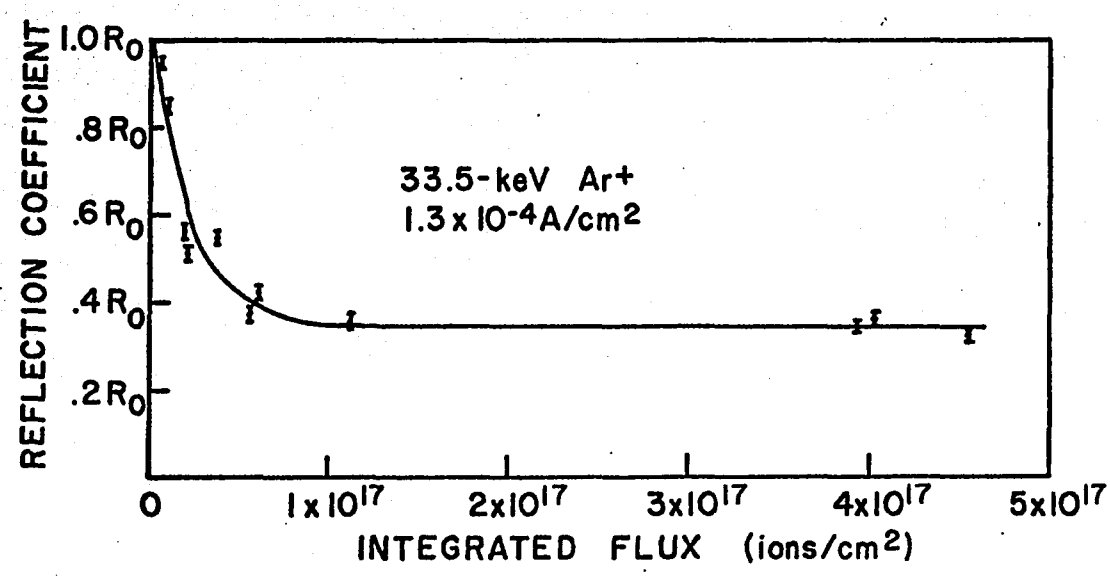

Fig. 15. Reflection Coefficient of Glass.
Reflection coefficient of glass (n_D = 1.5246) as a function of integrated flux of positive ions. (Hines[21])

atmosphere at 500°C removed the bluish tinge but changed the reflection coefficient only slightly. Indeed, annealing of Ar^+ and N_2^+ bombarded glass for three hours at its softening point (650°) in an argon atmosphere only partially restored the original condition.

In further work with quartz and vitreous silica, Hines and Arndt[18] determined layer depths and changes in refractive index brought about by H_2^+, D_2^+, He^+, Ne^+, Ar^+, Kr^+, and Xe^+ ions with energies from 7.5 keV to 59 keV. Corrections were made for the presence of a contaminant hydrocarbon film. In Fig. 16, the experimental points represent the combined effect of the radiation damage caused by the ions plus the effect of the contaminant film on the quartz surface. The dashed line is a theoretical curve, fitted to the experimental points at high fluxes, for the reflection coefficient ratio of a saturation bombarded quartz sample with a contaminant

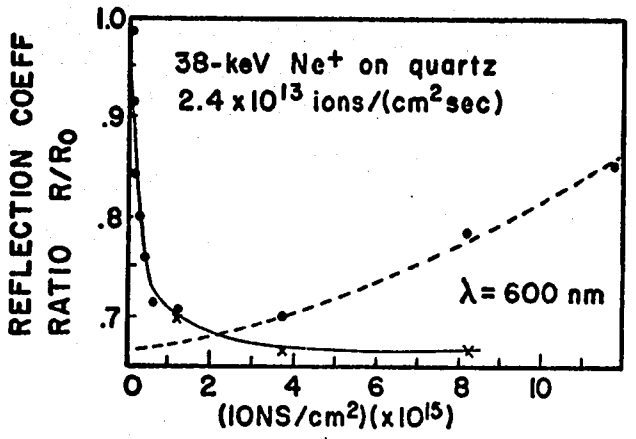

Fig. 16. Reflection Coefficient Ratio of Quartz.
Effects of radiation damage as derived from experiment.
Experimental points represent combined effect of radiation damage plus effect of the contaminant film on the quartz surface.
Dashed line is a theoretical curve for the reflection coefficient ratio of saturation bombarded quartz with contaminant film (see text).
Crosses are experimental points corrected for contaminant film.
Solid curve gives effect of radiation damage alone.
(Hines and Arndt[18])

film whose thickness is a linear function of the integrated flux. Extrapolating this curve to zero flux gives the saturation value R/R_o due to the radiation damage alone, and the difference between the dashed curve and the saturation value R/R_o gives the correction for the presence of the contaminant film. The crosses are the experimental points corrected for the contaminant film, and the solid curve gives the effect of the radiation damage alone.

Figs. 17 through 20 give typical results. Fig. 17 shows the increase in refractive index for vitreous silica. Figs. 18 through 20 show, respectively, the refractive index decrease of quartz, the effective depth, and the reflection coefficient ratio. These changes

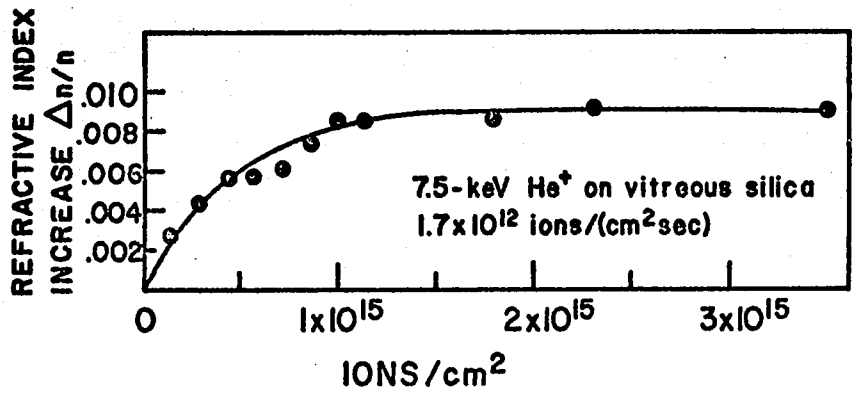

Fig. 17. Refractive Index Increase of Vitreous Silica. Increase in refractive index of vitreous silica as a function of integrated flux of 7.5 keV He^+ ions. (Hines and Arndt[18])

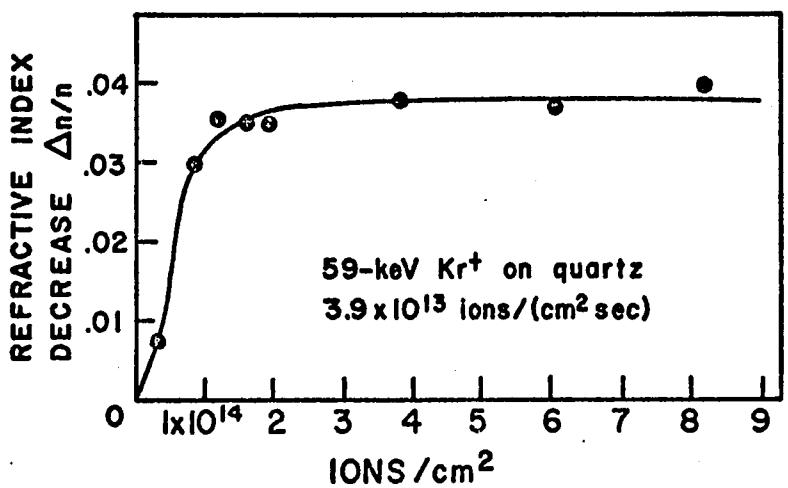

Fig. 18. Refractive Index Decrease of Quartz. Decrease in ordinary refractive index of quartz bombarded by 59 keV Kr^+ ions. Experimental points are obtained by fitting theoretical curves to the data shown in Fig. 20. (Hines and Arndt[18])

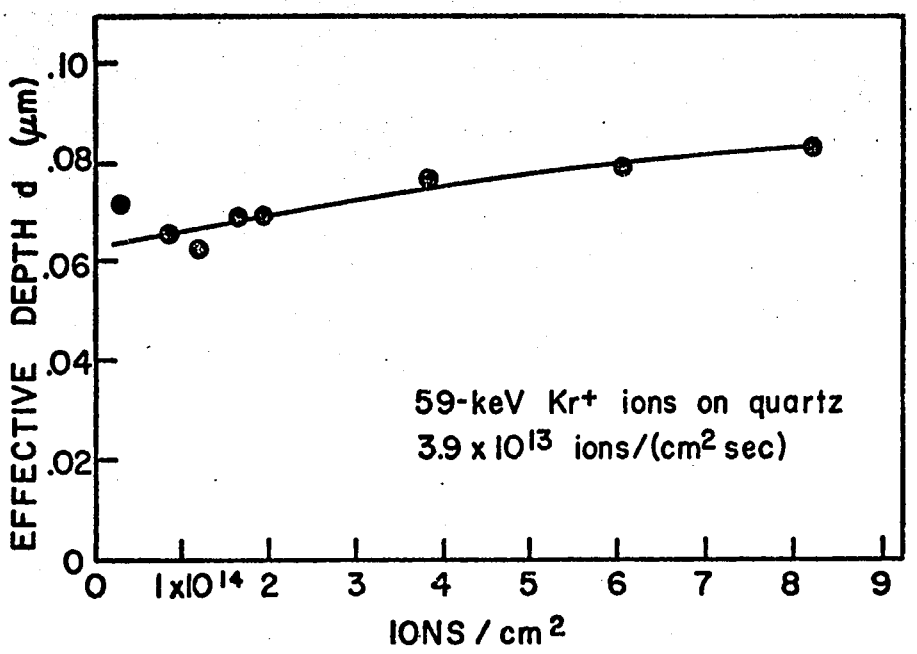

Fig. 19. Effective Depth of Bombarded Layer.
Effective depth of the layer produced when quartz is bombarded by 59-keV Kr^+ ions. The increase in depth for fluxes larger than that required for saturation (see Fig. 18) is attributed to the penetration of the high-energy knock-ons produced by the Kr^+ ions. (Hines and Arndt[18])

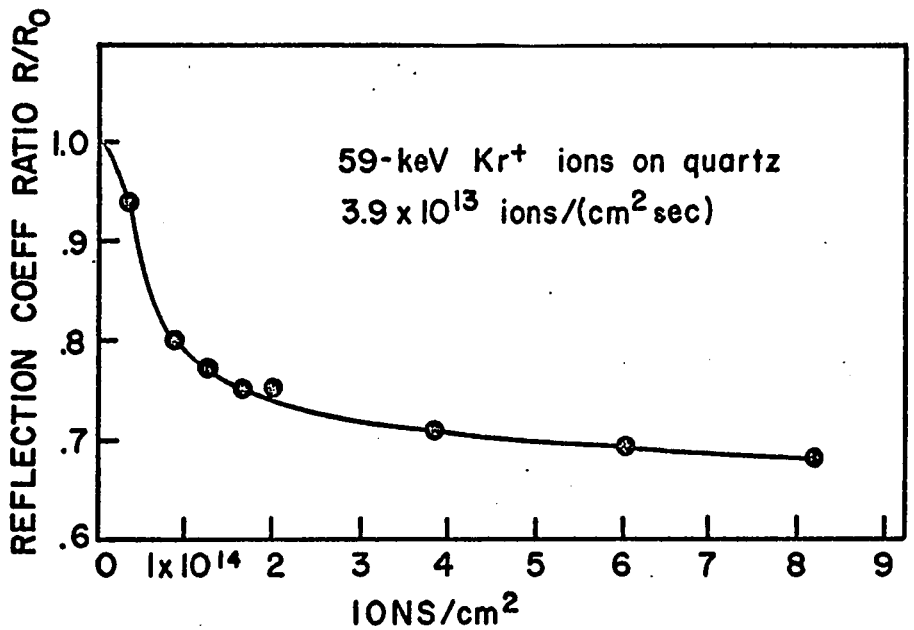

Fig. 20. Reflection Coefficient Ratio vs. Integrated Flux.
Reflection coefficient ratios ($\lambda = 550$ nm) vs. integrated flux for quartz bombarded by 59-keV Kr^+ ions. (Hines and Arndt[18])

are attributed to direct lattice displacement and are shown to be consistent with the known changes produced in quartz and vitreous silica by fast neutron bombardment. Thermal spikes are shown to be unimportant for knock-on atoms in quartz and fused silica with energies near 45 keV.

Schroeder, Bashkin, and Nester[8] observed similar changes in index in their work with BK-7 glass. Hines[35] then used the altered layers of quartz to determine ranges of 7.5 to 52 keV H_2^+, D_2^+, He^+, and Ne^+ ions in quartz. Under certain assumptions his results agree well with theoretical predictions. Typical results are shown in Figs. 21 and 22.

Secondary Electron Emission

Secondary electron emission will accompany ion bombardment of insulators, but apparently the only definitive measurements have been made by Batanov[36] using Soviet glass No. 46, which when heated to 400°C becomes conducting and can thus prevent surface charging. Batanov determined the variation of γ, the secondary emission coefficient, for H^+ and Ar^+ ions at energies from 200 eV to 2.5 keV and for H_2^+ and He^+ ions at energies up to 30 keV. The results are shown in Figs. 23 and 24.

Gas Trapping and Release

Carter and Grant[31] have investigated the trapping of inert gas ions in Pyrex glass for incident ion energies up to 250 eV, but their results can be regarded only as qualitative. They refer to other work along this line. Thermal desorption from glass occurs

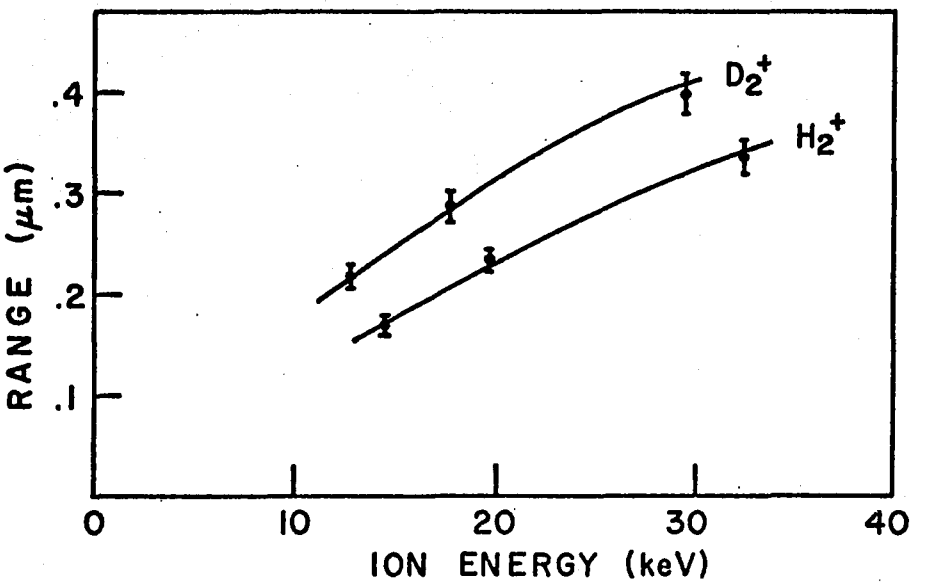

Fig. 21. H_2^+ and D_2^+ Range in Quartz.
Range in quartz of H_2^+ and D_2^+ ions as a function of ion energy. The molecular ions split into atomic particles as they enter the solid so that the range for atomic ions of a given energy will be equal to the range of molecular ions of twice the energy. (Hines[35])

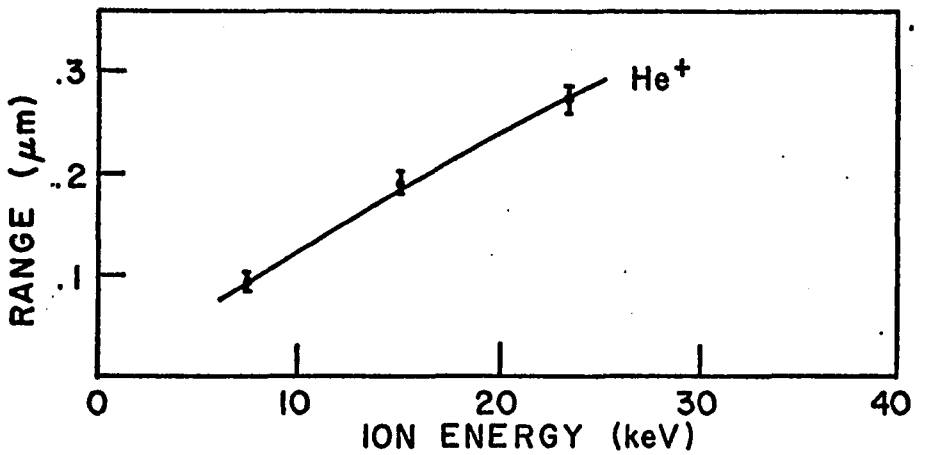

Fig. 22. He^+ Range in Quartz.
Range in quartz of He^+ ions as a function of ion energy. (Hines[35])

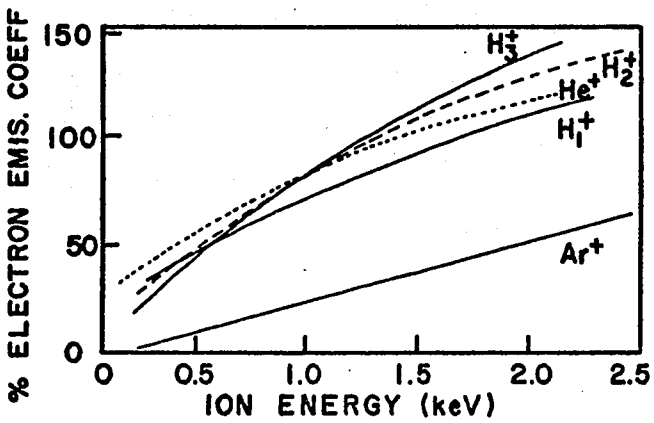

Fig. 23. Secondary Electron Emission, 0 - 2.5 keV.
Secondary electron emission coefficient for glass as a function of incident ion energy: Ar^+, H_1^+, H_2^+, H_3^+, and He^+. (Batanov[36])

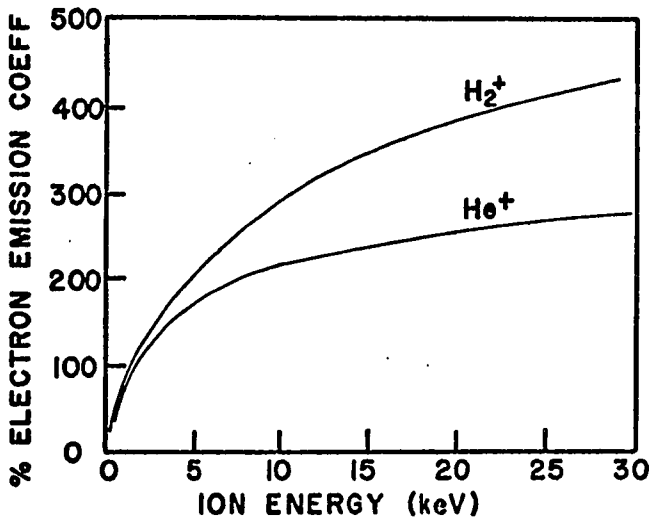

Fig. 24. Secondary Electron Emission, 0 - 30 keV.
Secondary electron emission coefficient for glass as a function of incident ion energy: H_2^+ and He^+.
(Batanov[36])

at room temperature and increases as temperature increases. Carter and Grant also mentioned studies on gas migration and release during ion bombardment. The release mechanism, thought to be other than normal target sputtering, has been called "gas sputtering."

Other Effects

Holland[37] has noted that, when a soda-glass target on a grounded cathode was bombarded by inert gas ions from a glow discharge, the glass surface in contact with the cathode became enriched with Na^+, probably due to positive charging of the bombarded surface and consequent migration of Na^+ ions away from the surface. Bills and Evett[38] have observed the decomposition of Pyrex and Nonex glass subject to ion bombardment, the glasses emitting Na and K atoms which in turn can condense on metal surfaces and produce insulating layers.

Summary and Conclusions Based upon Past Research

It is seen clearly that, in any experiment involving ion bombardment of insulators, great care must be taken in interpreting the results. To this writer's knowledge, only four papers have been published that try to present accurate erosion ratios for fused silica or glass. The data in two of these papers were obtained by bombardment in a gas discharge, which provides little control over the bombarding angle or ion energy; one of these experiments used the current-voltage characteristics of a Langmuir probe apparently without considering secondary emission. The other two papers presented the results of ion beam bombardment, and thus the experiments

were highly controlled. However, one work dealing only with Xe^+ ions and vitreous silica was limited to very small ion beam currents, 0.5 to 3 μA, and therefore sputtering quite small volumes of material, difficult to measure. The remaining ion beam experiment was done with Kr^+ ions at 60° on fused silica and an unspecified glass; this is the paper that equated the weight of a bombarded molecule to about 110 amu.

This review of past research does show that erosion ratios depend on temperature, ion mass and energy, angle of incidence, and nature of bombarded material. In addition there may be a dependence on pressure, for Yonts, Normand, and Harrison[39] have measured such a dependence in sputtering Cu with Ar^+ ions in the pressure range 4 to 8 x 10^{-5} Torr.

Quoting Gottfried Wehner in 1955[2]: "Sputtering of insulators should be a field of considerable interest, but the sketchy results to date do not seem reliable enough to be reported, and a definite need for systematic studies exists." Indeed, some studies have now been reported, and it is hoped that this paper will contribute to such systematic studies.

The early research at The University of Arizona was performed with Van de Graaff accelerators at energies from about 0.5 MeV to 1.8 MeV and with beam currents of usually well under 30 μA.

A thorough search of the literature concerning the ionic bombardment of glass led this writer to believe that more satisfactory results might be obtainable at considerably lower energies and higher beam currents. Fortunately these two aspects of the problem are not opposed to one another.

2

THE IONIC POLISHING SYSTEM

It was decided that a system should be constructed utilizing a duoplasmatron ion source. Duoplasmatrons are fairly recent developments in the field of ion sources, having H^+ current capabilities up to 0.5A.[40,41] Our experiments were to be carried out with disks of GE type 101 clear fused silica 1/16" thick by 1" diameter, and a duoplasmatron rated at H^+ current of 10 mA at 30 keV was deemed satisfactory. We will now describe the system which was designed and constructed by this writer for this research.

The Vacuum System

The ion bombardment of the fused silica targets occurred in a vacuum chamber. It is interesting to note that the chamber was a 6-inch Pyrex cross, i.e., a standard plumbing fitting of Pyrex glass. All types of standard fittings in sizes 6 inches and less are available along with rotatable flanges. The end bead of each glass fitting also has a groove that was readily adapted as an O-ring groove for vacuum sealing.

The cross was mounted in a vertical plane, thus providing a top and bottom arm in the vertical plane and two side arms in a horizontal plane. The ion source and lens were mounted on the top arm, providing an ion beam downward into the cross. The vacuum pumping system was connected to one side arm. This left the bottom and other side arm for instrumentation and target insertion. Only

the side arm was used, leaving the bottom with a blank flange. See Fig. 25.

Going from the cross toward the vacuum pumps, one first encountered a 6-inch-diameter flanged coupling, 7.5 inches long. The vacuum roughing line was welded to this coupling. The 2-inch roughing line proceeded to the mechanical pump by way of a bellows, water-cooled trap, and 2-inch air-operated solenoid valve. The trap restricted the migration of pump oil into the vacuum chamber. Also mounted on the flanged coupling were a thermocouple tube, an ionization vacuum gauge tube, and a vacuum-control tube containing a thermocouple and thermoswitch. Through its electronics, the vacuum controller was wired to shut off the diffusion pump and the duoplasmatron, should the vacuum pressure rise to any preset value in the range 10 to 150 μm. In addition, on the flanged coupling, there was mounted a valve and an 8 liter/sec Ion pump. The original intent was to use it as a holding pump to maintain a good vacuum in the cross overnight, leaving the diffusion pump off overnight. It proved more satisfactory to leave the diffusion pump on overnight pumping on the system. But the Ion pump was occasionally used to hold a vacuum in the chamber and in the duoplasmatron. The ions used were formed from research grade gas fed to the duoplasmatron through a controlled leak. On the flanged coupling was a 1/4" valve and copper tubing line which allowed a vacuum pumpdown on the input to the gas leak and also a complete pumpdown of the gas feed line, through the regulator and up to the gas cylinder.

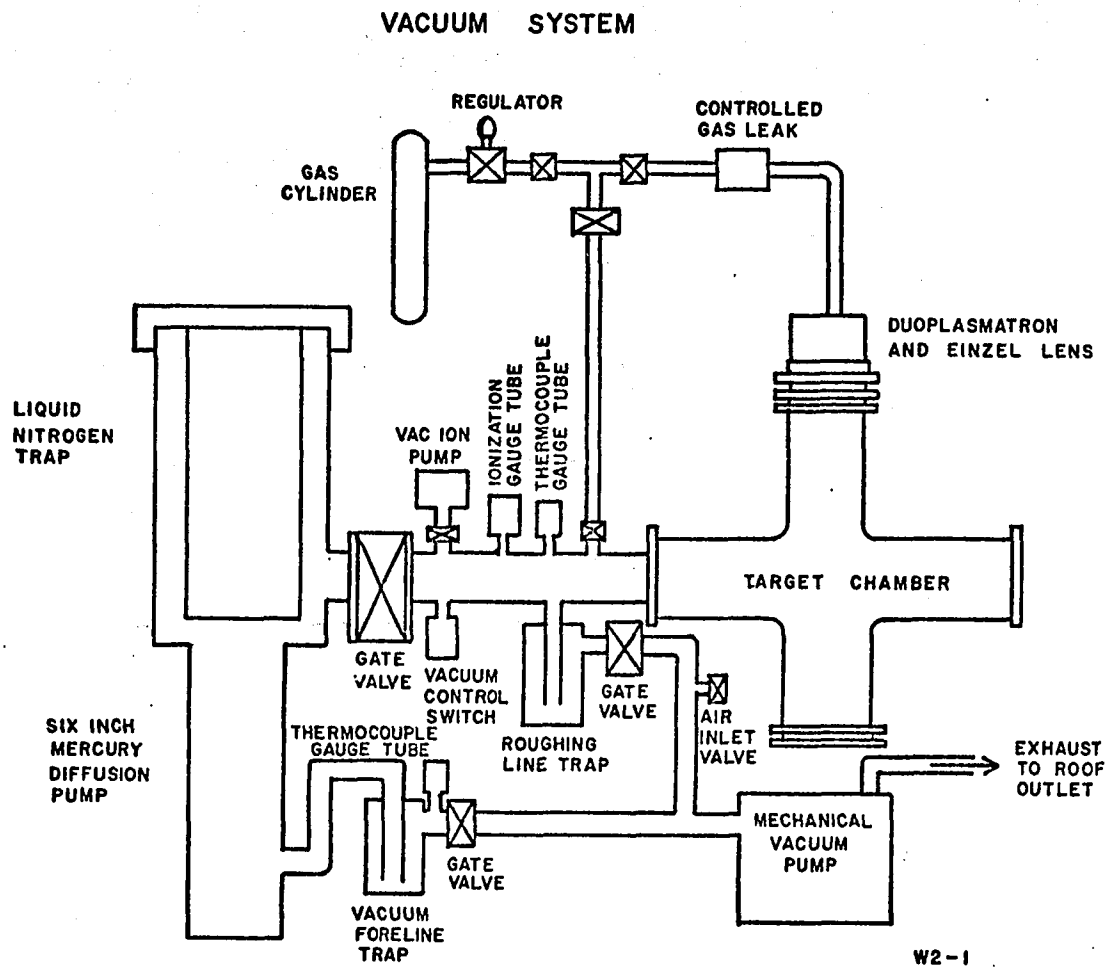

Fig. 25. Schematic Diagram of the Ionic Polishing Vacuum System.

The flanged coupling bolted onto a 4-inch hand-throttled gate valve that in turn was connected to a liquid nitrogen trap by means of an adaptive reducing coupling.

The liquid nitrogen trap was 26 inches deep, and the inner container, 8 inches in diameter. It had a capacity of about 20 liters, and when filled with liquid nitrogen had a holding time of over 24 hours when the system vacuum was 10^{-5} Torr or less. This trap mounted directly over the 6-inch mercury diffusion pump.

The 6-inch diffusion pump was baffled at its input to impede the movement of mercury vapor toward the vacuum chamber. This particular pump was chosen for two reasons. Hydrocarbon contamination had been a problem in previous experiments; with mercury as the pumping fluid we hoped to avoid that problem. The leak rate into the vacuum system of gas fed to the duoplasmatron was about 10^{-4} cc/sec at standard pressure and temperature. Calculation shows that this is about 10 1/sec at 10^{-5} Torr. The mercury pump was rated to have a pumping speed of about 460 1/sec at 10^{-5} Torr; thus, it had the gas-handling ability sought and in addition provided a reasonable pumpdown time. Pumping on the Pyrex cross, the duoplasmatron, and the instrumentation flange, the system pressure readily went to the 10^{-7} Torr scale in about 8 hours, the duoplasmatron filament requiring a few hours bakeout time. This was a satisfactory vacuum for duoplasmatron operation.

The fore line on the diffusion pump had a bellows, water-cooled trap, vacuum thermocouple tube, and a 2-inch hand throttle gate valve. The trap here served two purposes. It restricted the movement of mercury vapor into the mechanical pump, and it kept

mechanical pump oil out of the mercury pump. The mechanical pump had a pumping rate of 17.7 cfm.

An air line was run to the vacuum rack to supply air pressure for the roughing line valve and to supply over pressure for the transfer of liquid nitrogen.

This entire system was mounted in a framework of steel slotted angle 28 inches wide, 57 inches long, and 72 inches high. The mechanical pump rested on the floor, and steps were taken to keep vibration to a minimum.

The Cooling Systems

The diffusion pump required cooling with water to about 6°C. The duoplasmatron needed cooling to near room temperature with an insulating fluid. A water reservoir tank was built of stainless steel to supply water to a water Chiller by means of a standard well pump. It was this water that cooled the diffusion pump and the roughing line and fore line traps. The water then proceeded to a heat exchanger and cooled an insulating fluid being pumped through the exchanger and into the duoplasmatron and then into a reservoir. Freon 113 was the coolant originally recommended, and a Jabsco pump was supplied with this cooling system. Pumping Freon 113 we found the Jabsco pump to have far too much capacity, building up enough fore pressure to stop the driving motor. The impeller squeezing cam was replaced by a thinner one, but pressure still built up, and the noise was just bearable. It is this writer's understanding that Freon 113 is one of the most difficult substances

Fig. 26. Ion Beam System.
Lower left is six inch mercury diffusion pump with liquid nitrogen trap above and vacuum gauge controls on top. Center is vacuum manifold with gate valve and gauges leading to six inch Pyrex cross, the vacuum chamber containing targets. On the top arm of the Pyrex cross is a gate valve, einzel lens, and duoplasmatron. Mechanical pump is below cross. Control console on extreme right.

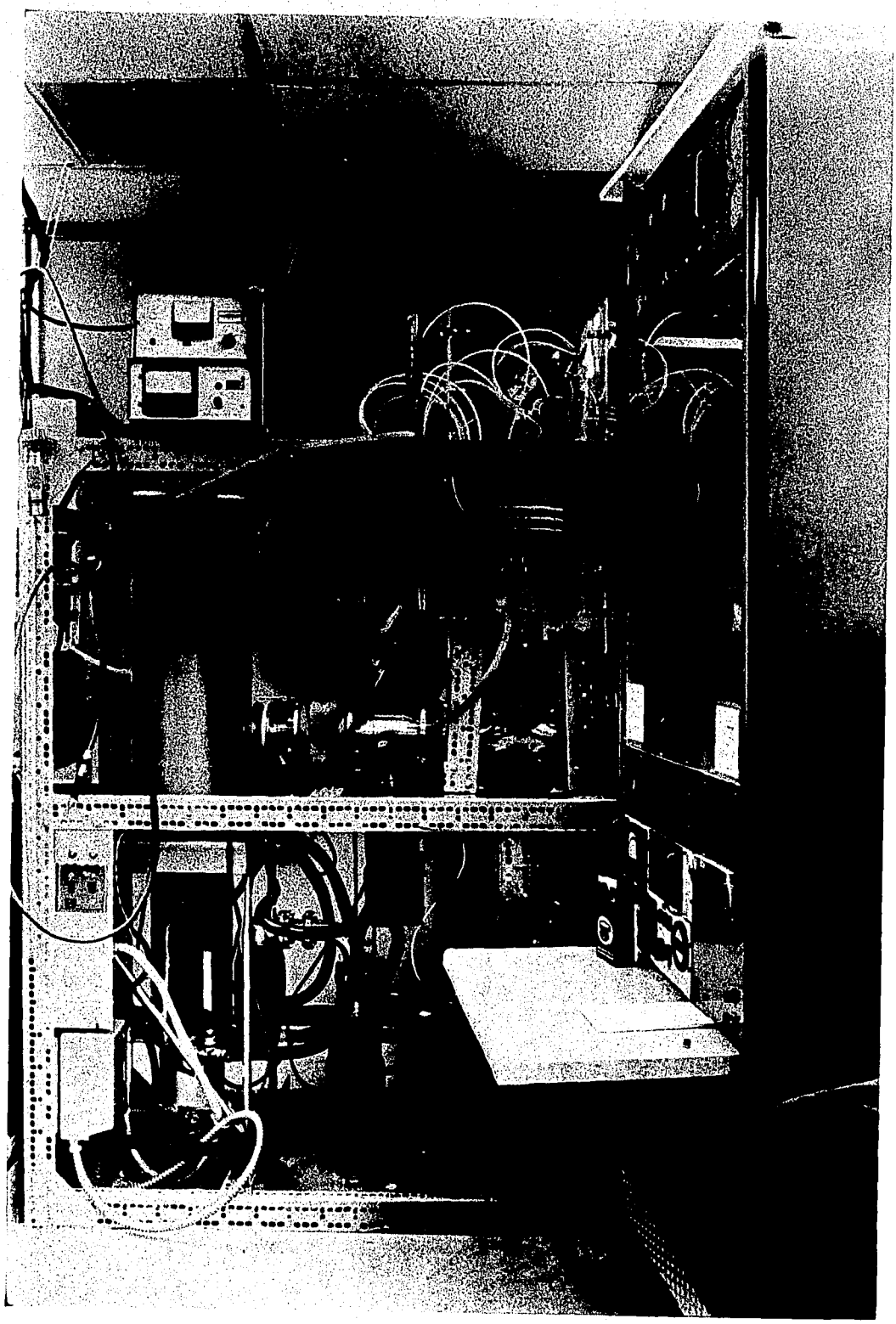

Fig. 26. Ion Beam System.

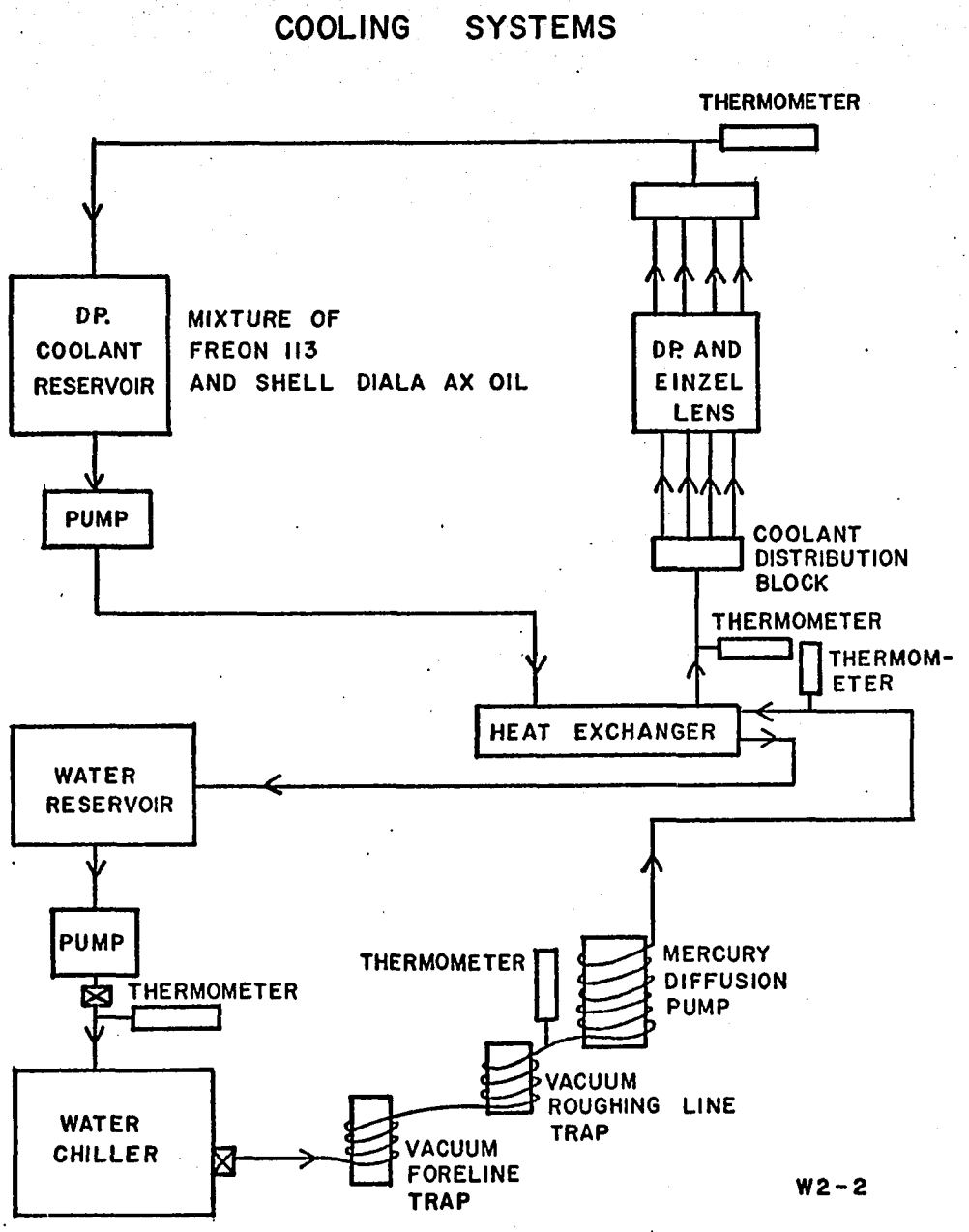

Fig. 27. Schematic Diagram of the Ionic Polishing Cooling Systems.

to pump. Ultimately we changed the pump to a Little Giant and the pump fluid to a 50-50 mixture of Freon 113 and Shell DIALA AX transformer oil. This proved satisfactory. We have been informed that a Dynapump such as that supplied with the ORTEC cooling system will satisfactorily pump Freon 113. The appropriate cooling lines were monitored by red alcohol thermometers.

All cooling lines and most cold surfaces were covered with a foam neoprene refrigeration insulating material. This covering also helped control water condensation from the air.

The cooling pumps, reservoirs, and chiller were mounted in a separate 4-level framework, 21 inches wide x 36 inches long x 60 inches high.

The Ion Source and Lens

The ion source and control element for this research was a Texas Nuclear Model 9406 duoplasmatron and associated Gap and Einzel lens (electrostatic), see Figs. 28 and 29. The duoplasmatron received research grade gases by way of a single - stage regulator and an Andonian Adjustable Leak. The output pressure on the regulator was adjustable from 0 to 60 psi, and it supplied gas to the controlled leak. The leak could supply gas at rates of about 10^{-4} to 10^{-2} cc/sec. The leak rate depended on how much twist was put onto a fine metal tube inside the leak, and a micrometer dial and lever arrangement supplied the twisting torque; this was a fine adjustment. A coarse adjustment could be made by twisting, through a degree or two, the 1/4-inch tube on the input side of the leak.

Fig. 28. Duoplasmatron Schematic Diagram.

KEY:
1. Duoplasmatron housing
2. Arc chamber
3. Solenoid chamber base
4. Solenoid support flange
5. Intermediate electrode
6. Filament support flange
7. Upper anode ring
8. Anode
9. Anode insert retainer
10. Anode insert
11. Bypass valve
12. Filament terminal
13. Filament terminal
14. Solenoid
15. Solenoid
16. Solenoid support washer
17. Filament
18. Insulator
19. Solenoid support

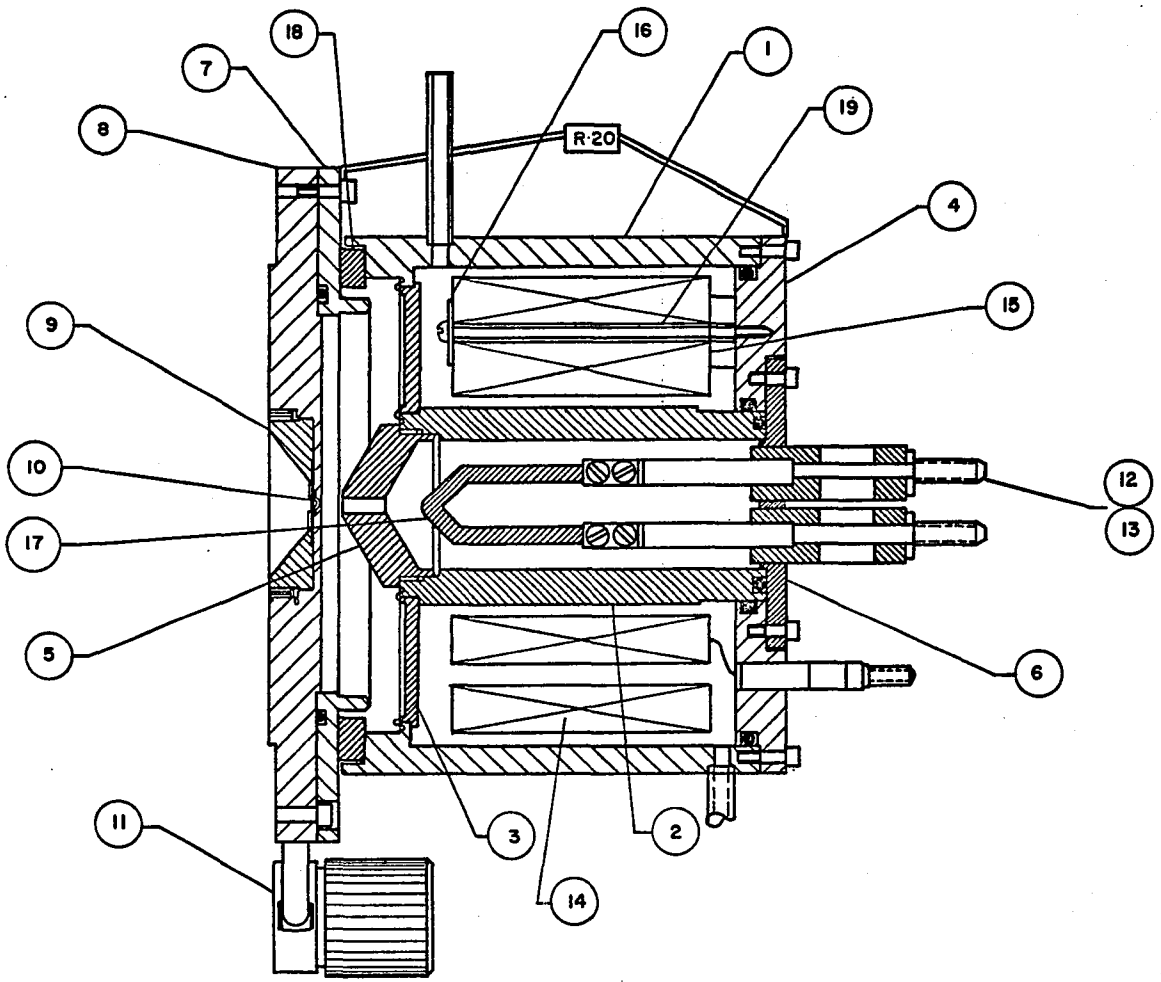

Fig. 28. Duoplasmatron Schematic Diagram.

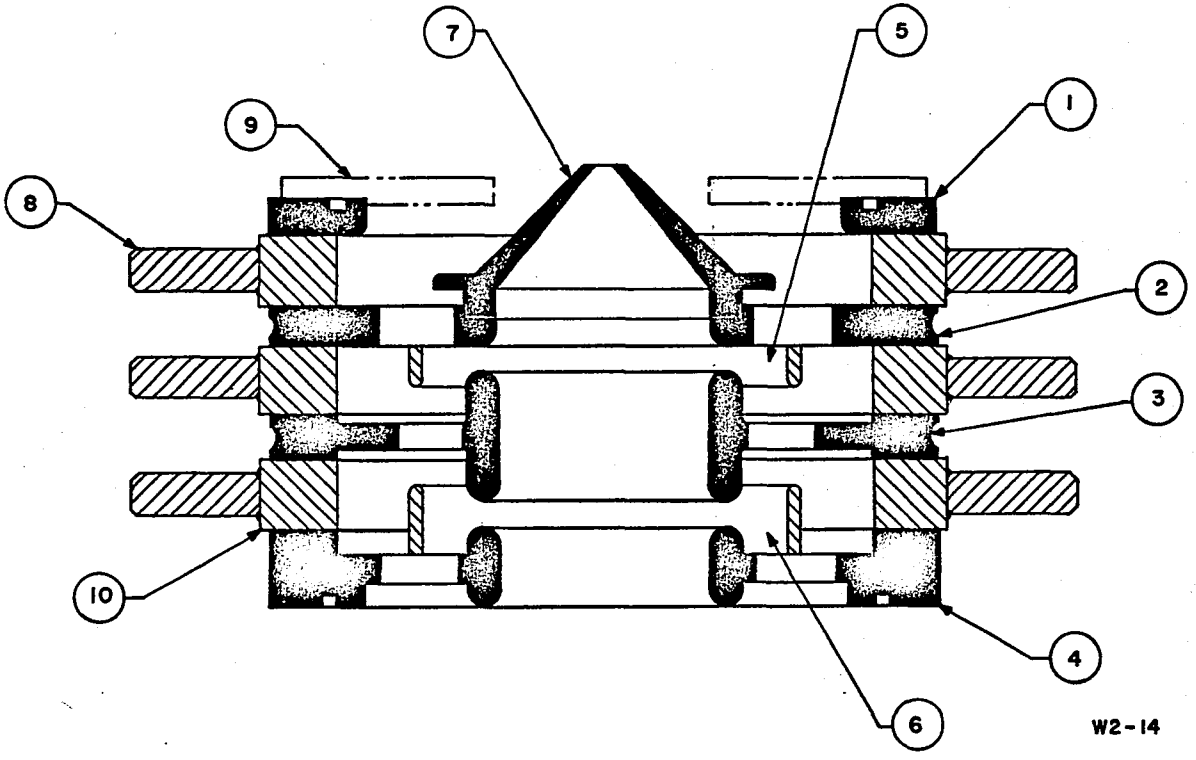

Fig. 29. Einzel Lens Schematic Diagram.

KEY:
1. Mating flange
2. Front electrode
3. Center electrode
4. Rear electrode
5. Guard Ring
6. Guard Ring
7. Extractor
8. Zap ring
9. Assembly ring
10. Insulator

Two set screws had to be first released while holding the tube in position. The input gas pressure also affected the leak rate.

In the duoplasmatron itself, see Fig. 28, there was an axial electron beam, originating at the filament cathode and accelerated through an intermediate electrode toward the anode plate. The intermediate electrode, constructed of magnetic material, provided electrostatic and magnetic focusing from which the source derived its name. It was biased at a voltage between the cathode and the anode and thus produced some electrostatic focusing of the electron beam. A solenoid developed a magnetic field between the intermediate electrode and the anode plate, thus magnetically focusing the electron beam. The magnetic field return path was through the anode plate, then through the small air gap near the intermediate electrode insulator.

If a gas was admitted into the ion source, atoms that enter the electron beam region are ionized. The resulting plasma flowed out of a small hole in the anode plate due to the pressure differential. The pressure inside the ion source was normally about 150 μm (1.5×10^{-5} Torr), and outside the ion source the pressure had to be in the 10^{-5} or 10^{-6} Torr region.

The aperture was in the center of the anode plate, and below it there was formed a plasma from which positive ions could be extracted. The duoplasmatron, therefore, was not an ion source unless an extraction electrode was placed below the source and the proper potential difference was developed between the extraction electrode

and the source. If the source was positive with respect to the extraction electrode, a positive ion beam would be extracted.

The duoplasmatron ion source was constructed entirely of metal and ceramic material. The anode, intermediate electrode, and housing were all steel. The vacuum-sealing plate between the magnet solenoid and the vacuum system was nonmagnetic stainless steel. The filament insulators and intermediate electrode insulators were ceramic. Copper was used to support the filament or cathode.

Electronics for the Ion Source and Lens

When operating, the duoplasmatron electrically floated at the ion extraction potential. It was therefore necessary that the electronics supplying power to the duoplasmatron also float at the extraction potential. In this manner we were able to set target assembly and extractor electrode (the gap lens) at ground potential. Alternatively we could have set the duoplasmatron and its electronics at ground potential and maintained target and extractor at a large negative potential, but the former method was more convenient.

The enclosure for all the duoplasmatron electronics was a cabinet, 30" wide x 30" deep x 85" high. Within this enclosure, supported on 4" diameter x 4" high polyethylene feet,was a 19" rack which supported the electronics which electrically floated at the extraction potential: Einzel lens supply; duoplasmatron arc, magnet, and filament supplies. This 19" rack was surrounded by approximately 4" of air and 1/8" polyethylene. A 3KVA isolation transformer by Del Electronics fed power to this isolated rack. Between primary

and secondary of this transformer was 50DCKV insulation so that the floating system was isolated from line voltage.

The Einzel lens supply was a Fluke Model 410B, 0-10,000 volts, 10 mA supply. The Einzel lens drew essentially no current so a 2 Meg, 50 watt bleeder resistor was installed at the output of this supply.

The filament supply, see Fig. 30, was a 5 volt, 30 Amp transformer powered by a variable transformer and current metered. The operating current was 25 Amp; the filament was platinum mesh coated with barium carbonate which after baking in the vacuum of the duoplasmatron was converted to barium oxide.

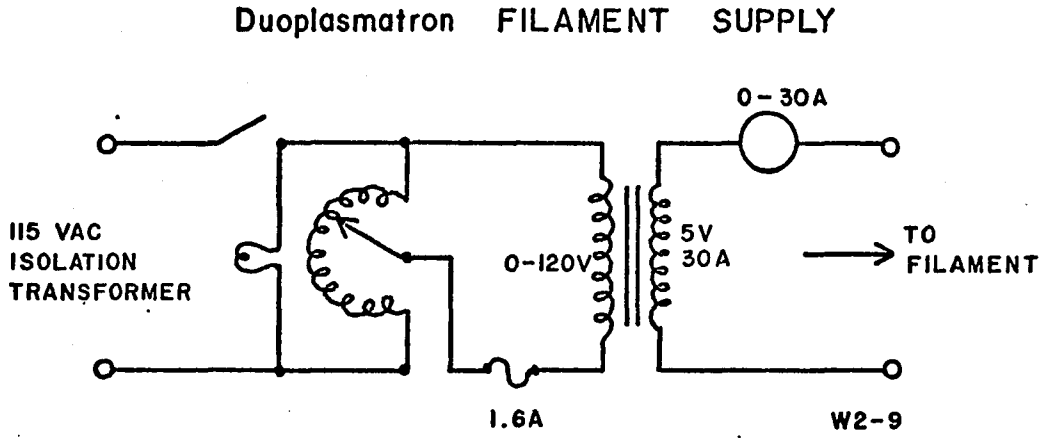

Fig. 30. Power Supply for Duoplasmatron Filament.

The magnet supply, see Fig. 31, utilized a full wave bridge rectifier and RC filter to supply up to 3 amp at about 100 vdc to the 36-ohm coil, the solenoid magnet of the duoplasmatron. It was current metered.

The arc supply, see Fig. 31, was adapted from plans supplied by Texas Nuclear. It utilized a full wave bridge rectifier, L section filter, and shunt regulator with Zener diode. We also added a 400-watt tungsten lamp as a ballast resistance. The output of this supply was current and voltage metered. The voltmeter, we found, served as an excellent indicator of relative gas pressure within the arc; it was sensitive to changes in pressure and had a quite immediate response to these changes. The voltmeter therefore became the indicator of the gas leak rate.

On the duoplasmatron was connected a 1K, 100-watt resistor between the anode plate and the intermediate electrode which somewhat balanced the arc voltage between intermediate electrode and anode, and intermediate electrode and filament. These four power supplies were referenced to the floating ground which was the extraction potential, obtained from a Sorenson Model 1030-20 H.V. supply and Sorenson L2 high voltage filter. The high voltage supply operated off a Sorenson C2 line regulator. See Figs. 32 and 33.

In the initial operation of the duoplasmatron we were troubled by numerous sparking and current bursts within the ion source due to metal cleaning up and apparently due to some vacuum leaks. Our initial arc and magnet supplies were highly regulated by somewhat delicate transistorized sensing and regulating circuits. When running, the arc and magnet consume about 300 watts, and fluctuation in this power quickly and repeatedly blew transisters and fuses in the original power supplies. We changed to the more brute force equipment described above, adding the 400-watt ballast to the

arc and also adding across the power input to the magnet a series of diodes to protect the magnet supply from transients or power failures.

These same transients took their toll on the extraction power supply and on the Einzel supply, and transient suppressors were added: RC combinations with the capacitors connected between the outputs and the appropriate ground.

These steps and better vacuum sealing seem to have eliminated the original problem. The duoplasmatron steadily supplied an ion beam without short-duration large transients.

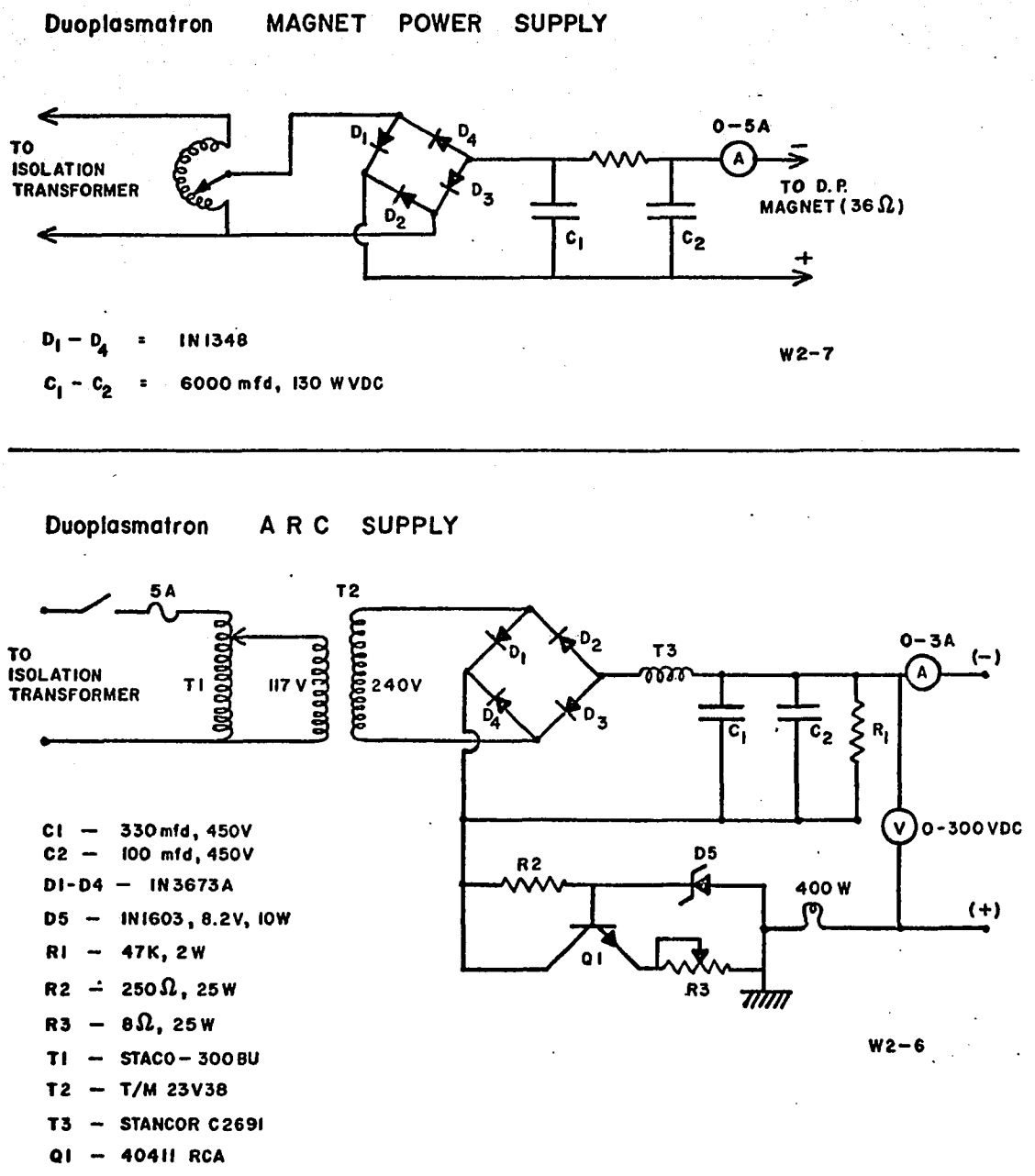

Fig. 31. Power Supplies for Duoplasmatron Magnet (Top) and Arc (Bottom).

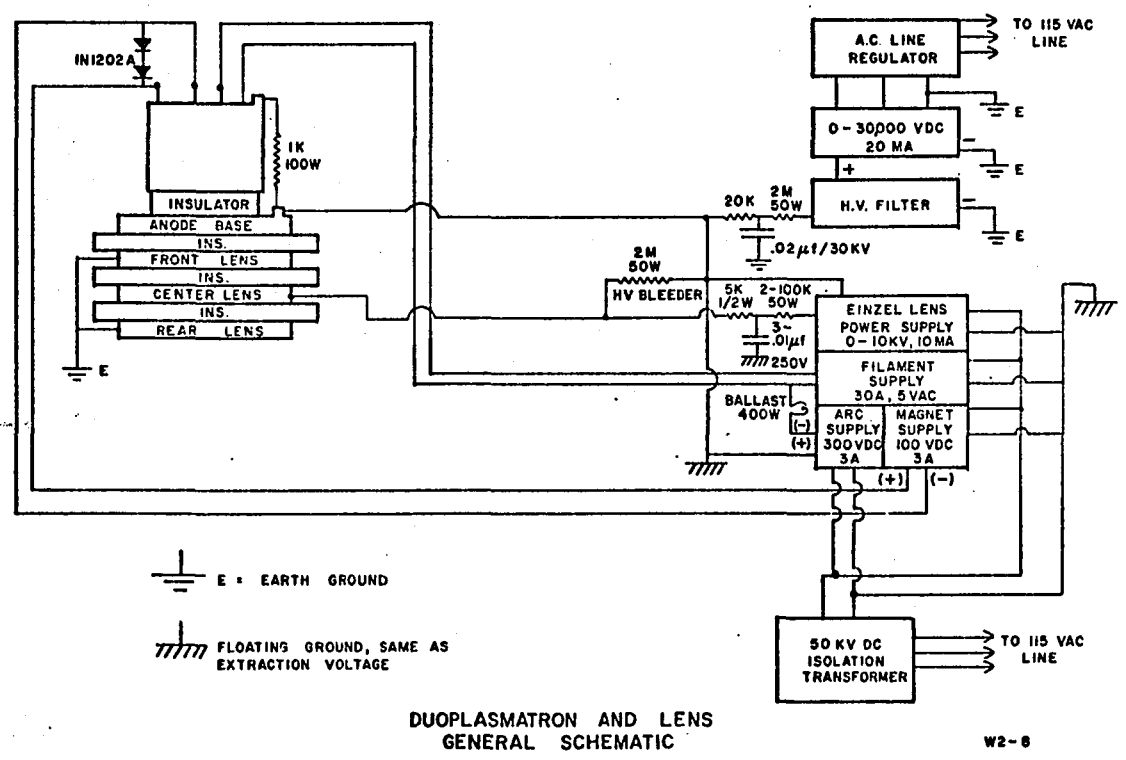

Fig. 32. Electrical Diagram, the Duoplasmatron and Einzel Lens.

Fig. 33. Ion Beam System.
Extreme left is cooling rack for diffusion pump and duoplasmatron. Extreme top of electronics cabinet is 0-30 Kv ion acceleration power supply. Immediately below is isolated compartment containing einzel lens supply, and supplies for duoplasmatron filament, arc, and magnet; these float electrically at the acceleration voltage. Below the compartment are controls for vacuum valve, neutralization filaments, ion beam monitor, and beam shutters. In the base of the cabinet is line regulator and isolation transformer.

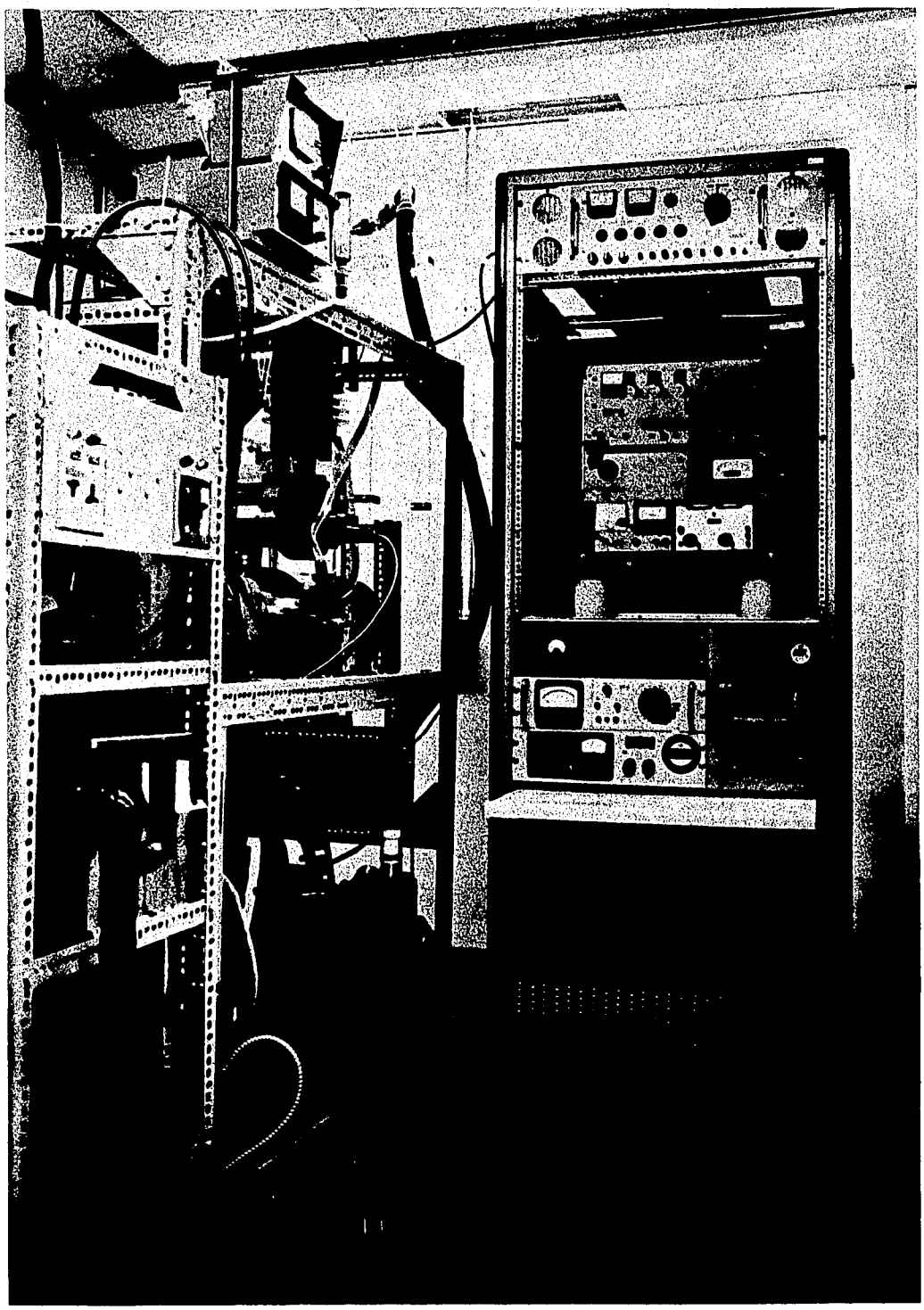

Fig. 33. Ion Beam System.

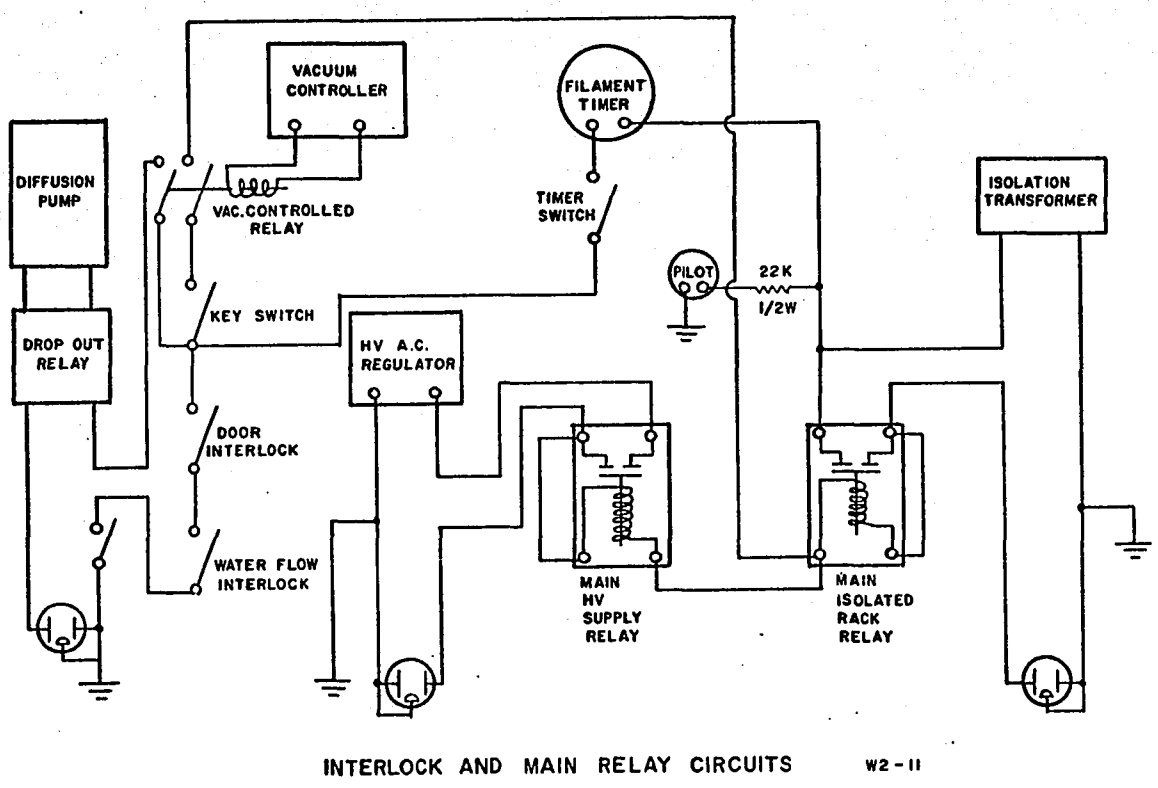

Fig. 34. Electrical Diagram, Vacuum System and Duoplasmatron Relays and Interlocks.

The Target Chamber and Monitoring System

The target assembly was installed in one horizontal arm of the Pyrex cross vacuum chamber. It mounted on a 10-inch-diameter stainless steel flange which vacuum sealed to the cross. The targets were mounted on a two-layer turntable which held a total of twelve targets. See Fig. 35. A stainless steel bellows and rotary feedthrough allowed lateral and rotary motion of the turntable. Any target could be brought into the ion beam path and each target was individually adjustable in angle of incidence to the ion beam. Angles used varied from 0° to 45° with this system. We found that

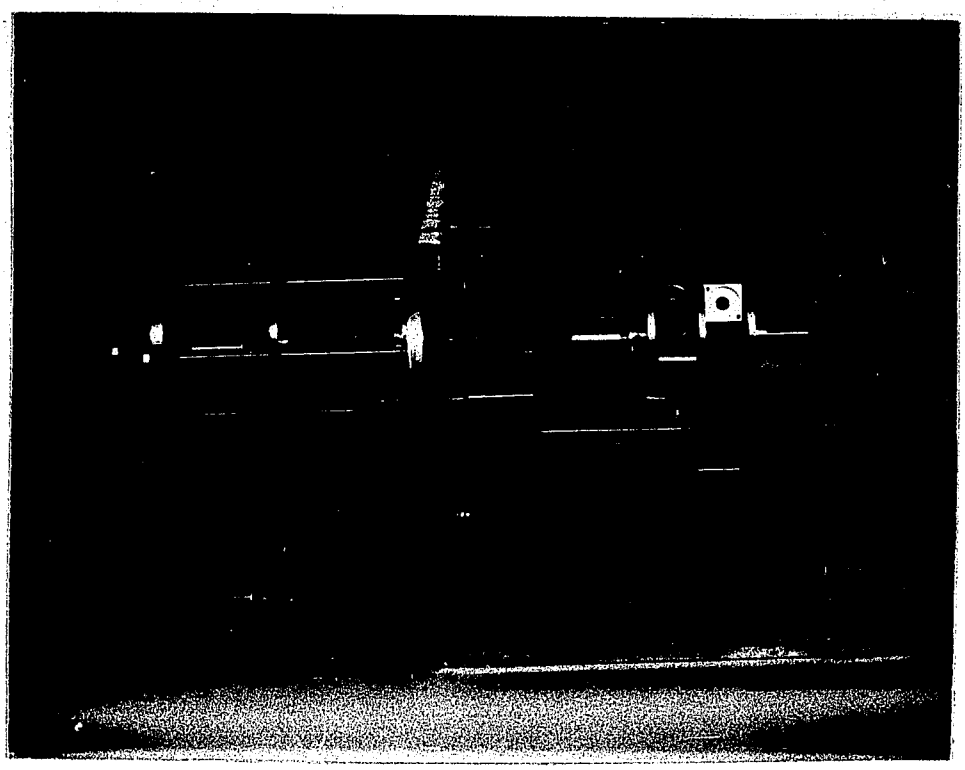

Fig. 35. Target Assembly Flange.

Target assembly flange showing bellows, sealed rotary and lateral motion feedthrough; double-decker target turntable; and frames supporting the Faraday cup, shutter, and shield plate. The flange is supported by a fixture.

for angles larger than 45° the targets did not present a large enough cross section to the beam. About 1.5 cm from the bombardment position was mounted a tungsten filament approximately 3 mm wide by 10 cm long which supplied electrons to neutralize any positive charge which might tend to accumulate on the target surfaces. See Fig. 36. The filament was operated at near 1450°C as determined with an optical pyrometer. We measured the emission current by biasing nearby metal parts 75 V positive with respect to the filament, obtaining a maximum current of 680 μA, assumed to be more than adequate for all our bombardment runs. See Fig. 37.

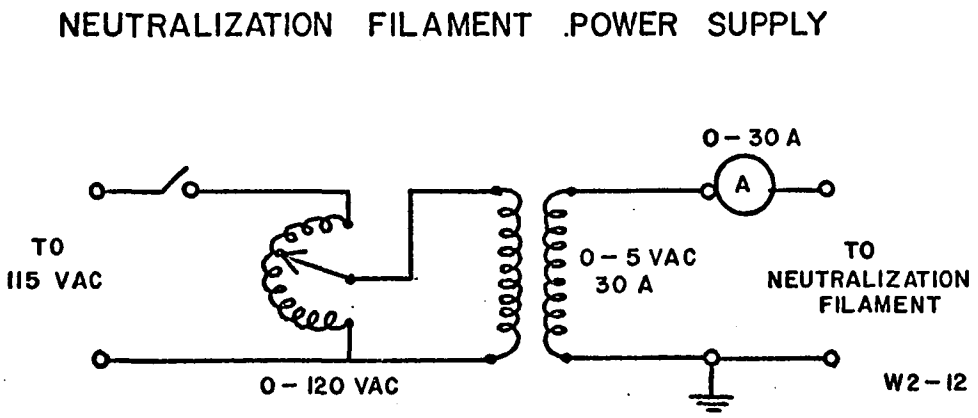

Fig. 36. Power Supply for the Neutralization Filament.

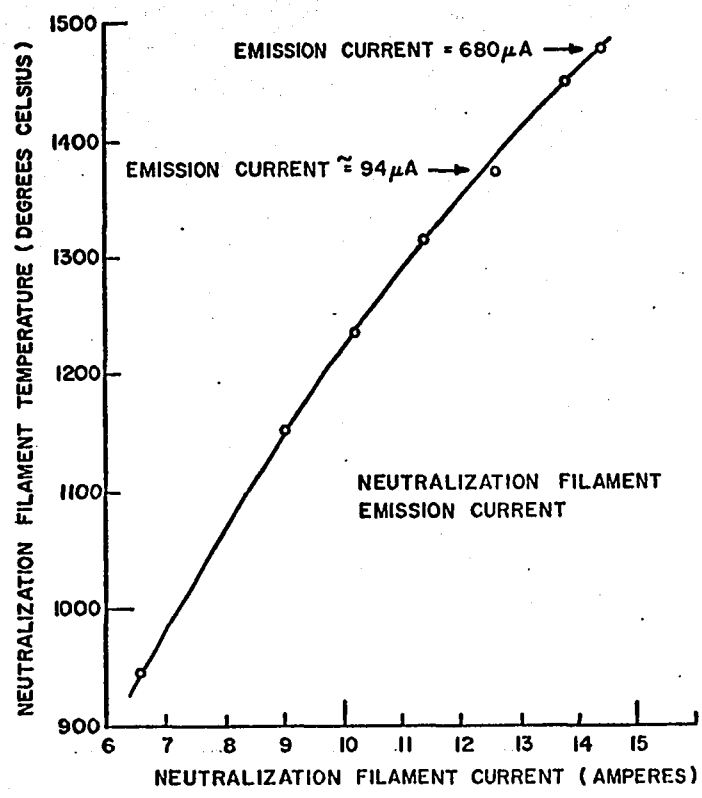

Fig. 37. Temperature and Electron Emission Characteristics of the Neutralization Filament.

Above the turntable was a frame assembly which held a solenoid actuated Faraday cup and shutter, a shield plate, and bias plate. The ion beam was directed down through apertures in the shield plate and bias plate and through a hole in the frame, thence to the target. The Faraday cup slid on the frame under the bias plate. To read beam current, the cup solenoid was actuated, swinging the cup concentrically under the hole in the bias plate into the beam path. The bias plate was negative with respect to the cup to suppress the emission of secondary electrons from the cup. Typical bias curves are shown in Fig. 38.

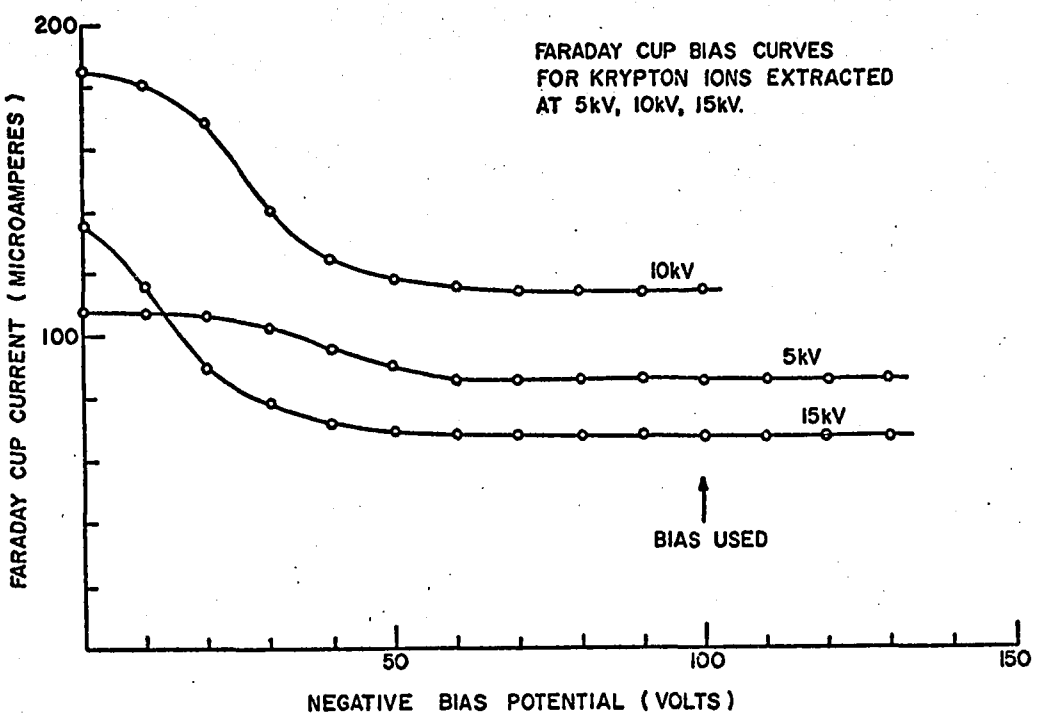

Fig. 38. Typical Faraday Cup Bias Curves.

For the Faraday cup and bias circuit, see Fig. 39. Fig. 40 shows the solenoid circuit, which included a clock that ran only when both shutter and cup were out of the beam. This clock monitored the exposure time of the target to the beam. The shield plate was electrically insulated from the bias plate by glass spacers and was grounded. It protects the frame assembly, wires, and solenoids from stray particles outside the main beam.

The inside diameter of the Pyrex cross was 6 inches; therefore the target assembly and feedthroughs were confined on the mounting flange to within the area of a 6-inch-diameter circle.

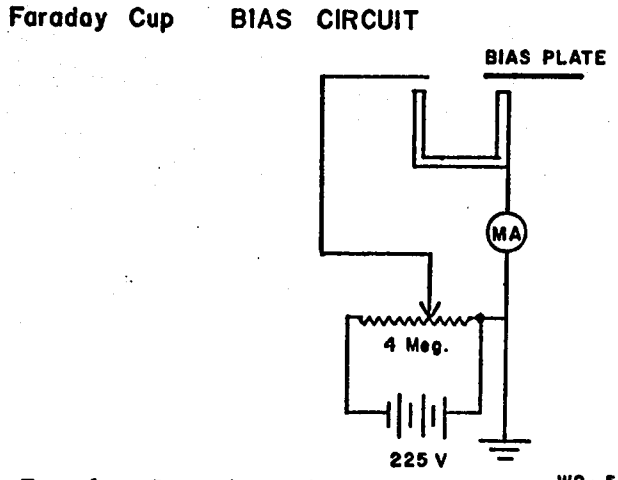

Fig. 39. Faraday Cup Bias Circuit.

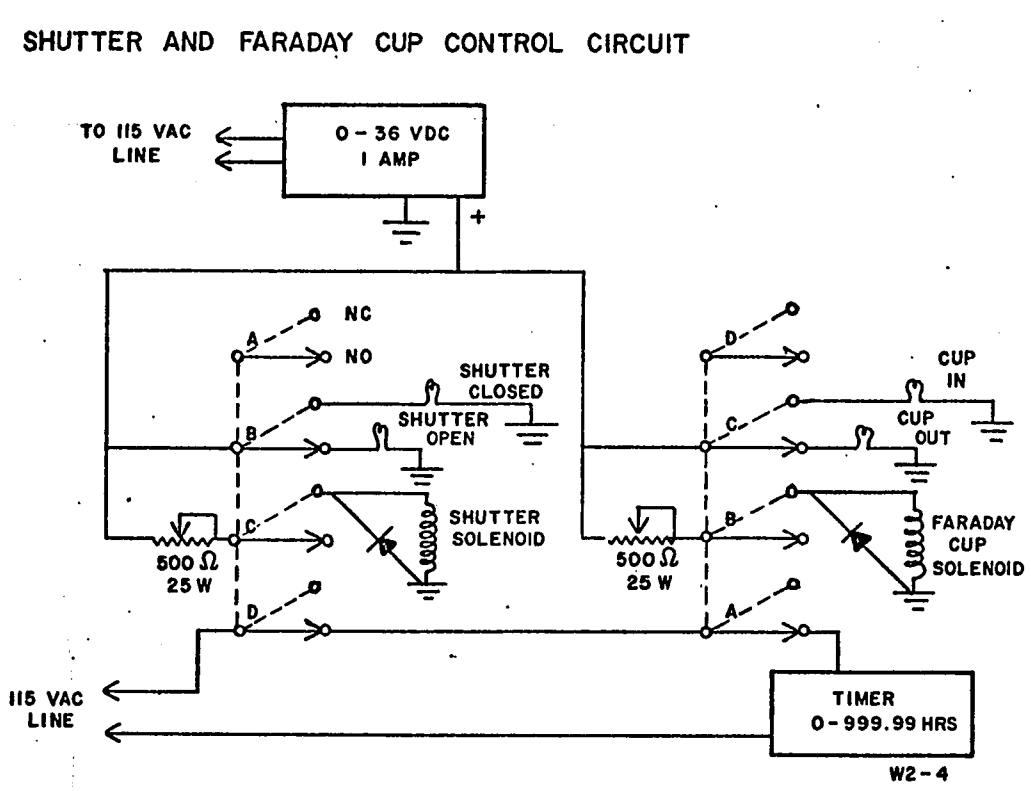

Fig. 40. Shutter and Faraday Cup Control Circuit.

3

EXPERIMENTAL PROCEDURES

Once the system was constructed the actual bombardment runs could be made. First the target holders had to be aligned so that the angle of bombardment would be known, after which the targets themselves had to be numbered, cleaned, weighed, and otherwise made ready. After the targets were inserted in their holders and the system pumped down, the actual beam production, bombardment, and beam current monitoring were carried out. Initially some vacuum problems developed which were solved. We also investigated, experimentally, the temperature increase of the targets due to bombardment.

Target Alignment and Preparation

Our first problem in alignment was to determine the path of the ion beam at the target turntable. The turntable was removed and in its place a copper foil installed. The shield plate had not been used so that when the beam was turned on and left divergent it cleaned an area on the shield plate and, after passing concentrically through the aperture, it cleaned a circular pattern on the copper foil also. The centers of these two cleaned areas were taken as the ion beam axis.

Fiducial marks were made on the vacuum cross and on the target assembly flange so that it could be replaced on the cross in the same position, a position which, as measured by a machinist's

level, made the frame assembly parallel to the anode plate of the duoplasmatron, i.e., making the ion beam perpendicular to the frame assembly. The flange and target assembly was removed and placed on an analog fixture. The centers of the two cleaned areas were marked and a laser beam lined up on both. Two auxiliary pinholes were aligned with the laser beam. These auxiliary pinhole apertures were then firmly fastened to the fixture and with the laser beam they formed an optical light beam analog to the ion beam. See Fig. 41.

The targets were General Electric Type 101 clear fused silica discs, ground and polished, one inch diameter, 1/16 inch thick. To prepare the targets they were first scribed with an identifying number and then cleaned: the surfaces were washed and scrubbed by hand and in a sonic cleaner in an Alconox solution, then rinsed three times in distilled water in the sonic cleaner, after which they stood on edge for about 5 minutes in nitric acid or warm chromic acid; they were then removed and rinsed with running distilled water and rinsed three times in distilled water in the sonic cleaner, dried rapidly with a heat gun and after cooling placed individually in numbered closed plastic containers. Throughout this cleaning procedure and henceforth the targets were handled only with clean stainless steel tongs.

The targets were then weighed with a Mettler balance which read to micrograms. Each target was weighed at least 5 times and a zero reading taken for each weighing. Intuitively we considered these readings to be accurate within ± 10 micrograms, but a computer

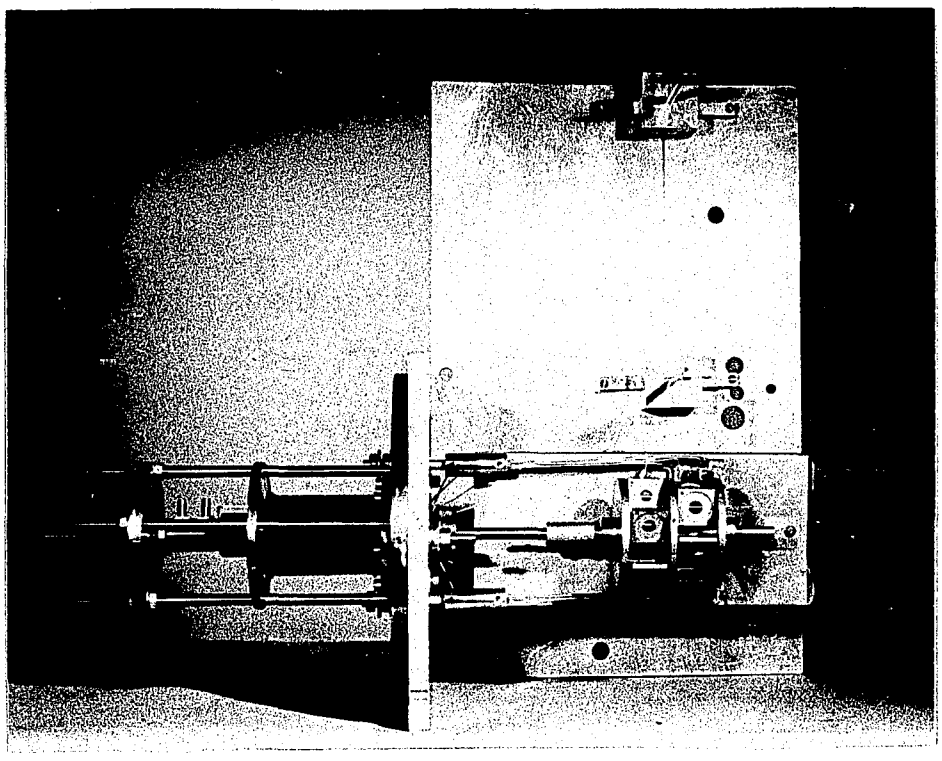

Fig. 41. Target Assembly Flange on Analog Fixture.

Target assembly flange on analog fixture, showing laser beam pinholes aligned in ion beam direction.

program was used to calculate the standard deviation and probable error in these weighings. Errors in general will be discussed later.

The targets were placed in their individual holders on the target turntable. A clean microscope slide cover glass was placed under each target to shield the target back surface from material sputtered from the adjacent target. Each target holder was individually adjustable in angle; the turntable was rotated centering a target at the aperture, then the target holder was adjusted until the laser beam was incident at the correct angle as determined by the total angle between incident and reflected laser beams. Three target holders were set for each of four angles of incidence, 0^{o}, 15^{o}, 30^{o}, and 45^{o}, and firmly fastened in that position. The turntable rotation is controllable from the air side of the target assembly flange, and fiducial marks for each of the 12 target positions were scribed on the air side adjacent to an indicating pointer that rotated with the turntable. Thus from the air side of the flange any of the 12 targets could be brought into the ion beam path. See Fig. 42. As determined by the reflected laser beam, the targets were resettable for angle of incidence to the beam to better than $\pm\frac{1}{2}^{o}$, but because two sets of fiducials were used to align a target and because fiducials were used in the original alignment analog, we estimated that the angle error may have been as large as $\pm 2^{o}$. After bombardment the targets were removed and reweighed and the eroded mass was calculated. The surfaces of selected targets were analyzed for smoothness; this is discussed later.

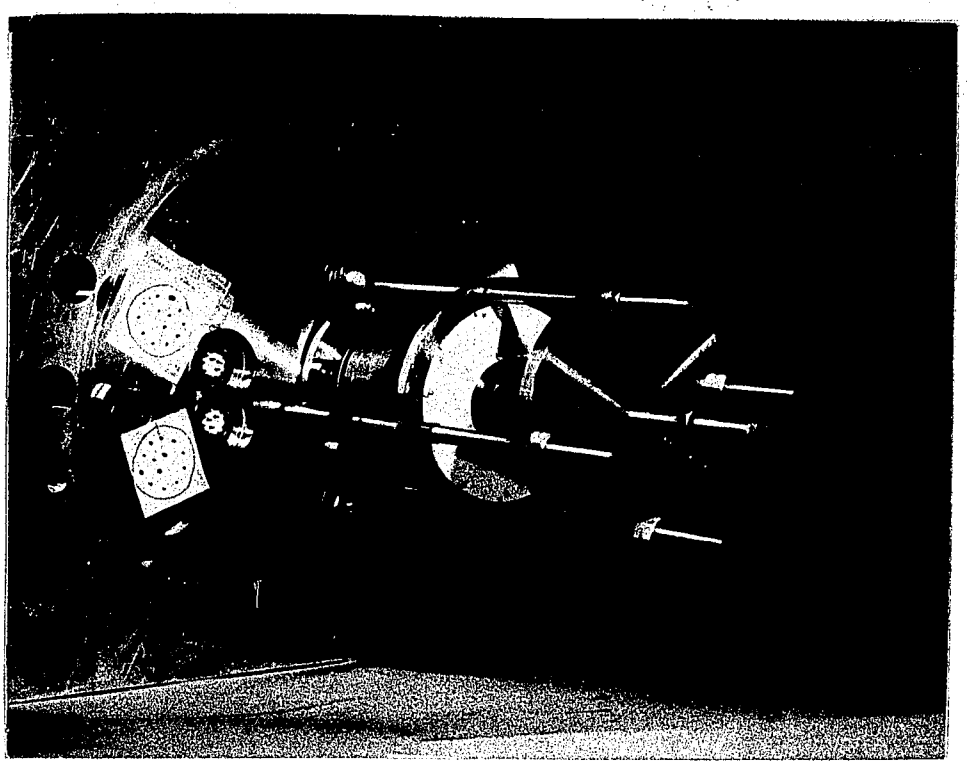

Fig. 42. Target Assembly Flange, Air Side.

Target assembly flange, air side, showing electrical pins for connection to: shutter and cup solenoids, cup and its bias circuit, and shield plate. Large bolt type feedthroughs for neutralization filament current, and fiducials for turntable position are also shown.

Ion Beam Production and Monitoring

When the targets were in place in the vacuum system, the gas for ion production was selected and installed in the gas feed system. The gas line was evacuated including the gas leak and regulator; it was evacuated up to the cylinder, pumped down to about 5×10^{-6} Torr, after which the cylinder was opened and the input pressure to the gas leak set at about 8 psi over one atmosphere. The duoplasmatron filament, having previously been baked, was brought up to temperature, which required 25 A, and allowed to outgas. After the filament was well outgassed, the gas leak was opened and an arc struck, magnet current was supplied, and the extraction and Einzel lens voltages turned on, the Faraday cup having first been placed in the ion beam path. Extraction voltage was set, the arc and magnet then adjusted, usually for maximum beam current. See Fig. 43. The target was exposed and the final adjustment on the Einzel lens was made by observing the fluorescent pattern on the target. The neutralization filament was then brought up to temperature. See Fig. 44. Time and beam current were monitored approximately every 0.1 hour for the duration of the bombardment run, using the properly biased Faraday cup. The beam current meter was calibrated against a ½% Weston microammeter.

The beam current drifted, generally slowly, during a run, and we approximated the drift as linear so that beam current versus time in our approximation would appear as in Fig. 45. The bombardment dose is represented by the area under these curves. A computer program was written to calculate these areas. See Appendix I. We looked at the problem as the summing of small trapezoidal areas.

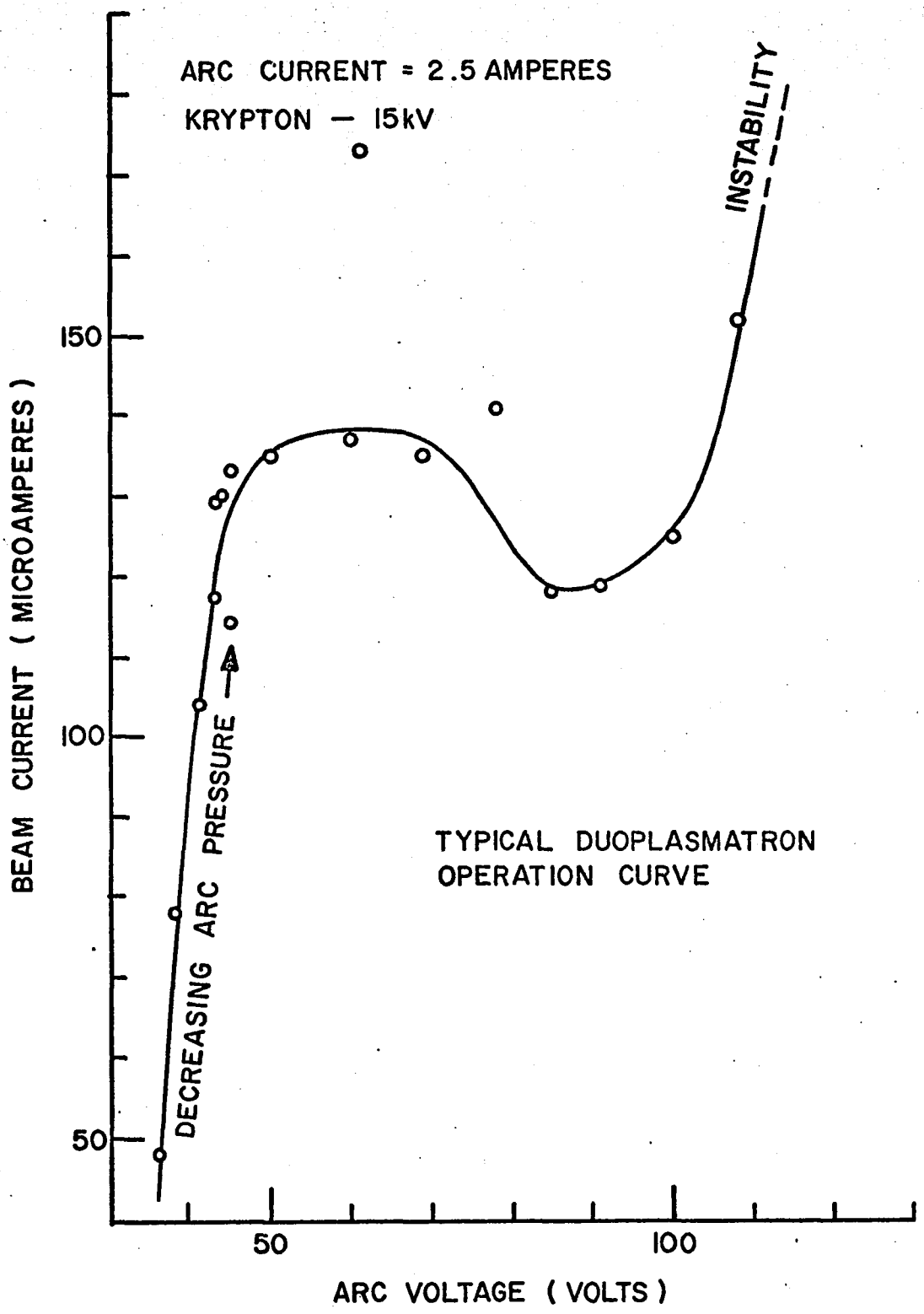

Fig. 43. Typical Duoplasmatron Operation Curve.

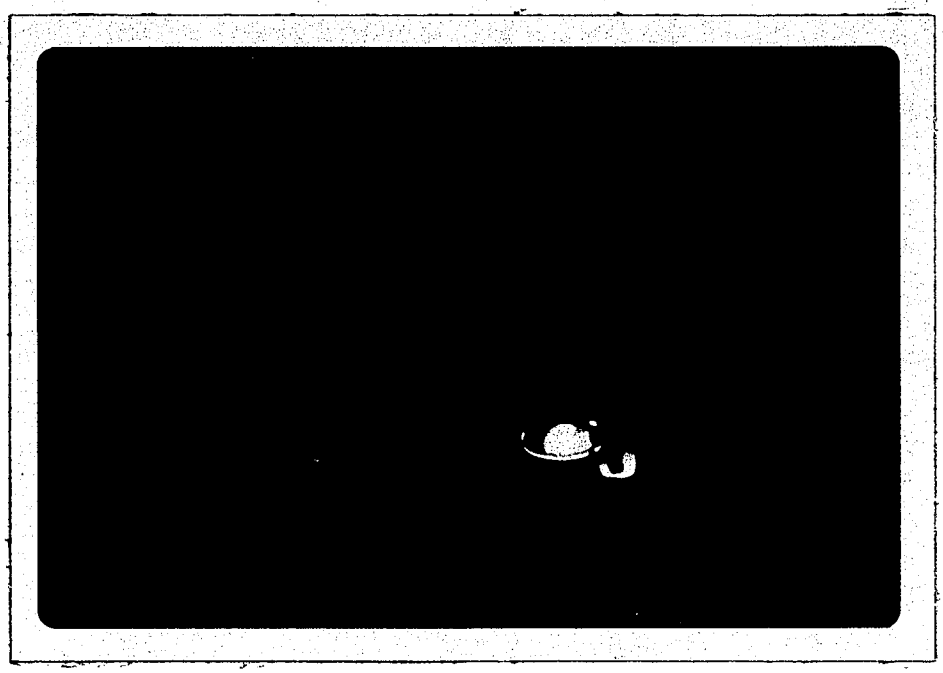

Fig. 44. Target Under Ion Bombardment.

Target under ion beam bombardment, showing fluorescence and glowing neutralization filament. Filament temperature has been lowered for this picture.

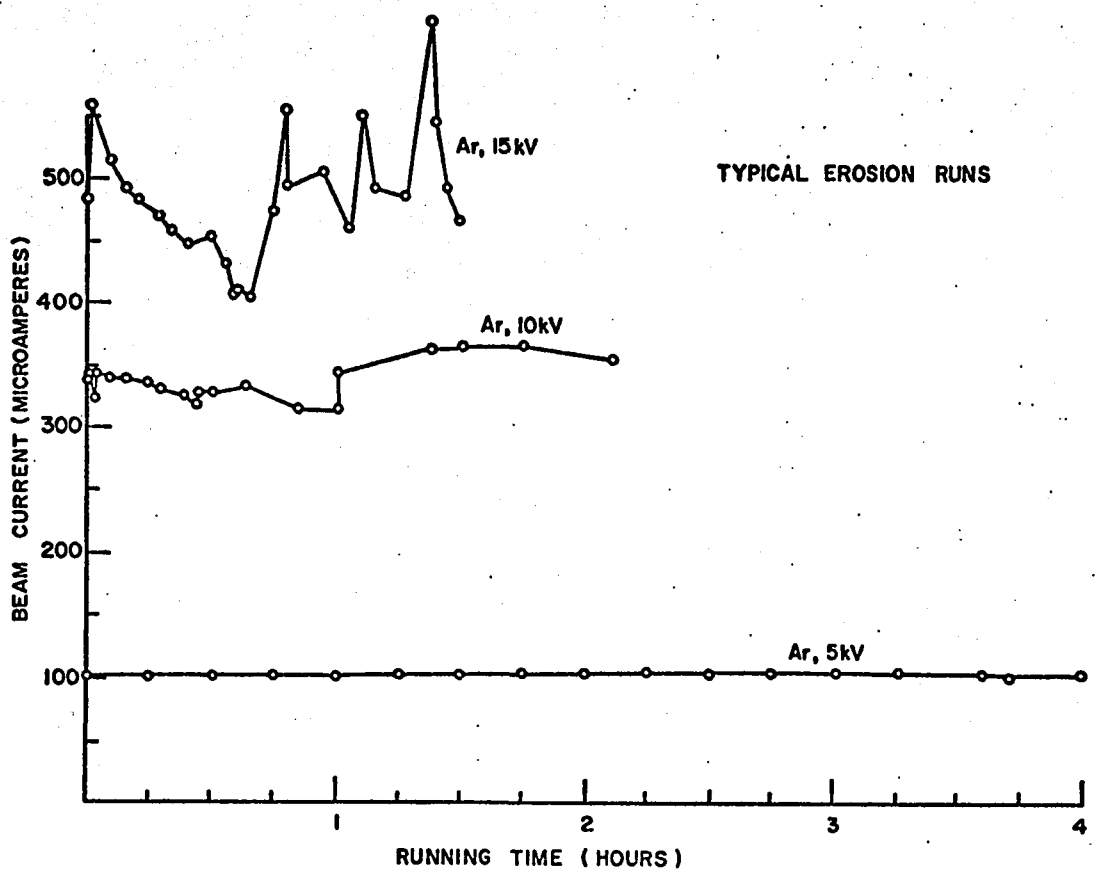

Fig. 45. Typical Erosion Runs.
Ion beam current versus running time for three typical runs, giving some indication of beam current stability.

Because the drift was sometimes not linear and because there were occasional small current outbursts of short duration, we estimated that the microampere hour dose was never more accurate than ± 5%. Each bombardment run was individually considered and bombardment dose error estimates were assigned on the basis of the beam current fluctuations for each individual run. Of the 50 targets utilized for erosion ratio calculations, 22 were estimated to have dose errors of 5%, 14 estimated at 10%, 9 at 15%, and 5 at 20%.

A Vacuum Problem

We have already mentioned electronic problems and solutions associated with discharges in the duoplasmatron. Some of these discharges may have been due to very small intermittent vacuum leaks. Initially menthanol was the only agent used for leak detection. We determined later that an epoxy glue used to cement parts of the duoplasmatron together was soluble in methanol. The duoplasmatron was completely disassembled, cleaned and reassembled, after which leaks were still present, one type caused by thermal gradients apparently warping one of the lower duoplasmatron flanges. Using great care in bolting these flanges together, and by balancing the system warm-up with its cooling system, and by the use of a liquid vacuum sealout the leak problem was essentially eliminated as determined by helium leak testing.

Target Temperature

The maximum power input to our targets during these experiments corresponded to that from an ion beam of about 600 μA accelerated through 15 kV, therefore an incident power of about 9 watts. It was of some importance to know what surface temperature increases were to be expected due to these bombardments. A very rough approximation can be made using Fourier's law for heat conduction:[42]

$$Q = KA[dt/dx] ,$$

where Q is the thermal energy current to the target surface, K is the thermal conductivity, A the surface area, and [dt/dx] is the

temperature gradient. This equation refers to a steady-state condition. The back surfaces of the targets were in contact with a machined surface of stainless steel and if we make the approximation that this steel remains at room temperature, then letting A = 5cm^2, K = 3 x 10^{-3} cal-cm/cm^2-sec-°C, Q = 2.15 cal/sec (the equivalent of 9 watts) and making the approximation that

$$\Delta t = Q \cdot \Delta X / KA$$

and letting ΔX = .16 cm, we find a calculated approximate temperature increase of 23°C. In the actual experiments the beam area on the target was usually less than 1cm^2 so the effective value of A is smaller than 5 cm^2. Also the machined surface against the target back does not provide excellent thermal contact. Both of these factors would tend to yield a value of Δt greater than 23°C; thus we were expecting temperature rises due to the beam in the low hundreds of degrees Celsius.

We performed a very rough experiment by making a sandwich of two targets with a copper-constantan thermocouple between and another beneath the sandwich. The ion beam was incident on the top surface and we attempted to roughly measure the temperature gradient across the bottom layer of the sandwich and extrapolate the temperature gradient across the top sandwich layer to its surface where the beam was incident. We found, with a 270 μA beam of 15 kV Xe ions incident at 30°, the extrapolated surface temperature in the steady state to be about 334°C. Measurements indicate that heat from the neutralization filament of 85 watts power brought the

surface temperature into the 200-250°C range, thus leaving the ion beam responsible for a temperature rise of some 85-140°C.

The thermocouples being sandwiched as they were detracted from the thermal contact of the system so that during an actual run the surface temperatures probably did not rise as high as 334°C. But even 334°C is well below the annealing and softening temperatures, 1140°C and 1670°C, of clear fused silica. The thermocouples responded well in this experiment; we were easily able to tell when the beam was turned on and off.

Hines[21] estimated a temperature rise of 95°C for lower beam current bombardment of a silica-soda-lime glass with 33.5 keV argon ions. His estimate and ours and our rough measurements verify that the macroscopic surface temperatures expected in these experiments are well below those temperatures where one could expect transformations in the structure of fused silica.

4

POST-BOMBARDMENT MEASUREMENTS AND CALCULATIONS

Determination of Eroded Mass and Eroded Mass Error

After bombardment each target was reweighed in an attempt to determine the amount of material eroded. The same Mettler balance was used, reading to micrograms. Again each target was weighed at least five times and from these weighings we obtained the mean weight and some statistical error data. See Appendix II for the computer program used. In this same appendix we have tabulated the mass loss for each target along with the statistically determined probable error.

In some of our early bombardments we restricted the diameter of the ion beam with stainless steel apertures. The ion beam sputtered metal from the edges of the apertures and the metal was deposited on the target surfaces, forming a dark film. The targets were secured in their holders by a stainless steel frame of inside diameter of 2.2 cm and when any part of the ion beam struck this frame it also sputtered metal onto the target surface, forming a reflective film. Both of these films would tend to increase the measured weight of the target.

By moving the ion source closer to the targets we were able to focus the main ion beam through apertures, 1.9 cm in diameter, without the main beam touching the aperture edges. We could observe this by allowing the vacuum pressure to rise until the beam became

visible by causing the residual gas to fluoresce. We also observed the size of the main beam at the aperture when a piece of glass was placed directly beneath the aperture and the pattern of fluorescence defined the beam size. And, of course, the beam size was visible due to fluorescence when the beam struck each target. Although the beam took on some strange patterns, which we believe were brought about by poor alignment of the Einzel lens during fabrication and by charge spreading of the beam, we saw no evidence of any part of the main beam being obstructed by an aperture.

Even though these precautions were taken some darkening did occur on some targets. When we observed the beam size by residual gas fluorescence we also observed a halo effect outside the main beam, an area of considerably less bright fluorescence apparently due to stray particles outside the main beam. We believe it was possible for these particles to sputter minimal amounts of metal from the apertures onto the targets, forming a slightly absorbing film. This film does not exist where the main beam struck the target.

Of concern here was the possible mass error such a film could contribute. The transmission of one such typical film was measured with white light and found to be 90%. This decrease in transmission, if due to a thin film of iron, would correspond to an iron film thickness of about 2 to 3 nm,[43] which we calculate would contribute a weight error of less than 8 to 12 μg. For most of the targets this would contribute an additional uncertainty in the range of 1% to 3% or less, but due to the great difficulty in attempting to estimate this error for each target, particularly in the presence of considerably

larger uncertainties, we have not included this contribution in the eroded mass data.

The targets fit snugly in their holders, but occasionally we found a target which had seemingly expanded somewhat during the bombardment and was more difficult to remove. At the time of removal the targets were at room temperature, as they were at insertion. We are aware of radiation compaction of fused silica, but because of these few observations we raise the question of a possible expansion due to ionic bombardment. Because of the tighter fit on removal for some targets, there was a possibility of micro-chipping at the edges. We have rejected most targets where chipping was obvious but have included 2 targets chipped for certain and one dubious target, in order to attempt to ascertain trends in erosion ratios and to set an upper limit for these ratios.

Determination of Ion Dose and Ion Dose Error

The eroded mass data was combined with the bombardment dose data to obtain the erosion ratio, the total bombardment dose being obtained by calculating the area under the ion beam current versus time curve. In addition to the fluctuations in beam current there are several other uncertainties related to bombardment dose. The ion beam was not analyzed; it was the raw beam from the duoplasmatron focused by the lens. As such we were not able to separate out singly or doubly ionized particles. We do not believe that conditions in the arc chamber were conducive to the production of large numbers of doubly charged ions, nor does the manner in which the

beam is extracted from the plasma just below the aperture plate seem to enhance the presence of doubly charged ions. Nevertheless some probability exists. In addition we were unable, with the unanalyzed beam, to make a distinction between charged and neutral particles. Both of these effects would contribute to erroneous measurements of bombardment dose. In addition, doubly charged particles, which would not be focused in the same manner as those singly charged, would have twice the energy capability for erosion. Small areas of depression on some targets, within the larger total beam area, may be due to neutrals in the beam, or they could be due to aberrational density increases in the charged beam. See Fig. 46. There also seems to be an erosion dependence on ion beam density.[44]

We also observed heavy erosion of the intermediate electrode of the duoplasmatron suggesting strongly that the atomic constituents of stainless steel were also present in the beam. See Fig. 47. The erosion of the electrode seemed to occur at a decreasing rate; that is, after we employed a new electrode most of the erosion seemed to occur during the subsequent 15-30 hours of running time and little more erosion after that. We estimated that some 40 mm^3 were eroded from the electrode, which, assuming all of it to be iron, is about 3×10^{21} atoms. During a typical run a bombardment dose of 300 μA-hrs is equivalent to the use of about 7×10^{18} ions. A great deal of the material sputtered from the electrode remains in the duoplasmatron, but it seems very likely that there were some quantities of it present in the ion beam. An analyzed beam would have allowed these to

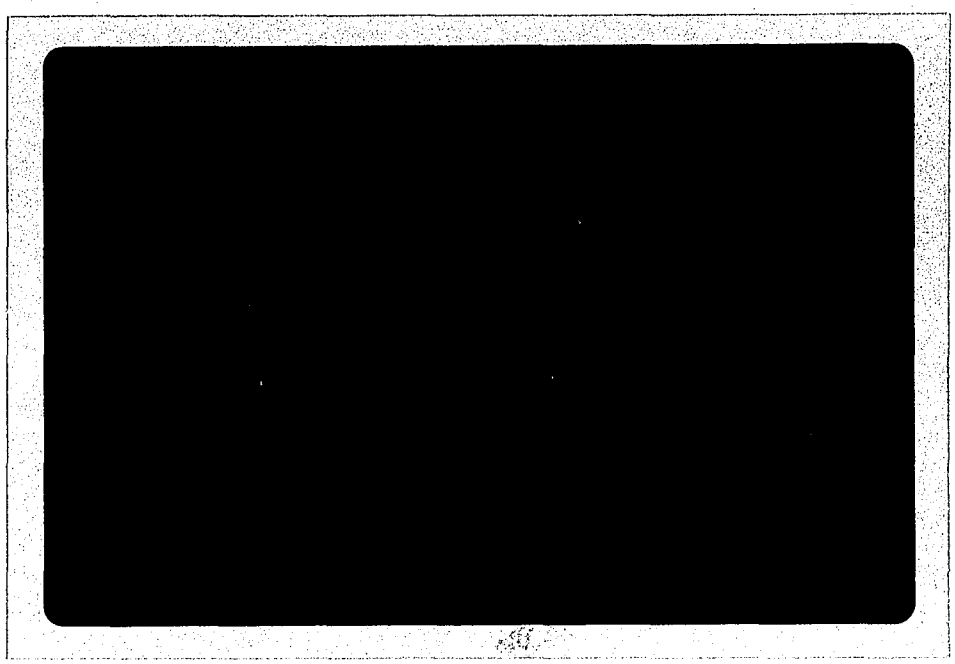

Fig. 46. Target After Bombardment.
Eroded rut in a target (just right of center). Target was silvered after erosion and some silver has been scratched off (near top) in another test.

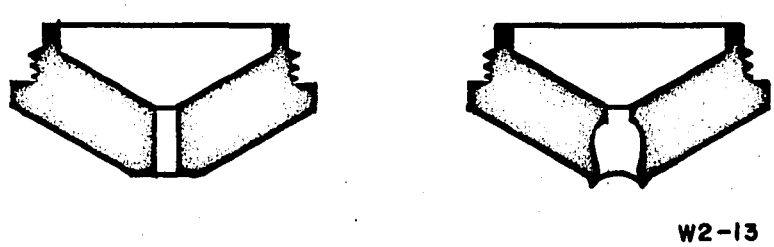

Fig. 47. Intermediate Electrode Erosion.
Duoplasmatron intermediate electrode before and after about 40 hours of running time, illustrating erosion in the plasma channel.

be separated out. These metal atoms may also have contributed to the dark film on the targets.

Lastly concerning the ion beam we are not certain of the effect of a charge buildup on the target surface. If such surface charge existed it could have altered the bombarding energy and the angle of incidence, and electron micrographs of the surfaces indicate that the angle of incidence may have been affected somewhat.

Display and Tabulation of Erosion Ratios

Erosion ratios vs. ion energy and vs. angle of incidence are plotted in Figures 48 - 55. Because of the uncertainties in the ion beam content and in the exact nature of the eroded material, the erosion ratio has been measured in terms of micrograms of target weight loss per microampere-hour of incident ion beam current, briefly, micrograms/microampere-hour. If one wishes to assume that the eroded material is SiO_2 and that all incident particles were identical and singly ionized, the equation for converting the erosion ratio to units of molecules of SiO_2 per incident ion is: (ER stands for erosion ratio)

ER (molecules/ion) = 0.447 X ER (micrograms/microampere-hour). If such a conversion of units was justifiable it would yield for these experiments erosion ratios principally in the range of 1 - 2 molecules/ion.

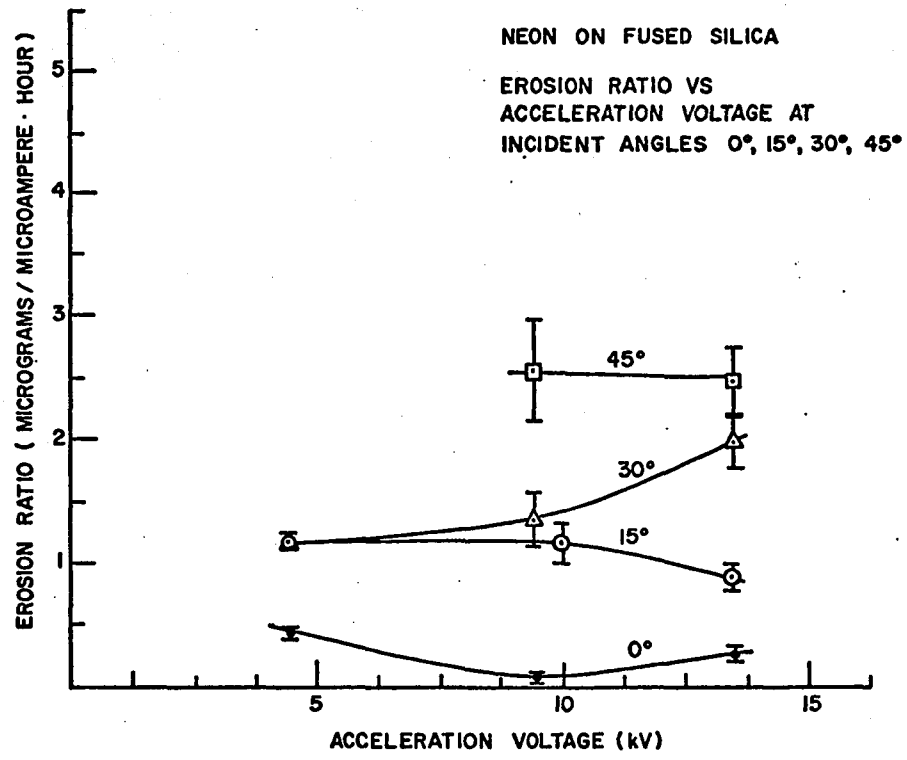

Fig. 48. Erosion Ratio Versus Acceleration Voltage, Neon on Fused Silica.

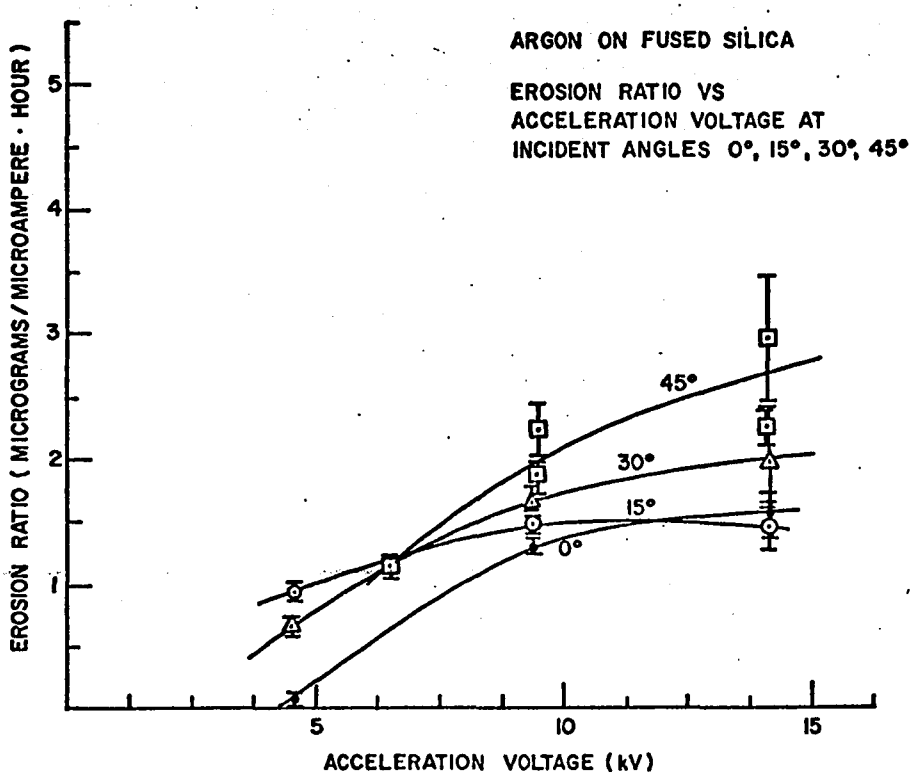

Fig. 49. Erosion Ratio Versus Acceleration Voltage, Argon on Fused Silica.

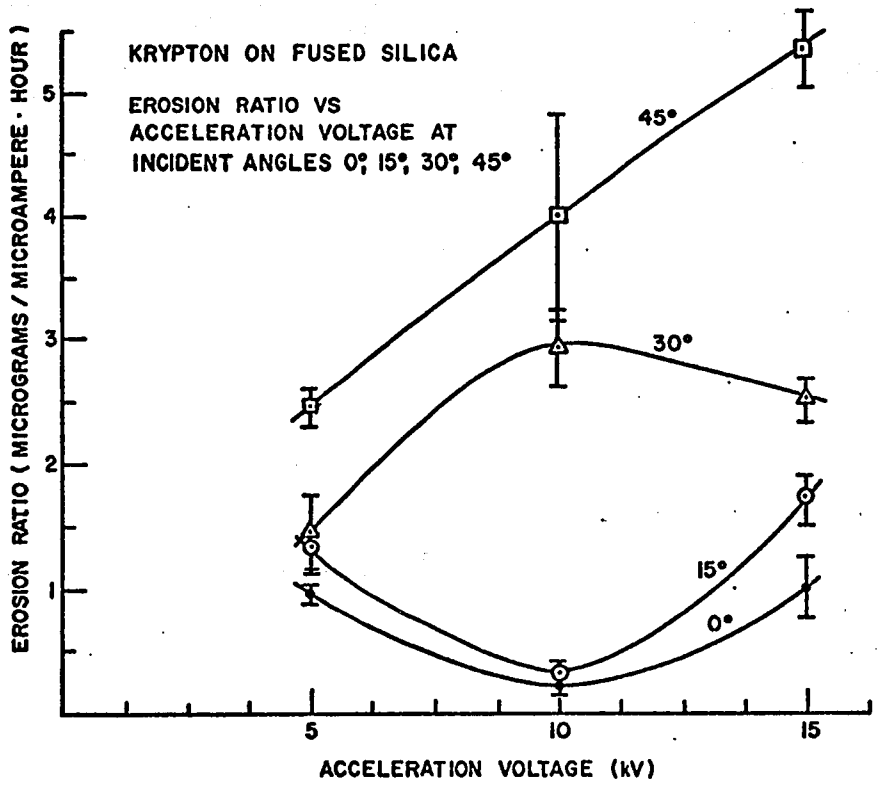

Fig. 50. Erosion Ratio Versus Acceleration Voltage, Krypton on Fused Silica.

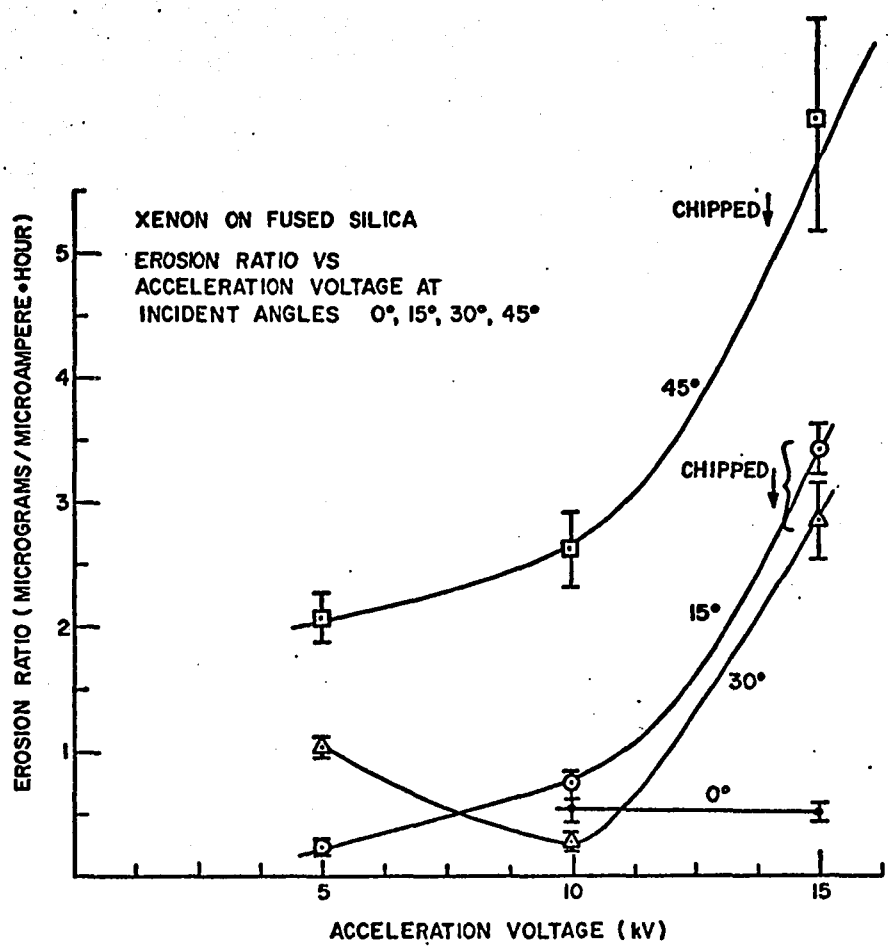

Fig. 51. Erosion Ratio Versus Acceleration Voltage, Xenon on Fused Silica.

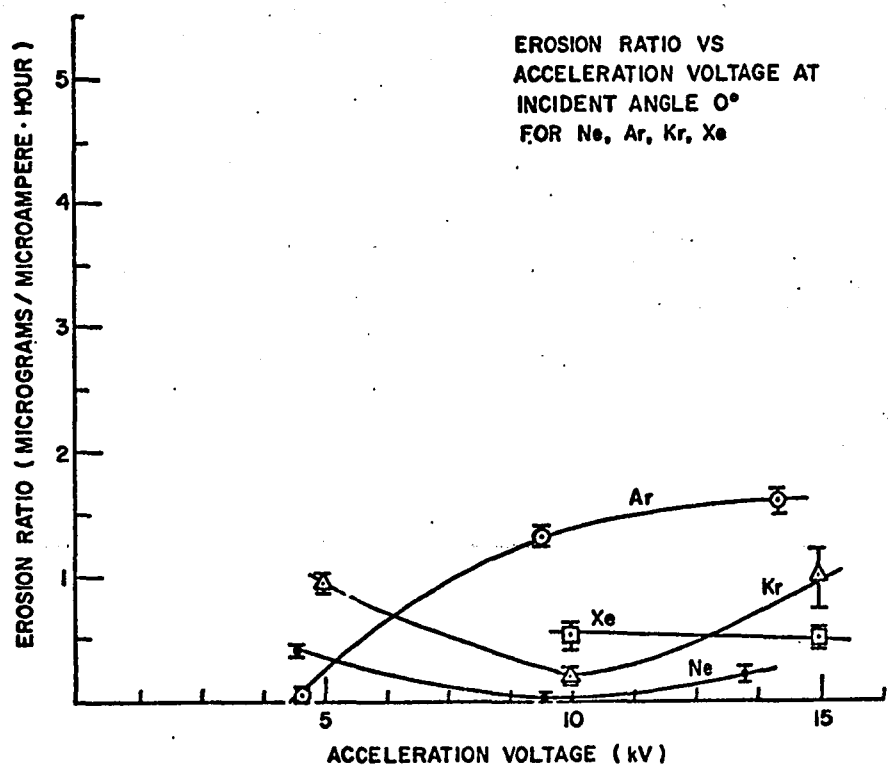

Fig. 52. Erosion Ratio Versus Acceleration Voltage, Angle of Incidence, 0°.

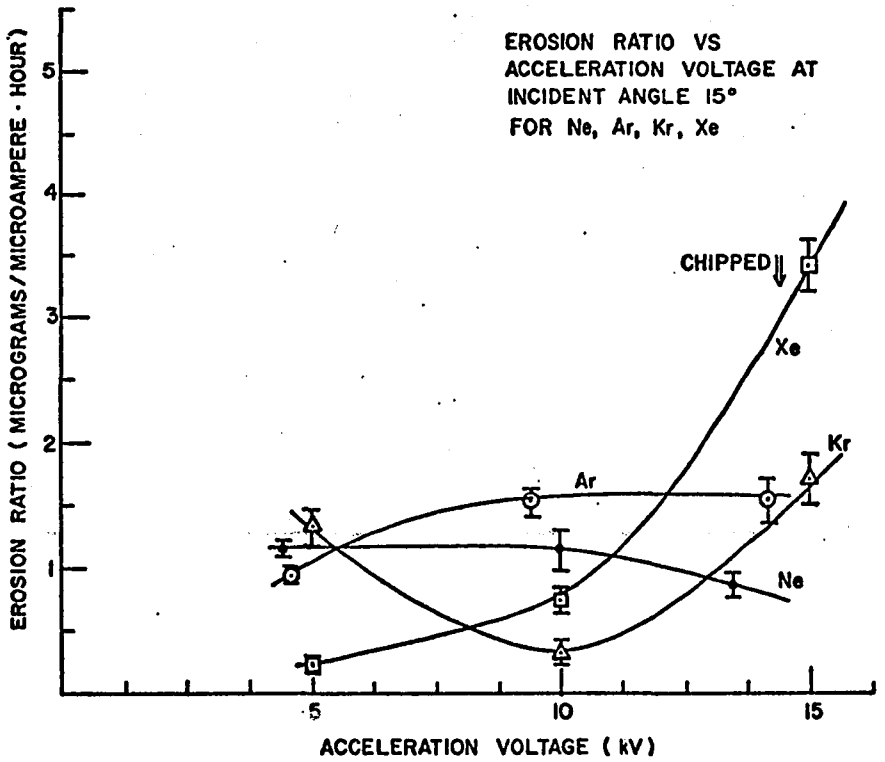

Fig. 53. Erosion Ratio Versus Acceleration Voltage, Angle of Incidence, 15°.

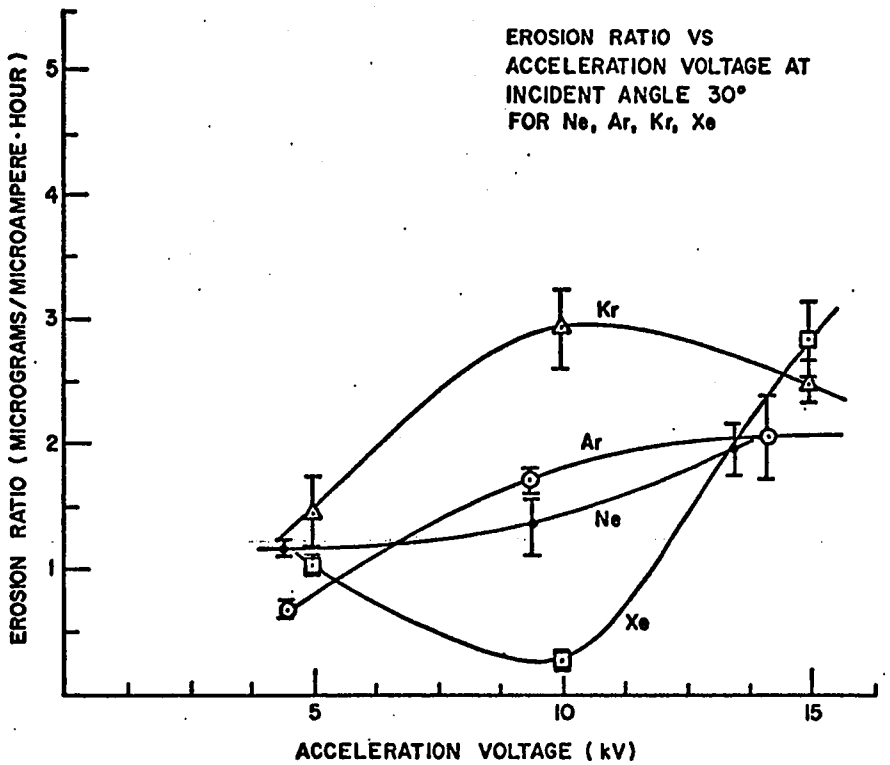

Fig. 54. Erosion Ratio Versus Acceleration Voltage, Angle of Incidence, 30°.

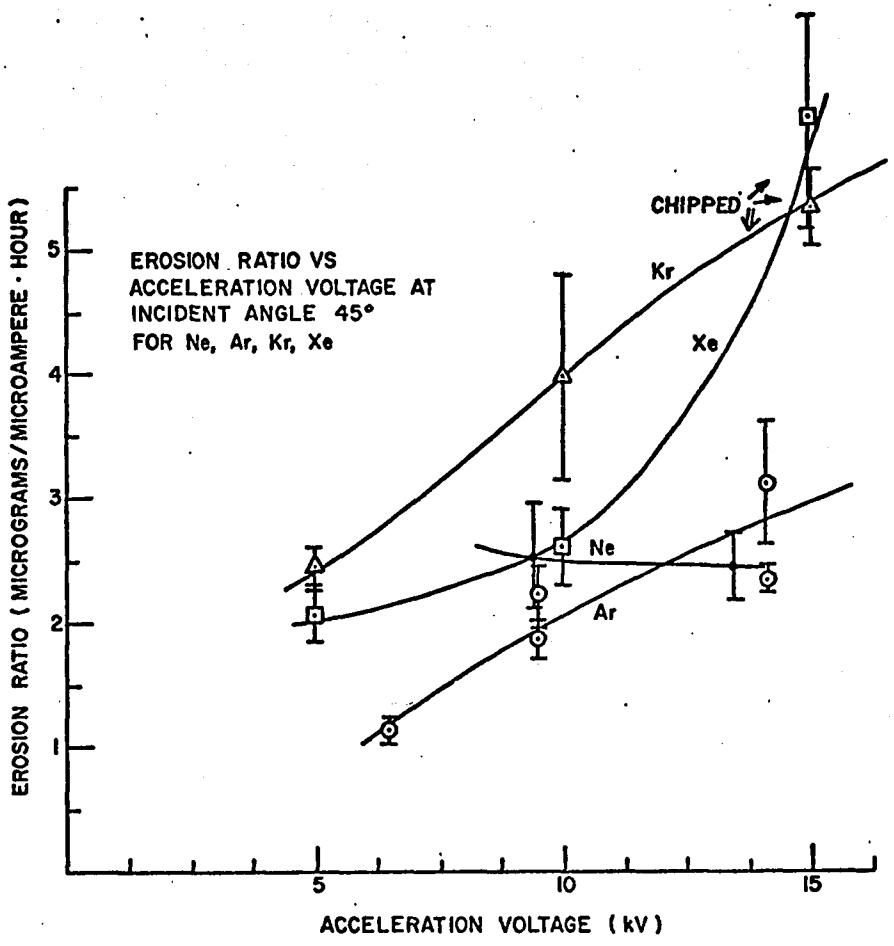

Fig. 55. Erosion Ratio Versus Acceleration Voltage, Angle of Incidence, 45°.

Table I. Erosion Ratios (μgm/μA·hr) as a Function of Ion Energy and Angle of Incidence. Error is estimated.

	0°	15°	30°	45°
		Neon on Fused Silica		
4.4keV	.440 ± .035	1.18 ± .07	1.17 ± .07	
9.4keV			1.37 ± .22	2.53 ± .43
9.5keV	.053 ± .032			
10 keV		1.14 ± .16		
13.4keV		.872± .096		
13.5keV	.27 ± .06		1.99 ± .22	2.43 ± .27
		Argon on Fused Silica		
4.6keV	.088 ± .034	.965± .068	.687± .062	
6.5keV				1.14 ± .09
10 keV	1.34 ± .08	1.55 ± .09	1.72 ± .10	1.88 ± .15
				2.22 ± .22
15 keV	1.61 ± .18	1.52 ± .24	2.07 ± .43	2.35 ± .14
				3.11 ± .50
		Krypton on Fused Silica		
5 keV	.981 ± .078	1.33 ± .15	1.46 ± .31	2.47 ± .15
10 keV	.23 ± .08	.369± .093	2.94 ± .32	3.99 ± .84
15 keV	1.03 ± .24	1.75 ± .21	2.51 ± .18	5.34 ± .32
		Xenon on Fused Silica		
5 keV		.24 ± .06	1.04 ± .08	2.08 ± .20
10 keV	.546 ± .100	.749± .080	.281± .070	2.61 ± .30
15 keV	.510 ± .070	3.43 ± .20	2.86 ± .30	6.09 ± .90

5

EXAMINATION OF POLISHED SURFACES

We were quite disturbed to observe some of the resulting surfaces. The roughness of some appeared as coarse as that of frosted glass. We have been unable to correlate this roughness with any experimental parameters; this pitting has occurred with all ions used, all angles and all energies. See Figs. 56-60.

Gross Observations of Gross Surfaces

On some of the grossly pitted surfaces there are continuous lines similar to those which have been observed with primary crazing of glass surfaces. On other surfaces the etching is faintly similar to that produced chemically; however, we rule out chemical etching in the normal sense of the word due to the care with which the silica samples were handled and stored.

We can conjecture as to other causes of pitting. The ion bombardment may have brought into appearance, conditions underlying the silica surfaces or conditions otherwise related to the past history of the targets. These targets were manufactured by fusing ½-in. to 2-in. (mixed) Brazilian quartz crystals in a vacuum furnace. The surfaces were polished by professional lapidaries, who first ground the surfaces to a relatively good finish and then polished with a standard jeweler's rouge. Conceivably, the ion beam could bring out grain boundaries or gas pockets in the glass. In the polishing process scratches are made in the surfaces with associated stresses in the surrounding material. The stresses remain even after the scratch

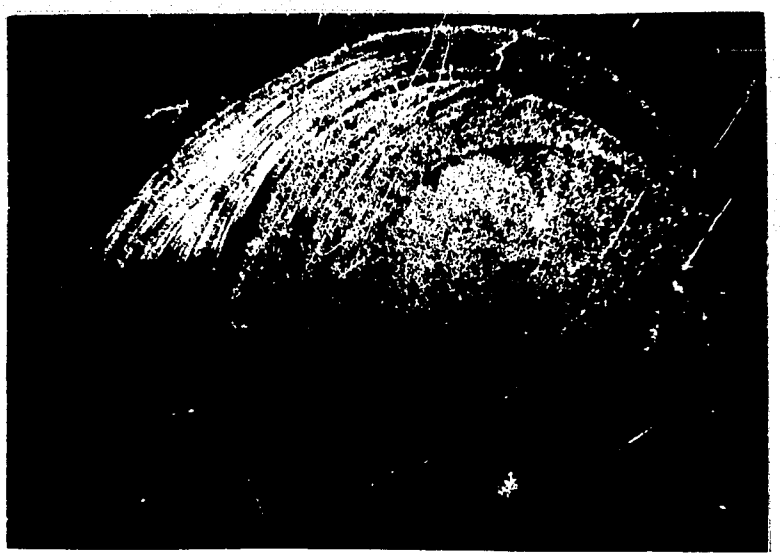

Fig. 56. Gross Pitting of Fused Silica by 15 keV Xenon Ions at 45°, Magnification 35X.

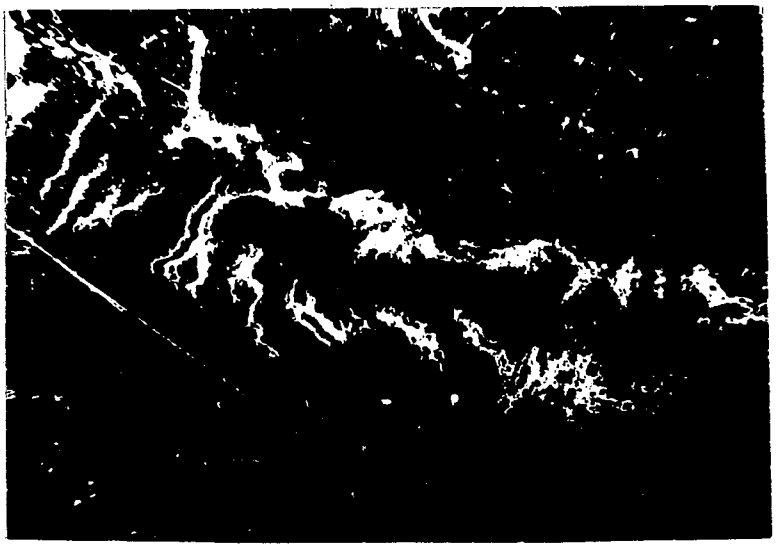

Fig. 57. Gross Pitting of Fused Silica by 15 keV Xenon Ions at 30°, Magnification 35X.

Fig. 58. Gross Pitting of Fused Silica by 10 keV Xenon Ions at 30°, Magnification 35X.

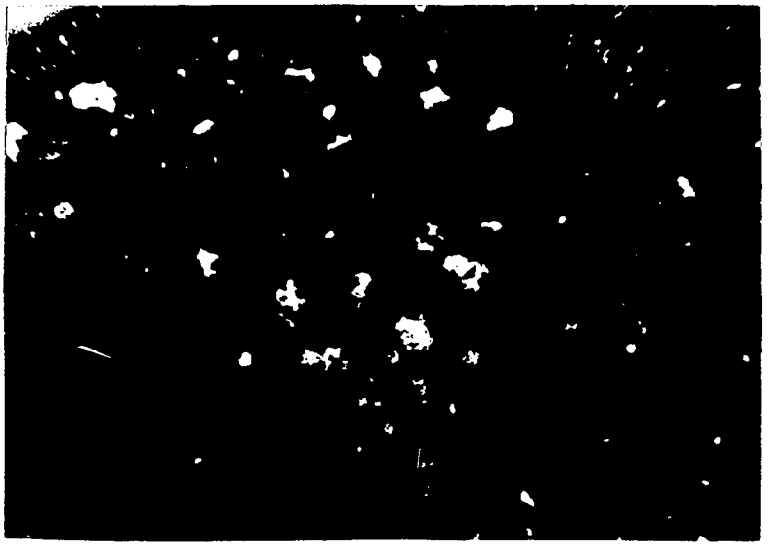

Fig. 59. Pitting of Fused Silica by 5 keV Xenon Ions at 0°, Magnification 35X.

is "polished out." Ion bombardment may bring out this past history of stress. The pitting may be associated with charge accumulations on the surface although, as mentioned before, steps were taken to eliminate this. Although we did not observe any, Lichtenburg figures will occur in glass under electrical stress.[45] Perhaps, a positive charge bombardment and possible imbedment can set up static electrical stresses on the surface which in turn affect the erosion pattern. Lastly, type 101 fused silica is not a pure material; it contains upwards of 200 parts per million of various substances other than SiO_2. In addition there was undoubtedly a surface layer of H_2O and $[OH]^-$ at the beginning of bombardments because the last cleaning step was a rinse in distilled water. Such surfaces are known for their catalytic action on certain types of chemical reactions.[46] Perhaps $[OH]^-$ and H_2O are responsible for some of these etch effects.

Thorough examination of all targets revealed that about 38% could be classed as having no pitting or very little pitting visible under an optical microscope at a magnification of 100. Fig. 61 is one such typical surface and it is to be compared with the gross pitting just mentioned. Apparently certain conditions will allow ionic erosion without gross disruption of the optical polish.

Examination by Electron Microscopy

We were concerned with just how smooth the surface finish was on this 38% of the targets so we turned to transmission and scanning electron microscopy (TEM and SEM) to see whether the microfurrowing observed by other workers was present here. Micrographs of grossly

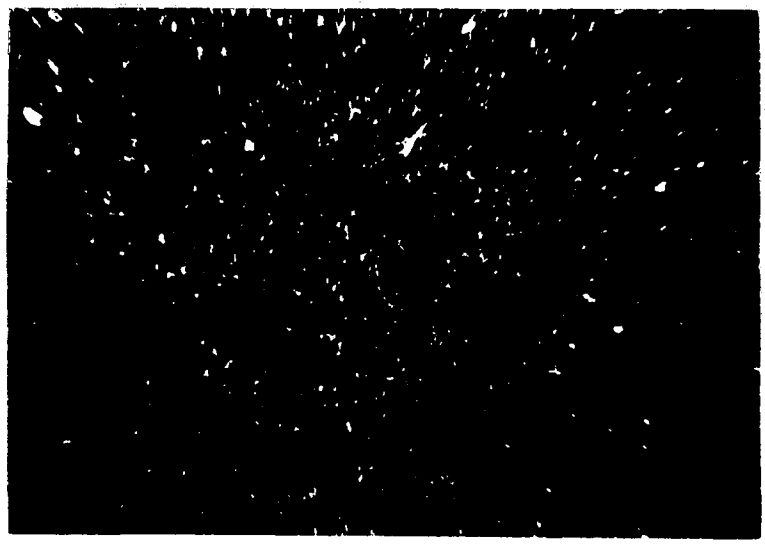

Fig. 60. Pitting of Fused Silica by 5 keV Xenon Ions at 45°, Magnification 100X.
Also see Figs. 64 and 66 for magnifications of 3,000X and 4,000X.

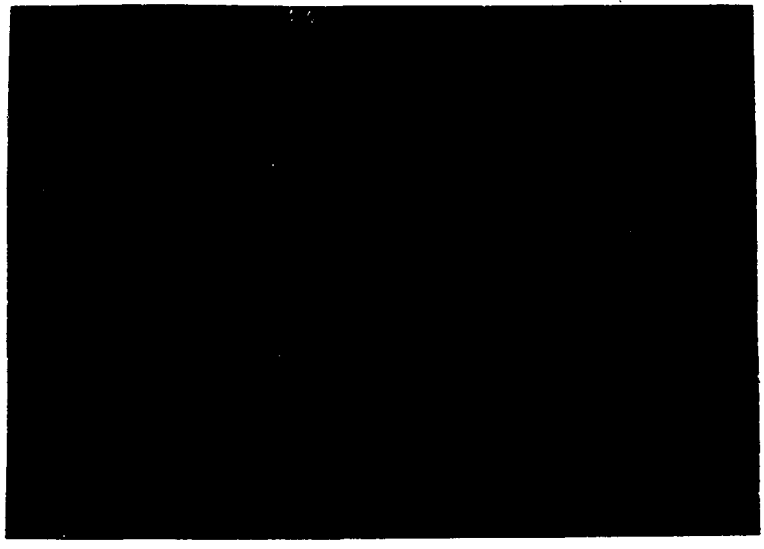

Fig. 61. Comparison Photograph Showing Very Little Pitting on a Target Bombarded by 4.6 keV Argon Ions at 45°, Magnification 100X.

pitted targets and a reference target were made by a professional laboratory. These illustrate more detail of the gross etching and pitting. Toward the end of the study this writer chose some of the optically best appearing surfaces for study by transmission electron microscopy alone. We made surface replicas by a double replication technique, the first of plastic and the second of carbon shaded with a platinum palladium alloy and these were examined with a 100-keV Hitachi microscope at Illinois State University. The furrowing that had been reported by other workers with 4-keV ions is still present with 15-keV ions.

We believe this study may shed some light on the formation of the micro-furrows. Fig. 62, a scanning electron micrograph, illustrates the furrows formed by 15-keV neon ions incident at 45°. The beam direction was approximately from the top of the photo to the bottom. Compare this picture with Fig. 63, 15-keV argon ions incident at 45°. Although the ion was different we believe these figures illustrate the manner in which the furrows may be built up from a large number of what appear to be microcraters. Notice also in Fig. 63 that the cratering is most prevalent along certain lines running from low left to high right. Could these be stress lines implanted in the original polishing of these targets? These lines are not taking the same direction that the furrowing will.

Fig. 64 shows another phenomenon encountered. This is the same target as Fig. 60 but now the magnification is 3000X. Similar appearing spikelike forms have shown up in other studies[47-49] and have been attributed to inclusion material of a different erosion

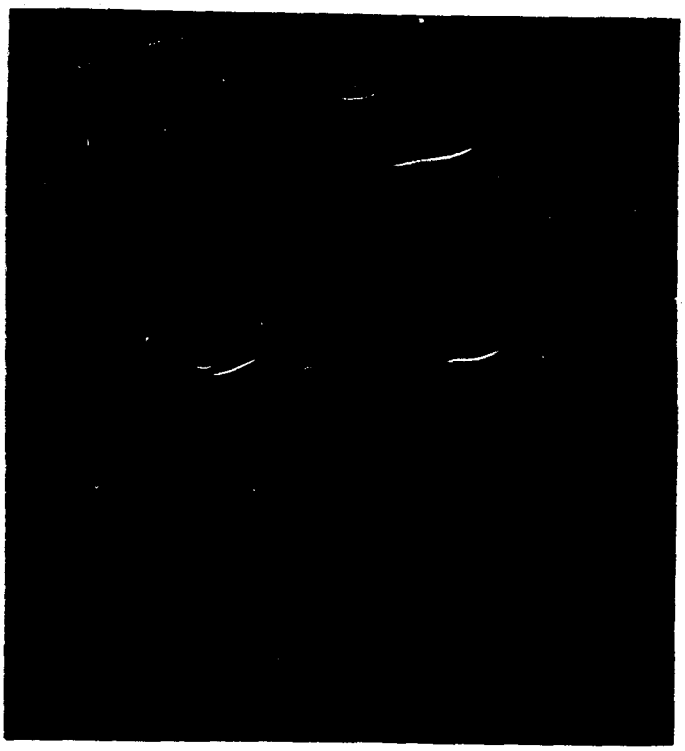

Fig. 62. SEM Micrograph, Fused Silica, 15 KeV Neon at 45°, Magnification 3,000X.
Scanning electron micrograph of fused silica surface bombarded by 15 keV neon ions at 45°, magnification 3,000X. The micro-furrowing reported earlier is still present at 15 keV.

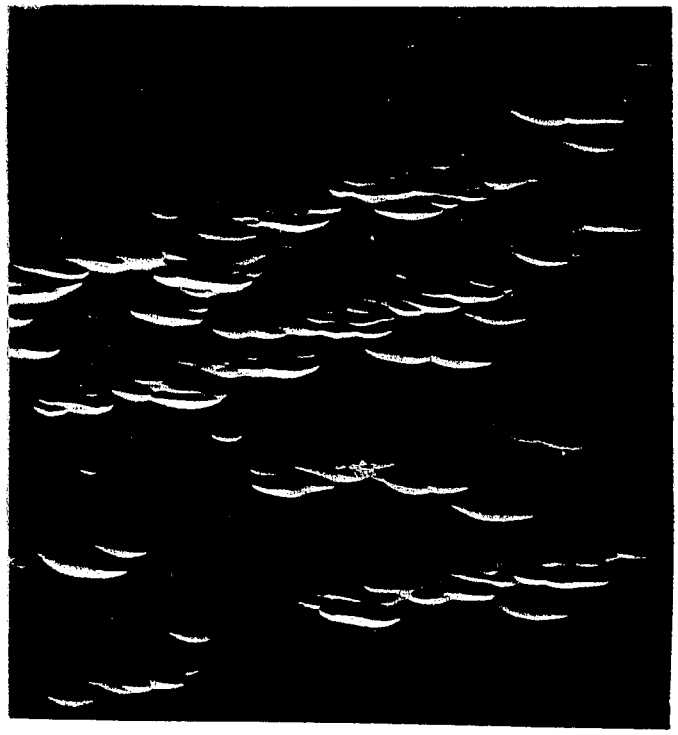

Fig. 63. SEM Micrograph, Fused Silica, 15 KeV Argon at 45°, Magnification 3,000X.
Scanning electron micrograph of fused silica surface bombarded by 15 keV argon ions at 45°, magnification 3,000X. We believe this area of the target shows the preliminary formations leading to the micro-furrows.

ratio. Fig. 64, however, is to be interpreted not as spikes but rather as depressions in the surface. The ion beam direction is the same as the longer dimension of the depressions and therefore perpendicular to the very slight micro-furrowing of the surface; but in the depressions themselves there is a slight furrowing parallel to the beam direction. Obviously such a surface is useless optically, unless one needs ground glass.

Fig. 65 is a scanning electron micrograph of an unbombarded surface as received from General Electric. There are no surface markings of any type at 10,000X.

Fig. 66 and 67 are transmission electron micrographs of, respectively, the spikelike appearing surface and a cratered surface; these are negative prints. Fig. 66 does reveal streaks, parallel to the ion beam direction, in the depressions and more clearly shows the micro-furrowing of the surface.

The above are examples of electron microscopy of the poorest surfaces. Figs. 68-70 are transmission micrographs of surfaces which appeared optically smooth to the unaided eye and at 100X with a visual microscope. The micro-furrowing is present and we have used the shadowing angle information to make estimates of surface roughness. Of particular interest is Fig. 69 where the bombardment angle was $0° \pm 2°$. In this figure there is a significant decrease in furrow spacing and surface roughness. It is apparent visually in these photographs. In the three Figs. 68-70 we have estimated the peak-to-peak surface roughness by assuming that a cross section of the furrows would appear as a saw-tooth or triangular wave of variable frequency.

Fig. 64. SEM Micrograph, Fused Silica, 5 KeV Xenon at 45°, Magnification 3,000X.
Scanning electron micrograph of fused silica surface bombarded by 5 keV xenon ions at 45°, magnification 3,000X. Some micro-furrowing is present. The spike-like appearing objects are depressions, unexplained. See Fig. 66, a transmission electron micrograph of this same target.

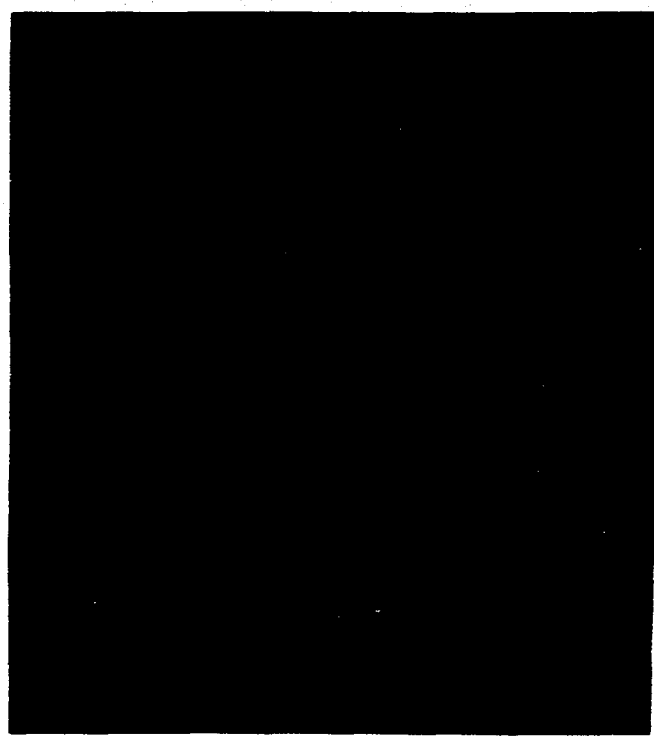

Fig. 65. SEM Micrograph, Unbombarded Surface, Magnification 10,000X. Scanning electron micrograph of an unbombarded surface of fused silica (a reference surface) showing essentially no surface features. Magnification 10,000X.

Fig. 66

Fig. 67

Fig. 66 (Left). TEM Micrograph, Fused Silica, 5 KeV Xenon at 45°, Magnification 4,000X.
Transmission electron micrograph (negative print) fused silica surface bombarded by 5 keV xenon ions at 45°, magnification about 4,000X. These are the structures which appeared spike-like in the scanning micrograph, Fig. 64.

Fig. 67 (Right). TEM Micrograph, Fused Silica, 15 KeV Argon at 45°, Magnification 4,500X.
Transmission electron micrograph (negative print) of fused silica surface bombarded by 15 keV argon ions at 45°, magnification about 4,500X. We believe this figure also shows the preliminary stages of micro-furrowing.

Fig. 68. TEM Micrograph, Fused Silica, 5 KeV Neon at 45°, Magnification 9,600X.
Transmission electron micrograph of fused silica surface bombarded by 5 keV neon ions at 45°, magnification 9,600X. The peak-to-peak roughness of the micro-furrows is estimated to be about 34.5nm. The furrow spacing is about 130nm. (The white areas are due to a breakup of the surface replica film).

Fig. 69. TEM Micrograph, Fused Silica, 5 KeV Xenon at 0°, Magnification 9,600X.
Transmission electron micrograph of fused silica surface bombarded by 5 keV xenon ions at 0°, magnification 9,600X. The peak-to-peak roughness is estimated to be 6.9nm with a spacing of about 45nm. The decreased perceptibility of the micro-furrows is due to the near normal bombardment angle, estimated to be 0° $\pm$ 2°.

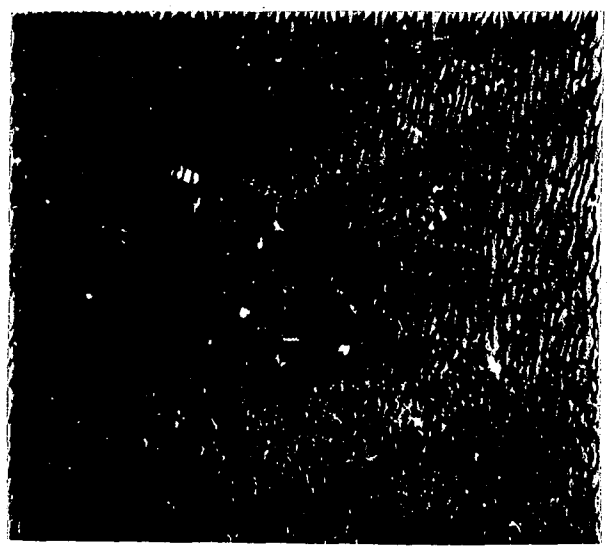

Fig. 70. TEM Micrograph, Fused Silica, 5 KeV Argon at 45°, Magnification 9,600X.
Transmission electron micrograph of fused silica surface bombarded by 5 KeV argon ions at 45°, magnification 9,600X. The peak-to-peak roughness is estimated to be about 13.8nm with a furrow spacing about 95nm. Note the additional fine pitting and cratering on this surface.

The shadowing angle was used to estimate the peak-to-peak height of the wave. In these three figures, which are typical, the roughness varied from 7 to 35 nm. The furrow spacing varied from 45 to 130 nm.

An Indirect Roughness Estimate

We were interested in comparing the above roughness estimates with those which could be obtained utilizing multiple beam interference fringes of equal chromatic order (FECO fringes). Bennett and Bennett[50] have reported an expression which under certain conditions can be used for calculating peak-to-peak surface roughness from measurements made on FECO fringes:

$$\sigma_{pp} = \lambda'\Delta\lambda/[2(\lambda-\lambda')],$$

where σ_{pp} is the peak-to-peak roughness, $\Delta\lambda$ the extreme width of the fringe having a mean wavelength λ, and λ' the mean wavelength of the adjacent fringe on the short wavelength side.

Fig. 71 is a FECO interferogram with interference fringes from two different bombardment areas and three sets of comparison spectral lines of mercury. Our measurements on this plate yield peak-to-peak roughness estimates of 23 nm for the upper set of fringes and 25 nm for the lower fringes. These measures are comparable with the range of 7 to 35 nm roughness obtained from the electron micrographs. The FECO method assumes that the heights of the surface irregularities have a Gaussian distribution; this is probably not exactly our case, but we believe our micro-furrowed surfaces are close enough to Gaussian for the FECO method to be employed for a roughness estimate.

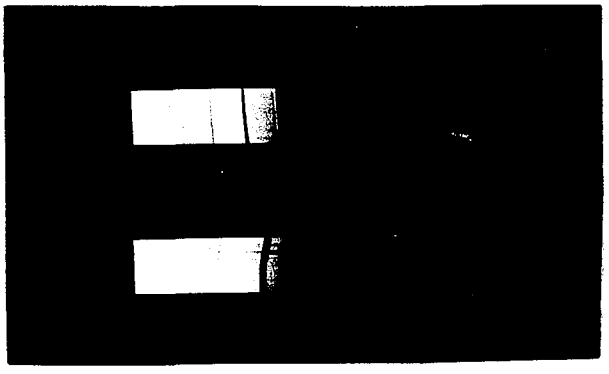

Fig. 71. FECO Fringes from Bombarded Surface.
FECOgraph also used to estimate surface roughness of bombarded fused silica. Two sets of reflection interference fringes of equal chromatic order from two different target areas are shown with three sets of mercury comparison spectral lines.

6

SUMMARY AND CONCLUSIONS

We have bombarded over 100 target discs of GE Type 101 fused silica, one-inch diameter by one-sixteenth inch thick, with ion beams of neon, argon, krypton, and xenon, at energies of 5 to 15 keV, the target surfaces at angles to the beam of 0°, 15°, 30°, and 45°. As a result, material has been removed from the surfaces indicating erosion ratios varying from 0.053 to 6.09 micrograms per microampere-hour. We believe we have satisfactorily monitored the beam currents incident on the targets. Precautions were taken in an attempt to eliminate charge buildup on the target surfaces. Although the erosion ratio data contain much uncertainty, a trend can be seen indicating an increase in erosion ratio as a function of energy and as a function of angle of incidence, measured from the surface normal. The data for argon, the best-behaved gas in the duoplasmatron, suggest the approach to a maximum in erosion ratio near 15 keV. Such a maximum is expected from general sputtering theory.[51]

The plotted data, however, do lack somewhat of a functional continuity with respect to ion mass, energy, and angle of incidence. We are tempted to attribute this to two principal causes. First, although we attempted to keep the ion beam incident area on the target uniform at about one square centimeter, we believe there were variations in incident ion beam density, observed as small areas of increased fluorescence on the target. These may have been caused by aberrations or nonuniform charge spreading of the ion beam, or by

accumulations of charge on the target surface. Secondly, examination of the eroded surfaces clearly showed that erosion took place in a variety of forms, suggesting that the past history of the surfaces may be a determining factor in the erosion process.

Though not all the bombarded surfaces were examined by electron microscopy, those surfaces which appeared of good optical quality visually and at 100X showed, on closer examination, micro-furrowing with estimated peak-to-peak average roughness from 7 to 35 nm and furrow spacing of approximately 45 to 130 nm. It is unlikely that such surfaces would be useful in optical work of high quality.

What is to be concluded from this study, specifically concerned with ion bombardment in the range 5 to 15 keV? From the examination of the polished surfaces we doubt that this energy range will be useful in optical figuring except at normal incidence, and more work might be done there to ascertain the best possible surface. A feasibility study of optical figuring has been recently reported[10] for ion energies upwards of 30 keV, but the investigations concerned normal bombardments only. Surface smoothness was based upon the results of light scattering experiments and electron microscopy and reported as cosmetically similar to good mechanical polishing, but no quantitative measures are given. It would be desirable to bombard at angles other than normal to take advantage of the increased erosion ratio, and we can only pose the question at this time about the surface roughness after oblique bombardments at energies exceeding 15 keV.

Concerning better values for erosion ratios we would strongly recommend magnetic separation of beam constituents so that one would

have better knowledge of the bombarding particle. We object to the conventionally used erosion ratio units of molecules/ion, especially in light of the work[23] which indicated that the sputtered material was $SiO_{1.6}$. These units are even more meaningless if the optical target material contains substances other than SiO_2. Some workers[10] have employed units of atoms/ion! We are dissatisfied with Faraday cup methods to measure beam currents and would rather have available some method for continuous monitoring without obstructing the beam or removing it from the target surface. Some workers[10] have placed the targets of optical material inside the Faraday cup and read beam current as the charge migrates or arcs to the inner cup surfaces. We question the effects of this on the quality of the optical surface. This writer feels, then, that magnetic beam analysis and a better, continuous, beam current measurement would greatly improve the data on erosion ratio. If at the same time one could find a way to assure the electrical neutrality of the target surface, this would also aid in stabilizing the erosion ratio.

We have said very little concerning the microscopic process by which material is eroded. Two processes are usually mentioned in conjunction with sputtering; they are transfer of momentum and sputtering by thermal spikes. Increased erosion with more glancing angles of incidence seems to give credibility to the momentum transfer process. This process could also account for erosion along boundaries or stress lines in the surface where the cohesive forces might be less. This was suggested as a result of some work with metals by Magnuson, Meckel and Harkins.[48]

The investigations of Hines and Arndt[18] led them to conclude that for 45-keV neon ions incident normally on fused silica, the penetration depth and volume of displacement were so large that the temperature rise of this volume was estimated to be 8.4°C. If the penetration depth is less, then the beam energy must be dissipated in a smaller volume and they estimate that neon ions of 3.4 keV could produce thermal spikes near the melting point of quartz, about 1500°C. We have operated near 3.4 keV as well as above it and it seems possible that some of our erosions were due to thermal spikes, particularly those with the larger ions of argon, krypton and xenon. We raise the specific question of whether the cratering we have observed, Figs. 62 and 63, was due to thermal spikes. We believe the cratering to be an early form of the microfurrows, and even though we bombarded at 15 keV, the targets were at 45° to the ion beam, implying a lesser penetration depth than in the work of Hines and Arndt and suggesting that thermal spikes cannot be ruled out as responsible for the cratering and subsequent, we believe, furrowing. We do not pretend that the work reported in this paper presents any conclusive evidence pointing to the specific erosion process.

There is a third possible erosion process, however, blistering and exfoliation due to trapped gass. Primak and Luthra[52] have suggested this process in which the bombarding ions are trapped beneath the target surface, coalesce, forming microbubbles of gas which could eventually burst, leaving a blistered effect on the surface. In metals they have observed this blistering along what they believe to be grain boundaries. In our work we have shown an instance of the

early cratering of fused quartz to occur along preferred lines not associated with the ion beam direction. Our bombardments, however, lack the energy necessary for any great depth penetration, say, more than about 40 nm[10,35] which is the same order as the roughness figures we have estimated for the surfaces. And some workers[10] have stated that the open structure of fused silica is sufficient to allow trapped gas to migrate to the surface and escape. The bombardment energies we have been discussing are available in electron beams, and perhaps some studies with such beams would allow differentiation between the effects of gas trapping and the effects of thermal spikes.

From the observations we have made it seems impossible to determine which, if any, of the above three processes dominated in our experiments. It was not the purpose of this paper to do so.

We speculate on three additional possible applications of ionic polishing. In the ruling of large diffraction gratings the lines near the end of the ruling become rather ragged due to the dulling of the diamond ruling tool. Perhaps this roughness could be removed by ion bombardment at near grazing incidence. Would it ever be possible to utilize the furrows themselves as a grating? Granted, the furrows we have illustrated lack uniformity, but they look much better on the surfaces of crystalline materials bombarded at large angles of incidence.[53] A furrow spacing similar to those we have shown, about 100 nm, if usable, would provide a grating of 100,000 lines/cm or 254,000 lines/inch. Lastly, if all the difficulties we have encountered were due to the electrical properties of our targets, ionic polishing may prove very useful in the development of metal mirrors.

The ionic polishing of optical materials is still in its infancy, and much more investigation remains to be done. Evidence of its fruitfulness lies in its impending commercial application. This writer would caution anyone initiating research in this area that he should be ready to accept and come to grips with all the problems inherent in bombarding insulators with electrically charged particles.

APPENDIX I

CALCULATION OF ION DOSES

This appendix contains: the computer program used to calculate the ion beam dose in microampere-hours; a sample entry of data for the program; and the computer output for that sample, which is a display of the actual data taken for that target, that is, a record of time and of ion beam current as read by the biased Faraday cup. The computer prints the total microampere-hour dose at the end of each run.

The computer reads the ion beam current at the beginning, I, and at the end, I1, of time intervals indicated by T and T1. It then takes the product $(I1 + I)\cdot(T1 - T)$ and moves on to the next time interval repeating the operation and accumulating the sum of these products. This sum represents twice the area under the ion beam current vs. time graph, therefore, twice the microampere-hour dose to the target. The computer divides by 2 then prints the actual dose as approximated by this program.

THE COMPUTER PROGRAM

```
100 FILES TARGA;TARGB;TARGC;TARGD;TARGE;TARGF
110 FOR A=1 TO 6
120 LET S=0
140 PRINT
150 PRINT
160 PRINT
165 READ #A,N
170 PRINT "TARGET";N
180 PRINT"TIME(HOURS)","CURRENT(MICROAMPERES)"
190 READ #A,T,I
200 PRINT T,I
210 READ #A,T1,I1
220 LET D=T1-T
230 LET J=I1+I
240 LET K=D*J
250 LET S=S+K
270 PRINT T1,I1
280 LET T=T1
290 LET I=I1
300 IF END #A THEN 320
310 GO TO 210
320 PRINT "TOTAL BOMBARDMENT DOSE IS  ";
330 PRINT S/2;
340 PRINT "MICROAMPERE HOURS"
370 NEXT A
380 END
```

SAMPLE DATA FOR COMPUTER PROGRAM,

IN THIS CASE THE FILE CALLED TARG B

```
50 56
100 0•0,484
101 •03,561
102 •1,515
103 •17,492
104 •21,482
105 •29,470
106 •34,459
107 •42,449
108 •50,453
109 •57,431
110 •59,409
111 •61,411
112 •67,406
113 •76,474
114 •8,556
115 •83,494
116 •95,506
117 1•06,461
118 1•11,552
119 1•17,492
120 1•28,487
121 1•38,634
122 1•40,546
123 1•44,492
124 1•5,467
```

COMPUTER OUTPUT OF THE SAMPLE DATA

TARGET 56

TIME(HOURS)	CURRENT(MICROAMPERES)
0	484
.03	561
.1	515
.17	492
.21	482
.29	470
.34	459
.42	449
.5	453
.57	431
.59	409
.61	411
.67	406
.76	474
.8	556
.83	494
.95	506
1.06	461
1.11	552
1.17	492
1.28	487
1.38	634
1.4	546
1.44	492
1.5	467

TOTAL BOMBARDMENT DOSE IS 730.82 MICROAMPERE HOURS

Table II. Summary of Bombardment Doses, and Estimated Bombardment Dose Error

Target No.	Bombardment Dose (μA·hr)	Estimated Error (%)
56	731	15
57	759	5
59	400	5
60	912	10
66	652	20
67	688	15
68	769	5
69	731	5
74	415	5
75	425	5
86	490	10
87	561	10
88	593	10
90	579	15
91	593	15
93	611	5
94	678	5
95	609	5
224	153	5
225	279	5
227	278	5
230	456	5
301	412	5
302	374	5
304	382	20
305	340	20
306	314	10
307	281	5
308	386	10
309	312	10
312	290	5
313	218	10
314	388	15
315	318	15
316	346	20
317	303	10
318	273	5
319	238	5
320	387	5
322	309	15
323	298	20
324	335	15

Table II, Continued

Target No.	Bombardment Dose (μA·hr)	Estimated Error (%)
325	394	15
326	347	10
328	429	5
329	428	10
331	404	10
353	316	10

APPENDIX II

TABULATION OF ERODED MASSES

The targets were weighed five or more times before bombardment and after bombardment. Gaussian error theory was used to calculate the probable error in these weighings and also the mean value of the weighings. A computer program for these calculations was adapted from one contained in an instruction manual in BASIC programming.[54] Only the variable significant figures in the weighings were used in these calculations. We list below the computer program and two lines of typical weight data and the computer printout. This is followed by a tabulation of all the mass loss and mass error data.

THE COMPUTER PROGRAM

```
100 LET N=0
110 LET S=0
120 LET S2=0
140 READ X
150 IF X=99 THEN 210
160 LET N=N+1
170 LET S=S+X
180 LET S2=S2+X*X
190 GO TO 140
210 LET M=S/N
220 LET V=(N*S2-S*S)/N/(N-1)
230 LET D=SQR(V)
240 LET P=.6745*D
280 PRINT "NUMBER","SUM","SUM-SQUARES","MEAN"
290 PRINT N,S,S2,M
310 PRINT "VARIANCE","STD. DEV.","PROB. ERR."
320 PRINT V,D,P
330 PRINT
340 PRINT
350 PRINT
360 LET N=0
370 LET S=0
380 LET S2=0
390 READ X
400 IF X<>999999 THEN 160
900 DATA 24,26,35,20,36,99
901 DATA 49,46,44,44,37,55,99
999 END
```

COMPUTER OUTPUT

NUMBER	SUM	SUM-SQUARES	MEAN
5	141	4173	28.2
VARIANCE	STD. DEV.	PROB. ERR.	
49.2	7.01427	4.73113	

NUMBER	SUM	SUM-SQUARES	MEAN
6	275	12783	45.8333
VARIANCE	STD. DEV.	PROB. ERR.	
35.7667	5.98052	4.03386	

Table III. Tabulation of Mass Data

Target No.	Mass Loss (μgm)	Probable Error (μgm)	Percent Error (%)
56	2162	15	1
57	1251	8	1
59	35	12	34
60	1399	9	1
66	1286	12	1
67	997	8	1
68	1141	13	1
69	949	9	1
74	285	10	4
75	410	10	2
86	1192	4	1
87	1115	9	1
88	517	6	1
90	1466	25	2
91	812	7	1
93	716	6	1
94	801	12	1
95	268	7	3
224	175	6	3
225	525	14	3
227	618	31	5
230	1022	8	1
301	22	12	55
302	367	11	3
304	558	8	1
305	1357	11	1
306	85	12	14
307	694	10	1
308	512	6	1
309	918	7	1
312	303	8	3
313	454	11	2
314	109	10	9
315	1937	5	.3
316	358	11	3
317	529	11	2
318	687	11	2
319	1270	16	1
320	290	18	6
322	71	15	21
323	110	6	5
324	82	9	11

Table III, Continued

Target No.	Mass Loss (μgm)	Probable Error (μgm)	Percent Error (%)
325	215	6	3
326	907	7	0.7
328	1471	7	0.5
329	1222	7	0.6
331	206	8	4
353	360	14	4

LIST OF REFERENCES

1. W. R. Grove, "On the electro-chemical polarity of gases," Phil. Trans. Roy. Soc. London 142:87, 1852.

2. G. K. Wehner, "Sputtering by ion bombardment," in *Advances in Electronics and Electron Physics, Vol. VII* (Academic Press, New York, 1955), pp. 239-298.

3. W. J. Moore, "The ionic bombardment of solid surfaces," Am. Scientist 48 (2):109-133, 1960.

4. H. S. W. Massey and E. H. S. Burhop, "The collision of positive ions and neutral atoms with surfaces," Chap. IX in *Electronic and Ionic Impact Phenomena* (Oxford U. Press, London, 1952), pp. 541-617 (2nd revised edition now also in print).

5. G. Carter and J. S. Colligen, "Sputtering," Chapt. 7 in *Ion Bombardment of Solids* (Amer. Elsevier, New York, 1968), pp. 310-353.

6. R. B. Gillette and B. A. Kenyon, "A study of proton-induced effects on reflective surfaces of space mirrors," NASA Contractor Report, NASA CR-1532, The Boeing Co., Seattle, Feb., 1970.

7. A. B. Meinel, S. Bashkin, and D. A. Loomis, "Controlled figuring of optical surfaces by energetic ionic beams," Appl. Opt. 4(12):1674, 1965.

8. J. B. Schroeder, S. Bashkin, and J. F. Nester, "Ionic polishing of optical surfaces," Appl. Opt. 5(6):1031-1034, 1966.

9. J. B. Schroeder and H. D. Dieselman, "Ellipsometric analysis of radiation damage in dielectrics," J. Appl. Phys. 40(6): 2559-2564, 1969.

10. J. B. Schroeder, H. D. Dieselman, and J. W. Douglass, "Technical feasibility of figuring optical surfaces by ion polishing," Appl. Opt. 10(2):295-299, 1971.

11. L. H. Narodny and M. Tarasevich, "Paraboloid figured by ion bombardment," Appl. Opt. 6(11):2010, 1967.

12. M. Tarasevich, "Ion beam erosion of rough glass surfaces," Appl. Opt. 9(1):173-176, 1970.

13. R. K. Burdett, "Superfine glass polishing with ions," SIRA Review, South Hill, Chislehurst, Kent, England, Oct. 1968, pp. 156-159.

14. "Glass polishing by ion beams," Research-Industry Techlink No. 328, Ministry of Technology, Station Square, St. Mary Cray, Orpington, Kent, England, May, 1969.

15. R. K. Burdett, "Ion beams in the optics industry," SIRA Abstracts and Reviews 23(8):281-284, 1968.

16. John Strong, *Procedures in Experimental Physics* (Prentice Hall, Englewood Cliffs, N.J., 1938), pp. 159-165.

17. G. S. Anderson, W. N. Mayer, and G. K. Wehner, "Sputtering of dielectrics by high-frequency fields," J. Appl. Phys. 33(10):2991-2992, 1962.

18. R. L. Hines and R. Arndt, "Radiation effects of bombardment of quartz and vitreous silica by 7.5-keV to 59-keV positive ions," Phys. Rev. 119(2):623-633, 1960.

19. A. I. Akishin, S. S. Vasil'ev, and L. N. Isaev, "Cathode sputtering of mica, fused quartz and glass by krypton ions," Izv. Akad. Nauk SSSR, Ser. Fiz. 26:1356, 1962. (Translation: Bull. Acad. Sci. USSR, Phys. Ser. 26(11):1379-1380.)

20. R. L. Hines and R. Wallor, "Sputtering of vitreous silica by 20- to 60-keV Xe^+ ions," J. Appl. Phys. 32(2):202-204, 1961.

21. R. L. Hines, "Radiation effect of positive ion bombardment on glass," J. Appl. Phys. 28(5):587-591, 1957.

22. R. A. Dugdale and S. D. Ford, "The etching of alumina and fused silica by sputtering," Trans. Brit. Ceram. Soc. 65:165-180, 1966.

23. G. V. Jorgenson and G. K. Wehner, "Sputtering studies of insulators by means of Langmuir probes," J. Appl. Phys. 36(9): 2672-2674, 1965.

24. P. D. Davidse and L. I. Maissel, "Equivalent dc sputtering yields of insulators," J. Vacuum Sci. & Technol. 4(1):33-36, 1967.

25. B. B. Meckel and R. A. Swalin, "Selective delineation of screw dislocations by cathodic sputtering," J. Appl. Phys. 30(1): 89-93, 1959.

26. A. I. Krokhina and G. V. Spivak, "Investigation of structural changes in dielectrics under the influence of heat, chemical etching and ion bombardment," Izv. Akad. Nauk SSSR, Ser. Fiz. 23:741, 1959. (Translation: Bull. Acad. Sci. USSR, Phys. Ser. 23(6):736-738.)

27. A. I. Krokhina and G. V. Spivak, "Concerning anisotropy of cathode sputtering of dielectrics," Izv. Akad. Nauk SSSR, Ser. Fiz. 24:694, 1960. (Translation: Bull. Acad. Sci. USSR, Phys. Ser. 24(6):701-704.)

28. A. I. Krokhina, G. V. Spivak, A. M. Reshetnikov, and R. I. Zhelninskaya, "Electron microscopic investigation of the structure of ceramic materials, brought out by ionic etching," Izv. Akad. Nauk SSSR, Ser. Fiz. 27:1224, 1963. (Translation: Bull. Acad. Sci. USSR, Phys. Ser. 27(9):1199-1202.)

29. A. I. Krokhina and G. V. Spivak, "Disintegration of ceramics and glasses under ion bombardment," Izv. Akad. Nauk SSSR, Ser. Fiz. 28:1483, 1964. (Translation: Bull. Acad. Sci. USSR, Phys. Ser. 28(9):1386-1389.)

30. M. Navez, C. Sella, and D. Chaperot, "Electron microscope study of the effects of ionic bombardment on glass," in *Ionic Bombardment--Theory and Applications*, International Symposium of the National Scientific Research Center, Bellevue, 4-8 December 1962 (Gordon and Breach, New York, 1964), pp. 339-355.

31. G. Carter and W. A. Grant, "The ion bombardment of glass," Phys. and Chem. of Glasses 7(3):94-100, 1966.

32. W. Primak, "Radiation-induced stress relaxation in quartz and vitreous silica," J. Appl. Phys. 35(4):1342-1347, 1964.

33. A. E. Ennos, "The origin of specimen contamination in the electron microscope," Brit. J. Appl. Phys. 4:101-106, 1953.

34. J. Koch, "Reduction of optical reflectivity of glass surfaces resulting from ion bombardment," Nature 164:19-20, 1949.

35. R. L. Hines, "Ranges of 7.5- to 52-keV H_2^+, D_2^+, He^+, and Ne^+ ions in quartz," Phys. Rev. 120(5):1626-1630, 1960.

36. G. M. Batanov, "Secondary emission from No. 46 glass under the effect of positive ions of some gases," Fizika Tverdogo Tela 2(9):2048-2057, 1960. (Translation: Soviet Physics; Solid State 2(9):1839-1846, 1961.)

37. L. Holland, *The Properties of Glass Surfaces* (John Wiley, New York, 1964), p. 321.

38. D. G. Bills and A. A. Evett, "Glass, a disturbing factor in physical electronics measurements," J. Appl. Phys. 30(4): 564-567, 1959.

39. O. C. Yonts, C. E. Normand, and D. E. Harrison, Jr., "High-energy sputtering," J. Appl. Phys. 31(3):447-450, 1960.

40. C. D. Moak, H. E. Banta, J. N. Thurston, J. W. Johnson, and R. F. King, "Duo plasmatron ion sources for use in accelerators," Rev. Sci. Instr. 30(8):694-699, 1959.

41. O. B. Morgan, G. G. Kelley, and R. C. Davis, "Technology of intense dc ion beams," Rev. Sci. Instr. 38(4):467-480, 1967.

42. R. L. Powell, "Thermal conductivity," in *American Institute of Physics Handbook* (McGraw-Hill, New York, 1963), Sec. 4, p. 77.

43. P. Rouard and P. Bousquet, "Optical constants of thin films," in *Progress in Optics, Vol. IV* (North-Holland, Amsterdam, 1965), pp. 145-197.

44. Personal communication from G. Sanger, Optical Sciences Center, University of Arizona, Tucson (1970).

45. Personal communication from W. Primak, Solid State Physics Div., Argonne National Lab., Argonne, Ill. (1970).

46. R. B. Sosman, *The Phases of Silica* (Rutgers U. Press, New Brunswick, N. J., 1965), p. 352.

47. A. D. G. Stewart, "Investigation of the topography of ion bombarded surfaces with a scanning electron microscope," in *Proceedings of Fifth International Congress for Electron Microscopy* (Academic Press, New York, 1962), pp. D-12.

48. G. D. Magnuson, B. B. Meckel, and P. A. Harkins, "Etch effects from oblique-incidence ion bombardment," J. Appl. Phys. 32(3):369-374, 1961.

49. W. C. Nixon, "Scanning electron microscopy," Contemporary Physics 10(1):71-96, 1969.

50. H. E. Bennett and J. M. Bennett, "Precise measurements in thin film optics," in *Physics of Thin Films, Vol. 4*(Academic Press, New York, 1967), pp. 1-96.

51. K. B. Cheney, E. E. Rogers, and E. T. Pitkin, "Research on experimental evaluation of sputtering yield rates," USAF ARL 63-125, The Marquardt Corp., Van Nuys, Calif. (AD No. 415285), pp. 31-32, July, 1963.

52. W. Primak and J. Luthra, "Radiation blistering: Interferometric and microscopic observations of oxides; silicon; and metals," J. Appl. Phys. 37(6):2287-2294, 1966.

53. R. L. Cunningham, P. Haymann, C. Lecompte, W. J. Moore, and J. J. Trillat, "Etching of surfaces with 8 KeV argon ions," J. Appl. Phys. 31(5):839-842, 1960.

54. J. G. Kemeny and T. E. Kurtz, *Basic Programming* (John Wiley, New York, 1967), pp. 81-82.